Optimisation of electrolyte composition and operating parameters for the electropolishing of 304 stainless steel

Jeeten Nathoo

Department of Chemical Engineering
University of Cape Town
Rondebosch, 7700
South Africa

20 October 2003

A thesis submitted for the degree of Master of Science at the University of Cape Town

Acknowledgements

I wish to acknowledge and thank all the people who have played a key role in the completion of this thesis:

Foremost, to my supervisor Professor Alison Lewis, for giving me both this opportunity and invaluable guidance without which this thesis would not have been possible;

To Janet Basson for introducing me to electropolishing and for her assistance;

To Rob van Hille for his valued input and Francis Pocock, for her efficiency and administrative assistance;

To Douglas Hatfield, for helping in the development of the surface roughness imaging technique and Derek Charlton for all matters statistically related;

From the mechanical workshop, to David and Joachim for their ever-enthusiastic assistance and friendship. To Bill and Granville from the electronics workshop as well as to Martin and Kenneth.

Thanks to Ashton, Shilpa, Mandy and Ochieng of the Precipitation and Crystallisation Research Facility for their friendship, support and interaction;

To my family: my parents to whom I am eternally grateful, to my sister Jyoti and brother Nilesh. Lastly, to Kalpana who has and continues to make each day so special.

Synopsis

The success of an electropolishing process hinges on its ability to achieve the best surface finish, both in terms of smoothness and specular reflectance, in the shortest possible polishing time.

The work detailed in this report focused on research into the optimisation of electrolyte composition and operating conditions for the electropolishing of 304 stainless steel. In the light of the scarcity of precise information with regards to electrolyte compositions and operating conditions for the anodic dissolution of ferrous alloys in acid electrolytes, this research was carried out on behalf of a South African metal finishing company, with the following aims:

1. To minimise the polishing time for their current electrolyte (PS electrolyte), whose fastest polishing time was ten minutes;
2. To determine the optimal electrolyte composition, by establishing the influence that varying the ratios in which the three components: H_3PO_4, H_2SO_4 and a diol (G) (the exact identity cannot be revealed for propriety reasons) are mixed, has on the rate and quality of polishing. Subsequently, to test the performance of the new electrolyte versus that of the currently used electrolyte;
3. To investigate metal ion speciation occurring within the spent electrolyte and to evaluate the possibility of precipitating the dominant metal complexes, therefore maintaining a favourable concentration gradient for rapid electropolishing, as well as, extending the electrolyte's operation life.

A digital imaging technique, based on determining the surface roughness from a digitally acquired image of the surface viewed under a Nomarski microscope, was formulated and found to give the most accurate overall three-dimensional representation of the surface topography and was consequently used to compare differences in polishing quality. The surface roughness was quantified according to a Smoothness Index (SI), with a larger SI value representing a greater surface smoothness and consequently better surface finish than a lower SI value.

The results of the optimisation study on the polishing characteristics of the PS electrolyte - 304 stainless steel system revealed that the voltage - current density relationship did not exhibit a clear polishing plateau region. Thus, it was necessary to establish the optimal current density range by measuring the polishing quality at increasing current densities. The plateau was found to be between 1 and 2A/cm^2, with 2A/cm^2 providing a significantly reduced polishing time of 3 minutes. Hence, the excessive plant polishing time of 10 minutes could be primarily attributed to operating below the optimal current density. Accordingly, operating

the plant at a current density as close to $2A/cm^2$ as possible, based on limitations of the power supply, formed one of the most important recommendations to come out of this research.

The major findings relating to establishing the optimum electrolyte composition and operating conditions were that: compared to the electrolyte composition, the effect of varying the current density and temperature within the ranges investigated, showed insignificant impact on the polishing quality and rate. Electrolytes without H_3PO_4 did not undergo electropolishing. Furthermore, the H_3PO_4 - H_2SO_4 interaction was found to play the most significant role in terms of the electropolishing rate, with higher H_2SO_4 concentrations resulting in more rapid mass loss. Conversely, the interaction of increasing amounts of G with the two acids was found to have a positive influence on the polishing quality.

Based on Response Surface Methodology (RSM), the relationship between the polishing quality (SI) and rate (% mass loss) to the compositions of the components making up the electrolyte was established. The optimum electrolyte composition predicted by the simultaneous optimisation of the SI and percentage mass loss responses was found to be 14.24% G, 55.66% H_3PO_4 and 30% H_2SO_4 by volume. However, experimentally, an electrolyte containing 9.45% G, 45.275% H_3PO_4 and 45.275% H_2SO_4 was found to be the optimum for the electropolishing of 304 stainless steel, with the discrepancy between the two being attributed to limitations of the mathematical model.

Having established the metal ion speciation characteristics of the spent PS electrolyte, it was found that the precipitation of dissolved metal ions from solution in order to increase the rate of polishing and the electrolyte life was not viable. Consequently, decanting a portion of the spent bath and topping it up with fresh electrolyte appears to be the easiest method of improving the driving force for electropolishing and extending the operating life of the electrolyte.

The most important recommendations for future work relating to aspects of the electropolishing process include:

- Refining the PS electrolyte voltage - current density relationship by using smaller voltage steps;
- Performing experiments at a wider range of temperature in order to establish the impact of temperature on polishing quality and rate;
- Establishing a fundamental understanding of the roles played by the electrical conductivity, viscosity and diffusivity of the electrolyte on the electropolishing process, towards developing simulation capabilities for this process;
- Initiating pilot scale studies using the key results from this work before implementing the findings at industrial scale.

The foremost recommendation relating to experimental improvements is to grind all the metal specimens to the same surface roughness prior to polishing in order to alleviate surface roughness measurement errors associated with variations in irregularities on the surface.

Table of contents

List of appendices

List of figures

List of tables

Chapter 1

Introduction

Electropolishing is widely used in industry as a metal finishing technique for obtaining a smooth and lustrous surface finish on various metals. The effective reduction in metal surface micro roughness and consequent smoothing is achieved by the preferential dissolution of the metal at the convex locations on the metal surface in a concentrated acid or alkaline solution (Delayen *et al.*, 2001).

The success of an electropolishing operation hinges on the ability to achieve the best surface finish in terms of smoothness and specular reflectance in the shortest possible polishing time. Therefore, to maintain the edge over competitors, electropolishers do not willingly reveal exact electrolyte compositions, operating conditions and process secrets, resulting in a scarcity of precise information with respect to the electropolishing of various metals. Furthermore, comparatively little literature is available relating to the anodic dissolution behaviour of ferrous alloys in concentrated acid electrolytes under electropolishing conditions (Betova *et al.*, 2003).

This research was carried out on behalf of a South African metal finishing company with the primary aim of minimising the electropolishing time for 304 stainless steel, without compromising and possibly enhancing the smoothness and lustre of the metal surface. With the current shortest possible polishing time being 10 minutes, the minimum target for this project was reducing the polishing time to less than 10 minutes.

Broadly speaking, two issues control the rate of electropolishing:

1. The rate of metal ion transport from the metal surface through the anode film layer to the bulk of the electrolyte mixture, which is principally a function of the properties of the electrolyte and the operating current density.
2. The concentrations of dissolved metal ions in solution continually increases until it becomes high enough to considerably slow down and eventually prevent polishing altogether (Faust, 1976).

Therefore, the approach adopted for this research was initially to map out the performance of the currently used electrolyte, by determining the current density that would minimise the polishing time.

The second objective was to determine the influence that the ratios in which the three components: H_3PO_4, H_2SO_4 and a specific diol (G), whose exact identity cannot be revealed for proprietary reasons, are mixed has on the rate of polishing. The effect of the metal ion transport properties of the system are inherently tied up in the various electrolyte compositions investigated. In this phase of the work, the possibility of enhancing the polishing rate by determining the optimal electrolyte composition, using an experimental design based on Response Surface Methodology (RSM), was investigated. The effect of temperature and current density on the polishing performance was also investigated and this research culminated in the development of a mathematical model relating polishing quality and rate to electrolyte composition and operating conditions. Once established, the performance of the model-predicted optimum electrolytes were tested against the performance of the electrolyte currently used.

Secondly, metal ion speciation within the electrolyte at different conditions was thermodynamically modelled with the intention of identifying the particular metal complexes occurring. This information was used to investigate possible methods for the continuous or batch-wise removal of these dissolved metals from the electrolyte, therefore maintaining a favourable concentration gradient for rapid electropolishing, as well as, extending the life of the electrolyte.

The final aspect of this research involved the development of surface roughness measurement techniques to be used for the analysis of polished metal surfaces during this project. These methods quantified the level of surface roughness and enabled differentiation between the various degrees of polishing, allowing comparisons to be made.

Chapter 2

Background to electropolishing

2.1 The History of Electropolishing

The first reference to electropolishing appeared in 1912 when a patent for the finishing of silver in a cyanide solution was issued by the German government. The successful electropolishing of copper, in 1935, was the next advancement in the process after which a number of new developments in 1936 and 1937, mainly by Charles Faust, led to the discovery of solutions for the electropolishing of stainless steel, amongst other metals (Delstar Corporation, 1998).

Today, electropolishing is replacing mechanical metal finishing in an increasing number of situations due to its ability to produce a smoother surface and enhance the following: brightening, deburring, stress relieving and passivating.

2.2 What is electropolishing and how does it work?

Electropolishing is the smoothing of a metal surface by the electrolytic removal of metal, ion by ion, from the surface in a highly ionic solution by the passage of an electric current. It is the reverse of electroplating.

Figure 2.1 below shows a schematic representation of a metal surface before and after electropolishing.

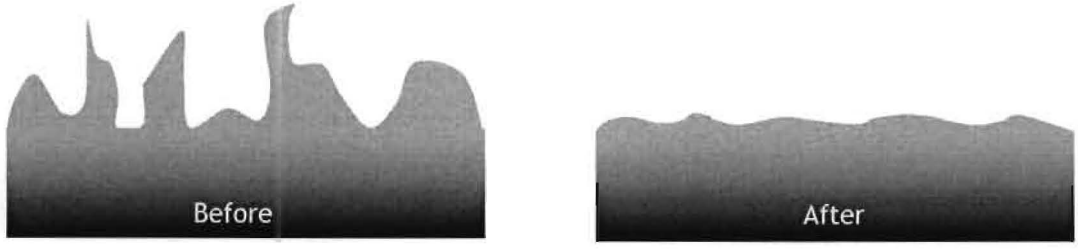

Figure 2.1: Cross-sectional schematic representing the micro-smoothening achieved by electropolishing

During electropolishing, the specimen to be polished is immersed in the electrolyte and made anodic (+) by means of a direct current. A metal cathode (-) immersed into the electrolyte completes the circuit as shown in Figure 2.2:

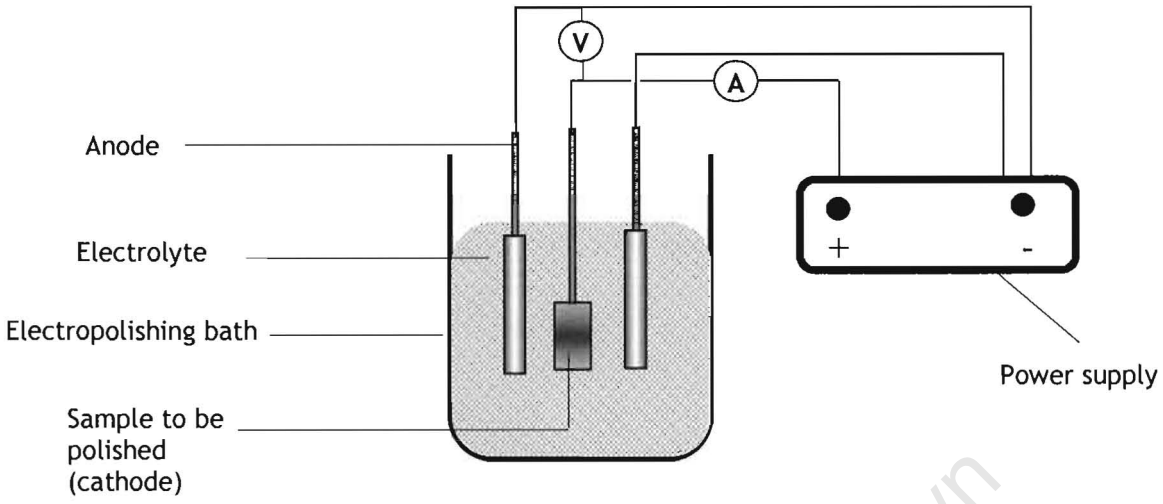

Figure 2.2: Schematic of an electropolishing cell

During the electropolishing process, the surface of the metal is covered by a film of varying thickness, which results from the reaction of products of the anodic metal dissolving in the electrolyte (Faust, 1976; Delstar Corporation, 1998). The film is thickest over the micro-depressions and thinnest over the micro-progressions, as shown by distances A and B respectively in Figure 2.3. The electrical resistance is smallest where the film is thinnest. As a result, metal dissolution occurs faster at the micro-projections as compared to the micro-depressions, therefore effectively removing the surface micro-roughness.

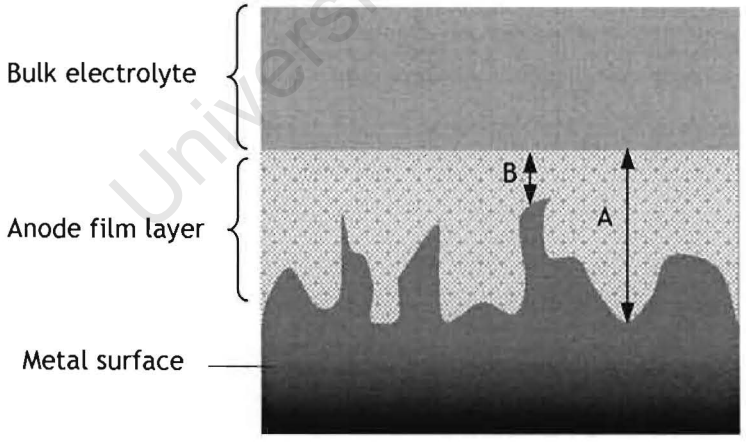

Figure 2.3: Schematic depicting the difference in anode film layer thickness between micro-depressions (A) and micro-projections (B)

Factors that affect the amount of metal removed are the current density, temperature of the bath, electrolyte and the type of metal being polished.

2.3 Benefits of electropolishing

Table 2.1: Some of the major benefits of electropolishing (Delstar Corporation, 1998)

Characteristic	Benefits of electropolishing
Physical appearance	▪ Enhanced smoothness and reflectivity ▪ No directional lines as with abrasive polishing ▪ Uniform lustre of shaped parts
Mechanical properties	▪ Reduced surface friction ▪ Retains grain structure and properties of bulk metal including fatigue strength ▪ Stress relieved metal surface
Corrosion resistance	▪ Increased corrosion resistance ▪ Increased surface ratio of chromium to iron in stainless steel
Ease of cleaning	▪ Substantially reduced contamination and adhesion due to surface micro-smoothness ▪ Surfaces are more easily and quickly cleaned ▪ Enhanced sterilisation of hygienically clean surfaces for food, drug, beverage and chemical processing equipment ▪ Best passivisation of stainless steel, brass and copper
Other important benefits	▪ Deburrs ▪ Sharpens edges depending upon rack position ▪ No hydrogen embrittlement ▪ Polishing of areas inaccessible by other methods ▪ Reduced annealing steps ▪ Large number of parts can be processed simultaneously

2.4 Disadvantages of electropolishing

Some limitations and disadvantages of electropolishing include (Metals Handbook, 1998):

- Most chemicals used in the preparation of electropolishing electrolytes are poisonous, flammable and in some cases potentially explosive. As a result only well- trained personnel with sufficient knowledge in the handling and use of these chemicals should be permitted to carry out the preparation and use of the electrolyte;
- The electrolyte and operating conditions for the electropolishing of different alloys may vary substantially and considerable time may be required to develop the procedure for a new alloy;
- Preferential attack may occur at the interface between two phases in multiphase alloys, resulting in uneven polishing;
- Depending on the number of different metals being polished by a single electropolisher, a large number of different electrolytes may be needed;
- Mounting materials constructed of plastic or metal may react with the electrolyte;
- The use of electropolishing for small specimens may be limited due to edge attack effects;
- The size of voids and inclusions may be exaggerated by the uneven attack on non-metallic particles and the adjacent metal.

2.5 Electropolishing equipment

Due to the similarities between an electroplating and an electropolishing operation, the equipment and layout are, not surprisingly, similar. An anodic work bar, which is connected to the positive terminal of direct current power supply, centres the work piece between two rows of cathodes, which are connected to the negative terminal of the power supply (Faust, 1976). An ammeter and voltmeter are connected in series and parallel respectively, while a current controlling device is generally used to maintain the current at the correct current density.

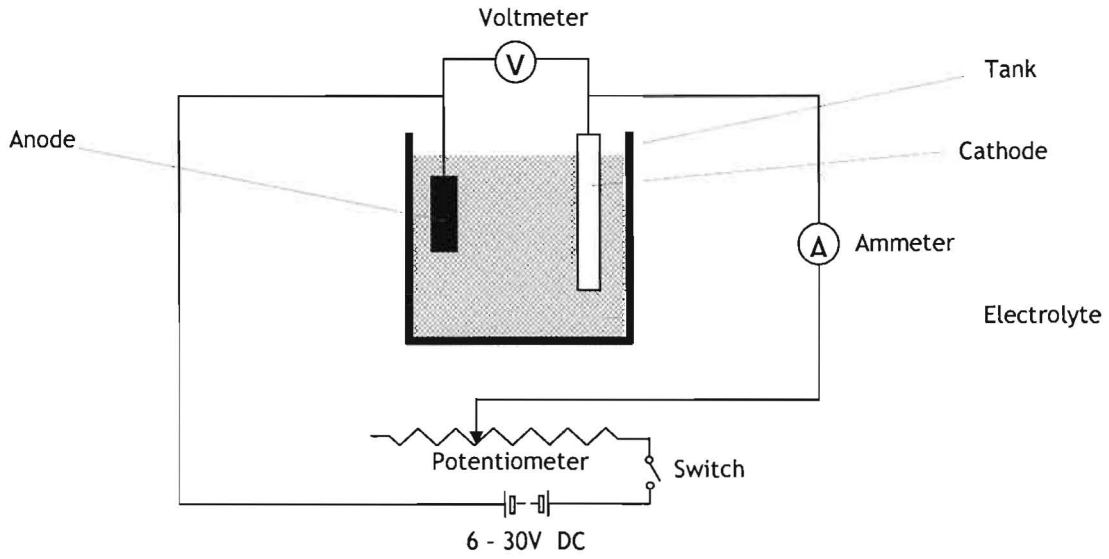

Figure 2.4: Circuit diagram of a typical electropolishing system

2.5.1 Racks

The pieces to be electropolished are placed on racks, which in turn are positioned on the work bar. Racks are usually constructed of copper and titanium with brass, stainless steel or titanium spring-loaded clips or fingers to hold the work piece. In order to ensure uniform current distribution through the work piece, when immersed between the cathodes, correct placement of the work piece on the rack is vital.

2.5.2 Cathodes

Suspended from the cathode bar, the cathodes are rods or flat strips usually made of lead, copper, stainless steel or carbon depending on the temperature and electropolishing operation. Their placement on the cathode bar determines how well the current is distributed.

2.5.3 Polishing baths/tanks

These tanks are usually made of stainless or mild steel and are either lead or plastic lined. However, the plastic lined tanks are limited to electropolishing operations where the temperature is considerably below the melting point of the plastic lining.

2.5.4 Direct current

A rectifier supplies the direct current used to drive the electropolishing process. The voltage rating depends on the size of the bath and the electrolyte being used. This usually ranges between 9 to 24 volts and is capable of supplying a current in the range of 150 to 500

amps/ft^2 (Faust, 1976). The direct current source is placed at a distance from the tank for emergency shutdown whilst a secondary control panel is placed at the tank.

2.5.5 Temperature control

Although electropolishing is an exothermic process and a significant amount of heat needs to be removed from the tank, heating is also required during start up when the tank contents need to be heated to the correct temperature for optimal polishing. Cooling/heating coils and electric immersion heaters are commonly used for this purpose. The heat transfer equipment is sometimes made cathodic to prevent chemical attack.

2.5.6 Agitation

Agitation of the work piece prevents gas streaks at apertures and extensions of the piece. Most often, the work bar with the racks holding the pieces is agitated from side to side. In some situations, an inert gas is sparged through a perforated pipe placed diagonally at the bottom of the tank.

2.5.7 Ventilation

Electropolishing baths using inorganic acids or alkalis as the electrolyte discharge hydrogen gas at the cathode and oxygen at the anode. This bubbling creates a froth at the electrolyte surface, which, together with the gases given off, may ignite if a spark is produced when the contact between the rack and the work bar is broken. To avoid this, exhaust ducts need to be installed to provide enough airflow to maintain a hydrogen to air ratio of less than 1 to 30 (Faust, 1976).

2.5.8 Cleaning and rinsing

Before electropolishing a work piece, any grease, oil or solid particles must be removed to obtain the best polishing. Whereas vapour degreasing and alkaline cleaning are commonly used for this pre-treatment step, the removal of residual surface contaminants is achieved using hydrochloric and nitric acid.

After electropolishing, the work piece is placed in a warm agitated rinse tank followed by a warm spray rinse and finally a hot rinse with demineralised water to prevent any water spots during drying. Dilute nitric acid is sometimes used in the post treatment of stainless steel.

2.6 Electropolishing process steps

The flow chart below shows a typical electropolishing process cycle (Faust, 1976):

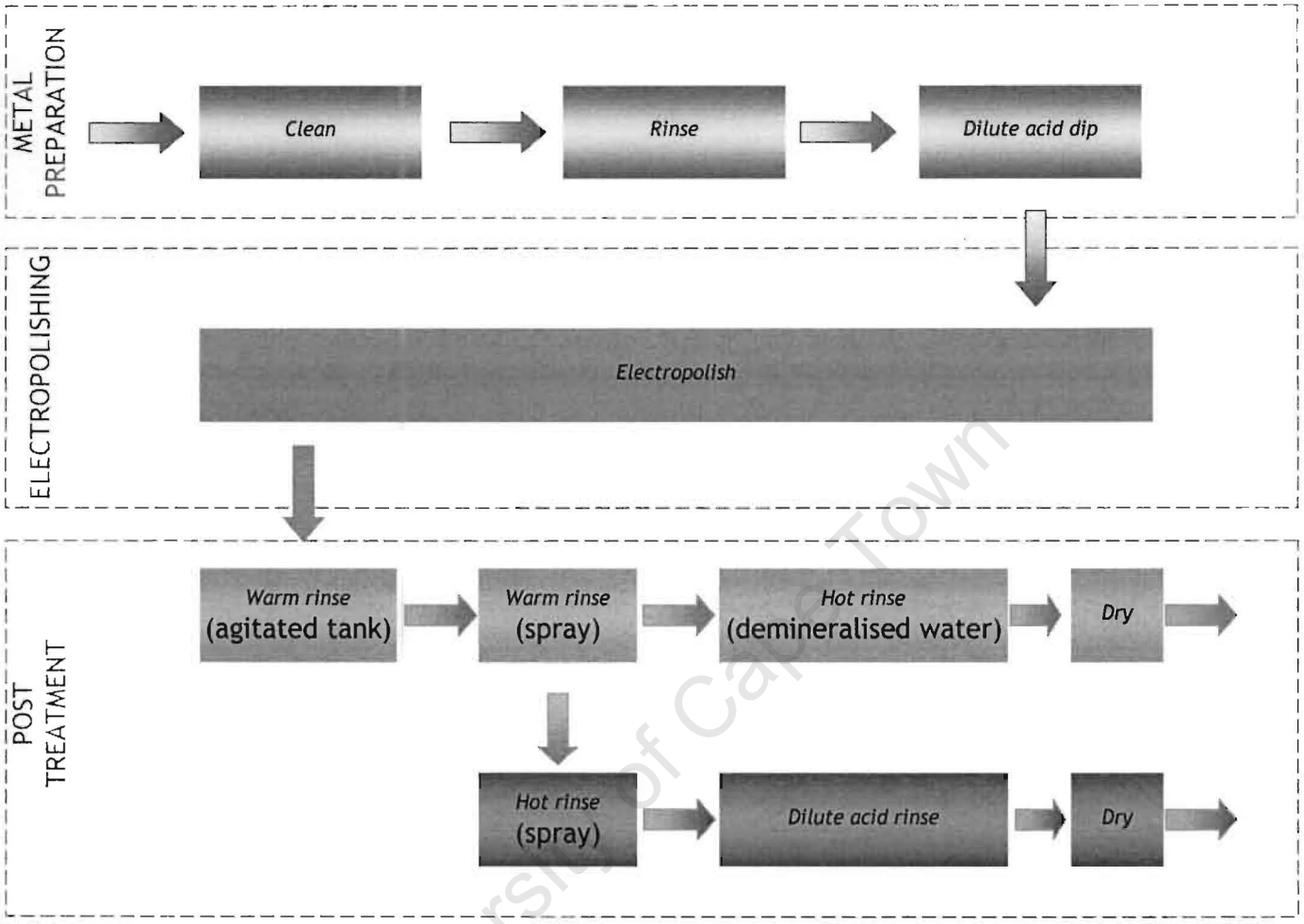

Figure 2.5: Flowchart of typical electropolishing process cycle

2.7 Properties of electropolishing electrolytes

The best electrolytes are those consisting of relatively large sized anions with a small ionic charge (Faust, 1976). Furthermore, the most successful electrolytes have the following characteristics (Metals Handbook, 1998):

- They must be fairly viscous;
- At electrolysis conditions, they must be good solvents for the metal being polished;
- They should contain large sized anions such as PO_4^{3-}, SO_4^{2-} or ClO_4^-. Additionally, large organic molecules improve electrolyte performance;
- Electrolytes should not attack the anodic work piece when there is no current flowing through the system;

- The electrolyte should be insensitive to temperature changes in addition to being able to function efficiently at room temperature;
- The electrolyte and the chemicals making up the electrolyte should be stable during mixing and use whilst being safe to handle. It should be noted that most electrolytes do not meet this particular criterion.

2.8 Metals that can be electropolished

Although most metals can be electropolished, only the metals with fine grain boundaries, free of non-metallic inclusions and seams, give satisfactory results. Stainless steels are the most commonly electropolished alloys whilst metals with high silicon, lead and sulphur content are the most problematic and therefore rarely, if at all, electropolished (Delstar Corporation, 1998).

Table 2.2 below lists the metals that are most commonly commercially electropolished:

Table 2.2: List of metals that can be electropolished (Delstar Corporation, 1998)

Low and high carbon steels	Titanium
Tool steels	Kovar
Aluminium	Inconel
Copper	Columbium
Brass	Leaded steel (low lead content)
Bronze	Beryllium
Nickel silver	Vanadium
Monel	Tantalum
Hastelloy	Silver
Beryllium copper	Gold
High temperature alloys Molybdenum, Nimonic, Waspaloy, Tungsten)	

2.9 Properties of 304 stainless steel

Stainless steel is an iron based metal containing various levels of chromium and very low carbon levels. The different compositions give each steel its unique strength and hardness as well as its specific corrosion and heat resistance.

Type 304 stainless steel is by far the most widely utilised, owing to its exceptional combination of corrosion resistance and machinability.

The chemical composition of 304 stainless steel is shown in Table 2.3 below:

Table 2.3: Chemical composition of 304 stainless steel

Element	Weight percent
Carbon	0.080
Manganese	2.000
Phosphorous	0.045
Sulphur	0.030
Chromium	18.000
Nickel	8.000
Iron	71.745
Nitrogen	0.100

2.10 Some commonly used electrolyte mixtures for electropolishing stainless steel

Table 2.4: List of commonly used electrolytes for electropolishing stainless steel

H_3PO_4 [wt %]	H_2SO_4 [wt %]	Other [wt %]	Current density [A/ft^2]	Temperature [°F]	Reference
41	45	Water-14	200-350	170-230	Faust, 1976
56		Chromic acid-12; water-32	100-1000	80-175	Faust, 1976
90		Glycerine - >50	>20	>200	Hensel, 2003
	15	Citric acid-55	>100	200	Hensel, 2003
63	15		50	80-175	Hensel, 2003
56	27	Diethyleneglycolmonobutylether-7			Hensel, 2003
40	13.5	Lactic acid-33	75-300	160-200	Hensel, 2003
	10-60	Chromic acid-12	150	175-212	Hensel, 2003

Chapter 3

Electropolishing theory

3.1 The fundamentals of metal dissolution/corrosion

When a metal is placed in contact with an electrolyte, be it an acid or an alkali, by giving up an electron to the metal surface, an atom leaves the metal lattice and enters the liquid phase as an ion. Simultaneously, a reduction reaction takes place on the metal surface, which accepts this electron. This dissolution process continues until the metal is entirely consumed provided that the system shifts towards thermodynamic stability (Hoare *et al.*, 1981).

On account of the surface asperities on the metal surface, the oxidation reaction or metal dissolution takes place at the peaks whilst the reduction reaction takes place at the valleys, which are protected by a film created by the accumulation of electrons at the metal surface. The reduction reaction usually involves the evolution of hydrogen gas from H^+ ions or the formation of H_2O or OH^- from O_2. During this oxidation-reduction reaction within the metal, the current is carried electronically by the migration of electrons from the active sites (peaks) to the protected sites (valleys), whereas between the two sites, the current is carried electrolytically by the migration of metal ions within the electrolyte (Hoare *et al.*, 1981).

By providing an external driving force for the reaction, the corrosion/dissolution rate of the metal can be increased. The external driving force potential is generally in the form of a direct current (DC) supplied by a rectifier. The corroding metal is made anodic with respect to the counter electrode. By manipulating the applied potential, the rate of dissolution can be increased or decreased. This externally manipulated, accelerated oxidation-reduction reaction forms the foundation of the anodic dissolution process employed in electropolishing and electro-chemical machining processes.

In most cases, it is impossible to continually increase the rate of metal removal by increasing the potential. This is due to the fact that at a critical anodic potential, most metals become passive in any given electrolyte as depicted in Figure 3.1, which shows the potentiostatic curve for an anode in an electrolyte (Hoare *et al.*, 1981).

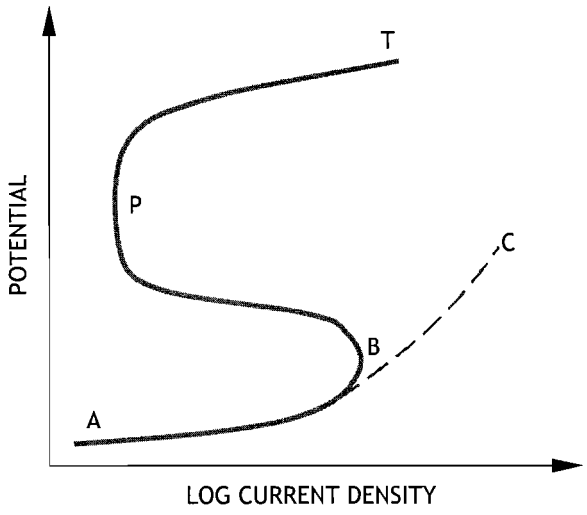

Figure 3.1: Sketch of an idealised, steady state, potentiostatic polarisation curve obtained on a given anode in a given electrolyte.

Below the threshold potential at point A, the rate of corrosion is zero. This is the region of cathodic protection. In the absence of a passive film, as the current increases, the rate of corrosion also increases along the curve towards point C. However, at the initiation of passive film formation (point B), the current starts to fall off as the film increasingly blocks off the active sites. When the surface is completely covered by the protective film (point P), the current is at its lowest and signifies the passive region. With a further increase in the potential, the protective layer begins to disintegrate (point T), exposing the surface layer once again for further attack. At this point additional electrochemical processes such as the evolution of O_2 start to take effect.

It follows that, the current density as well as the components making up the electrolyte play a pivotal role in the formation and breakdown of the anodic film and consequently the superiority of one electropolishing operation over another. Clearly, for good electropolishing, the applied current density should be at or above the limiting current density so as to produce and maintain a sufficiently thick anodic film on the metal surface so as to protect the valleys on the surface whilst allowing dissolution of the peaks.

3.2 Anodic levelling & anodic brightening

In general, electropolishing can be divided into two processes:

1. Anodic levelling/macro-smoothing, which results in the removal of surface roughness of heights greater than 1μm (Landolt, 1986).
2. Anodic brightening/micro-smoothing, which results in the removal of surface roughness of heights that are comparable to the wavelength of light (less than 1μm) and consequently result in surface brightening.

Although the levelling and brightening processes usually occur simultaneously, it is possible for a surface to undergo levelling without brightening and vice versa. Anodic levelling is driven by the concentration of current lines at the peaks of the surface asperities, resulting in a higher dissolution rate and levelling of the peaks. Anodic brightening depends on whether or not the surface is crystallographically etched. Consequently, anodic levelling is commonly treated as a current distribution problem whereby the surface is assumed to be homogeneous from a kinetic perspective. Conversely, anodic brightening which involves the removal of atoms from the metal lattice is treated as a surface kinetics and passivation behaviour problem (Landolt, 1986).

3.3 *The electropolishing current density - voltage relationship*

Figure 3.2 below shows a typical current density verses voltage curve for an electropolishing process:

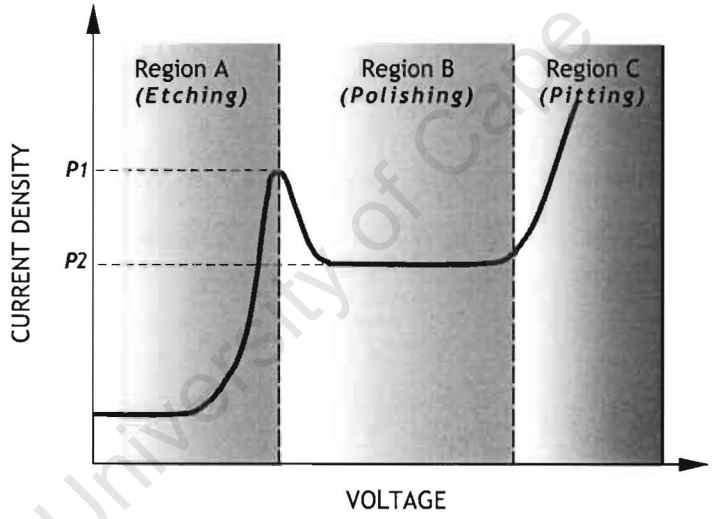

Figure 3.2: Typical current density-voltage relationship for an electropolishing process

At the lower voltages (Region A), the system is initially inert. However, with a slight increase in the voltage, the current rises sharply to a maximum point (P1) at which time the metal surface is etched. With a further increase in the voltage (Region B), the current falls off and stabilises at a steady value (P2). In this region, further increases in the voltage have no effect on the current density, which remains, at a level of P2. This is the region in which the thick anodic film forms on the metal surface, electropolishing it. At higher voltages (Region C), the current rises sharply due to the evolution of gas bubbles that consume more current. The evolution of gas bubbles at these high voltages causes a breakdown of the anodic film, exposing the surface depressions to attack, consequently pitting the surface (Hoare *et al.*, 1998).

Experimentally, predominantly salt solutions exhibit a well-defined limiting current region, unlike concentrated acid solutions (the exception being the copper - phosphoric acid system).

3.4 Faradays Laws

The relationship between the quantity of electricity flowing and the amount of material liberated, which was established by Faraday, led to the formulation of two laws (Twidwell *et al.*, 1992):

1. The amount of electrochemical decomposition produced at an electrode is proportional to the quantity of electricity (coulombs) passing through the circuit.
2. The amounts of different substances produced by the same quantity of electricity will be proportional to their equivalent weights.

Consequently, one equivalent of any substance will be liberated by oxidation, by a Faraday, F, which is equal to 96 500 coulombs.

$$W = \frac{EIt}{96500} \qquad \text{(Equation 1)}$$

where

w = weight		[grams]
E = equivalent weight		[atomic weight/valence]
I = current		[Amps]
t = time		[seconds]

3.5 Mass transport issues related to electropolishing

This section summarises the different mechanisms that have been proposed in terms of describing the electropolishing system.

Founded on studies carried out on the copper-phosphoric acid electropolishing system, Jaquet cited in Hoare (1981), came to following conclusions:

- As electropolishing takes place in the limiting current region, the metal surface is covered with a salt layer of thickness greater than the surface roughness of the metal;
- Accordingly, as shown in Figure 2.3, the distance B between a peak and the salt film-bulk solution boundary is shorter with a smaller voltage drop along this path when compared to the distance A between a valley and the salt film-bulk solution boundary. Hence, the rate of metal dissolution is faster at the peaks than in the valleys, levelling the surface.

This mechanism was further extended by Elmore (Hoare *et al.*, 1981), who proposed that as the metal dissolves, building up the salt film on the anode surface, the rate of metal dissolution becomes limited by the diffusion of metal ions from the salt film to the bulk of the solution. This then sets up the limiting current. Furthermore, the rate of dissolution will be greater at the peaks than at the valleys due to a shorter diffusion path B as compared to that of A as shown in Figure 2.3.

Assuming that diffusion is the predominant mode of metal ion removal from the metal surface, the current density (j) is proportional to the concentration gradient $\partial C/\partial x$. For an anode of area A, located at x = 0; the current density is:

$$j = \frac{I}{A} = FD\left(\frac{\partial C}{\partial x}\right)_{x=0} \qquad \text{(Equation 2)}$$

where I = current [A]
F = Faraday constant [coul.cm^{-2}.s^{-1}]
D = diffusion coefficient of metal ions [cm^2.s^{-1}]
A = area [cm^2]

When the current has passed for a critical time period (t_0) and the concentration of metals at x=0 has reached the solubility limit (C_m), the salt film is formed. For time greater than t_0, the current is limited by the concentration gradient in accordance with equation 2. Analysing the growth of the diffusion layer by solving the diffusion equation yields (Hoare *et al.*, 1981):

$$D\left(\frac{\partial^2 C}{\partial x^2}\right) = \frac{\partial C}{\partial t} \qquad \text{(Equation 3)}$$

Elmore found that for a given acid concentration, the product of j and t_0 was a constant value. This value varies with acid concentration, because C_m is a function of acid concentration (Elmore, 1939; 1940). Elmore's findings confirmed that the electropolishing process in the limiting current region proceeds by a diffusion controlled mechanism.

Edwards (1953), whose findings were based on viscosity studies relating to the copper - phosphoric acid electropolishing system, proposed that electropolishing occurred via the acceptor mechanism. He concluded that the polishing process was independent of reaching a critical Cu^{2+} ion concentration at the anode surface but rather that the limiting step was the diffusion of the acceptor species (PO_4^{3-}) through the salt film to the Cu^{2+} ions at the anode.

Employing the acceptor mechanism, Wagner (1954) derived an expression accounting for the observation made with the copper-phosphoric acid system. Wagner considered a sine wave surface profile as shown in Figure 3.3:

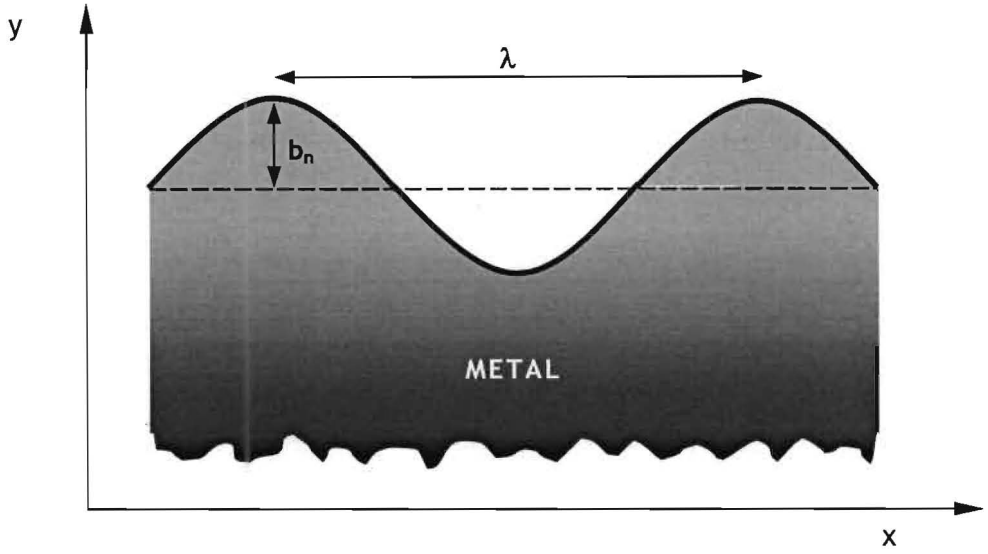

Figure 3.3: Sine-wave profile of anode surface

Wagner's solution predicts an exponential decay of profile amplitude with dissolution time (Landolt, 1986). Furthermore, as ▫ decreases, b_n also decreases, indicating that the amplitude of shorter sine waves decrease faster than that of longer waves, effecting surface levelling.

Lastly, electropolishing of iron in concentrated phosphoric and sulphuric acid was found to be controlled by the transport of dissolved Fe^{3+} ions from the anode surface, through the salt layer and into the bulk electrolyte (Datta *et al.*, 1992).

3.6 The anodic brightening mechanism

This section examines the proposed mechanism for attaining the morphological difference between a crystallographically etched and brightened surface as well as the electrochemical conditions resulting in these two different surface finishes.

By investigating the voltage-current density curves for metals polished in various acid electrolytes, Hoar (Hoare *et al.*, 1981) noticed their similarity to an anodic polarisation curve, such as the one shown in Figure 3.1. He proposed that at the initial peak of an electropolishing curve, a compact oxide film is formed at the metal surface. Accordingly, a metal ion can only leave the anode surface through a pore in this oxide film and the random distribution of pores indicates that there is random dissolution at the metal surface. Consequently, brightening of the metal surface is achieved as opposed to the etch patterns that are normally generated as a result of the preferential attack on certain crystal faces.

Therefore, whereas surface levelling is controlled by the diffusion of metal ions from the metal surface through the salt film to the bulk solution, brightening is accomplished by indiscriminate metal dissolution through the randomly distributed pores of the thin oxide film which lies below the salt film on the anode surface.

Chapter 4

Development of techniques & instrumentation for measuring polishing quality

At the outset of this project, it was established that being able to quantify the level of polishing would add significantly more value in terms of determining whether or not any particular electrolyte composition or operating parameter resulted in better polishing at a faster rate. Using the rate of mass loss only as an indicator for the rate of polishing is limited in this respect as a higher mass loss, although indicative of a faster dissolution rate, does not necessarily imply a good surface finish. A successful method would need to be able to distinguish differences in surface roughness in situations where the human eye was unable.

The American Society of Mechanical Engineers (ASME) (1996), defines total ruggedness or roughness profile of a surface as consisting of two components; a waviness profile component and a roughness profile component, as shown in Figure 4.1:

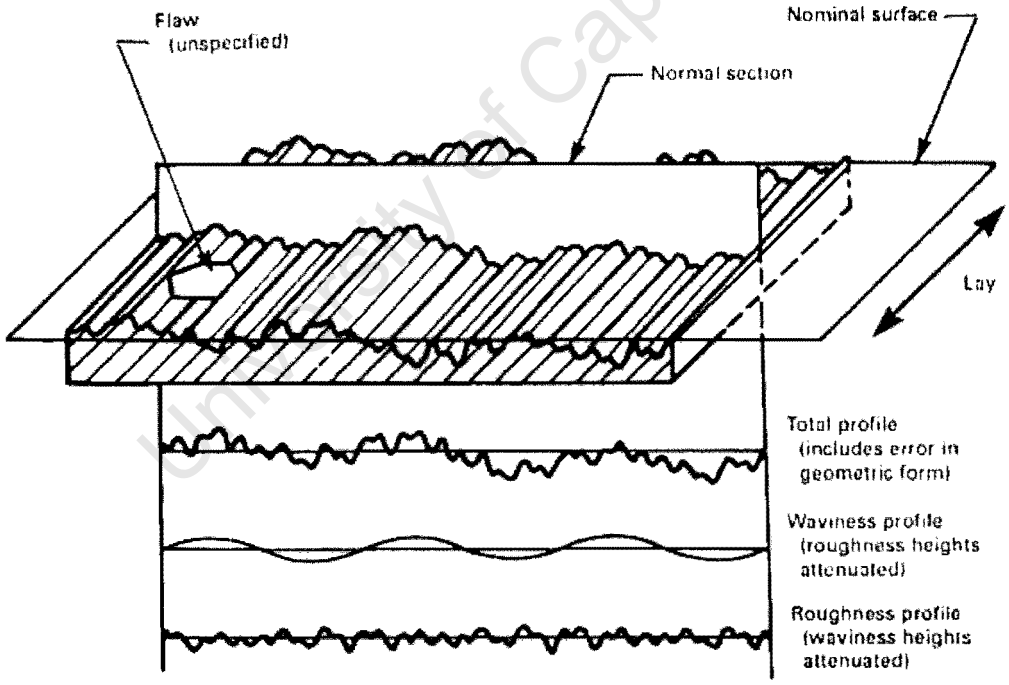

Figure 4.1: Schematic representation of surface roughness and waviness (ASME, 1996)

The roughness component describes the finer irregularities typically in the sub-micron range on the surface, whose characteristics are usually as a result of the production process. The waviness component describes the more widely spaced component of the total profile. Hence, the roughness component can be viewed as superimposed on the waviness profile of the surface (ASME, 1996).

The methodology used in the characterisation of surface roughness can be divided into contact and non-contact processes. For this project, the modification of one contact method and the development of two non-contact methods were undertaken. Based on the order in which they were investigated, these included:

1. Design and construction of an instrument capable of measuring the light scattering characteristics of the polished surface as an indicator of surface roughness (non-contact method).
2. Surface roughness measurements based on a surface-tracing stylus, with a modification to improve the accuracy of the measurement (contact method).
3. Development of a machine vision/image processing technique to measure surface roughness from a digitally acquired image using a Nomarski microscope (non-contact method).

Of the three methods investigated, (2) the surface tracing stylus and (3) digital image processing techniques were successful, whilst (1) development of the instrument to measure the diffraction of a beam focussed on a polished surface was discontinued due to technical limitations and time constraints. The fundamental aspects, as well as the operating procedures for these three methods, are presented in the following sections of this chapter.

4.1 Measuring the surface roughness based on light scattering

4.1.1 Operating principles

The development of this non-contact technique for quantifying the metal surface roughness was based on the principle that surfaces with different roughness scatter collimated light to different extents (Younis, 1998). The microscopic waveform of the surface profile modulates the incident light beams into scattered beams of varying intensities. Thus, the difference in intensity of the scattered beam over a range of angles between two metal surfaces being compared, is indicative of their relative surface roughnesses.

4.1.2 Development and operation of equipment

A schematic diagram of the set up constructed for this purpose is shown in Figure 4.2:

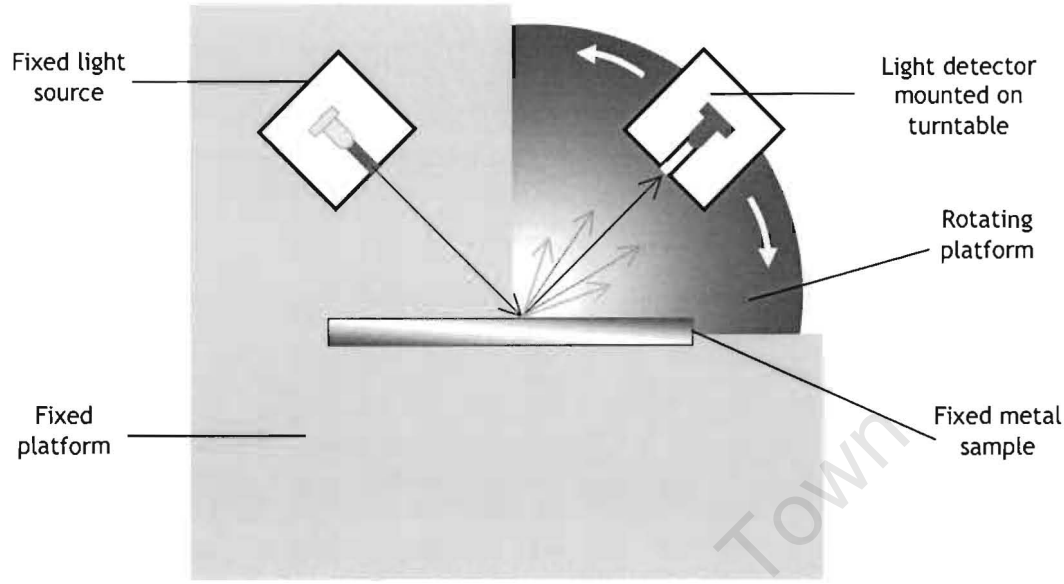

Figure 4.2: Top view schematic diagram of set up used to measure surface roughness based on extent of light scattering

This apparatus worked by focussing a columnar light beam onto the metal surface and measuring the intensity of the scattered light at angles up to 45° on either side of 90° to the light source. As a rougher surface would scatter the light beam more extensively than a smoother surface, a plot of the intensity of the reflected light verses the angle would exhibit a relatively low reflected light intensity over a wide range of angles. In contrast, a smooth surface would show a higher reflected light intensity at a much narrower range of angles. Consequently, this difference in responses could be used to quantify the relative roughness between surfaces.

The light source in the form of a light emitting diode (LED) was mounted in a precision machined PVC block of dimensions 20mm x 20mm x 20mm, with a 0.5mm opening on one face. This opening served to channel a nearly columnar light beam on to the metal surface. The light detector used was a phototransistor mounted in an identical block to the LED. The electrical circuit used to drive the LED and phototransistor was developed based on the circuitry for a similar light-measuring device. The amplified signal from the photo detector was then relayed to a data capturing PC, which also controlled the movement of the light detector.

The stepped angular movement of the light detector was achieved by mounting it on the turntable of an old floppy disk drive and connecting it to a stepper motor by means of lever arm as shown in Figure 4.3 below:

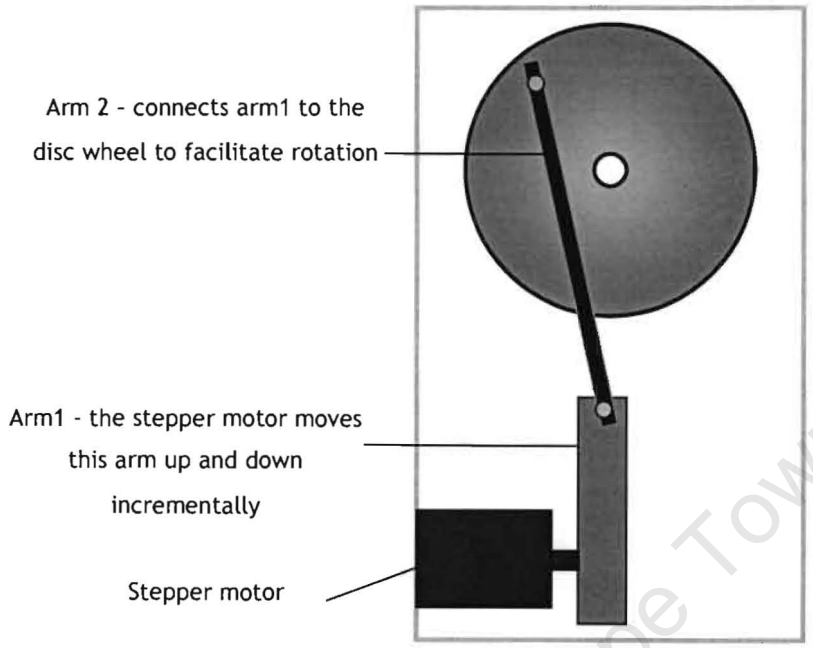

Figure 4.3: Bottom view of modified floppy disk drive used to rotate light detector

4.1.3 Findings

On testing this device, it was found that although the electrical and mechanical components worked as they were designed to, the phototransistor was too sensitive. Consequently, it acted a switch, with readings amounting to little else but logic hi/lo signals. Due to time constraints associated with obtaining a less sensitive phototransistor, further work on this particular project was discontinued in favour of the contact based stylus method.

4.2 Stylus based surface roughness measurement

Surface profile and roughness determination using a stylus was achieved by direct mechanical contact with the work piece. Figure 4.4 shows a diagram of a basic stylus instrument.

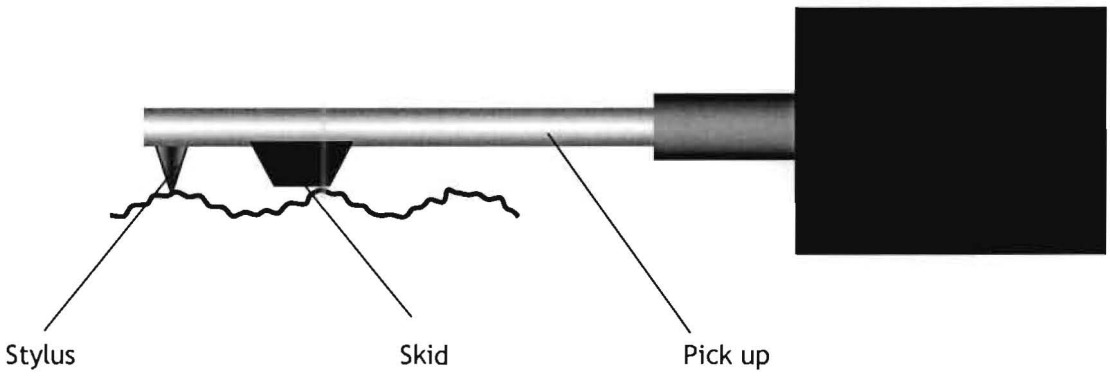

Figure 4.4: Diagram showing the principle components of a stylus instrument

The unit consisted of a transducer, an amplifier, a traverse unit and a metering or chart recording system. The pick-up was supported on the work piece by the skid. As the stylus was dragged across the surface, it traced the surface profile with changes in amplitude or height causing a variation in the mutual inductance within the transducer. This change in mutual inductance changed the phase of a high frequency carrier signal, which was amplified and demodulated to represent the surface profile. The final signal was then either logged and evaluated by a data-capturing device or recorded by a chart recorder.

The most common measurement unit used to describe the roughness of a surface is R_a. R_a is the average value of the departures from its centre line, for a given sampling length as shown in Figure 4.5 below:

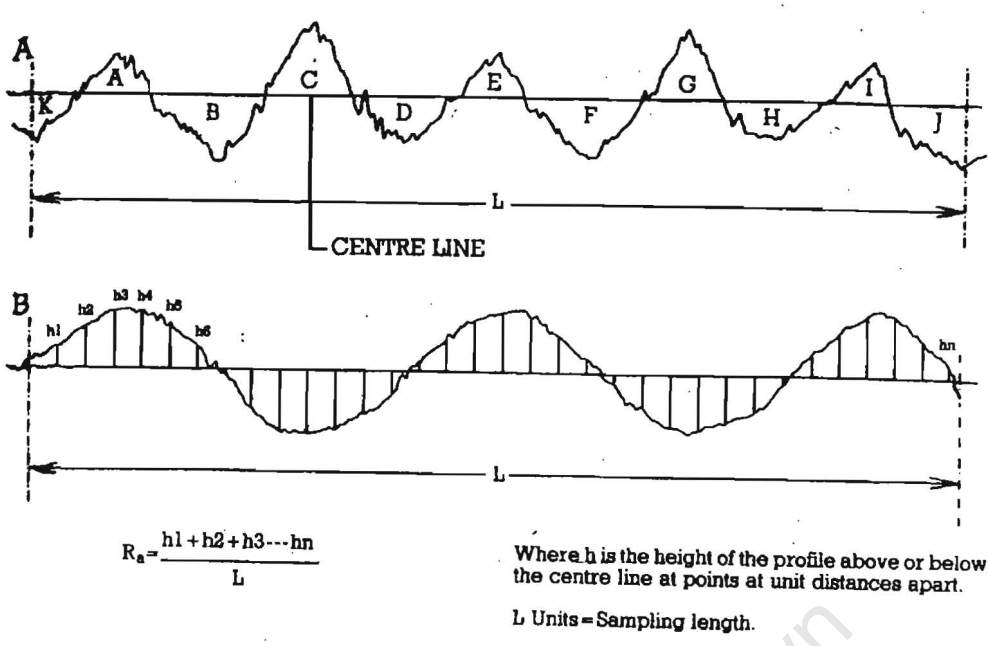

Figure 4.5: Derivation of R_a (Taylor-Hobson, 1995)

4.2.1 Taking a surface roughness measurement

These measurements were taken using a Taylor Hobson Surtronic 3P stylus. For each reading taken, the metal specimen was placed in a vice with the surface to be measured facing upward. The stylus tip was then carefully placed on the metal surface by holding the pick up. A traverse length of 13mm was specified on the units' selection panel and the measurement initiation switch engaged after which the corresponding R_a value was displayed on the unit's display panel. This reading was recorded and the procedure repeated for two more readings at different locations on the surface. The average of the three readings was used as the final surface roughness measurement.

4.2.2 Problems encountered with the stylus based measurement and the solutions formulated

Initial surface roughness measurements showed considerable variation between the three readings (see Table 4.1). This could be attributed to a number of inherent limitations and disadvantages associated with using a stylus-based measurement.

Firstly, surface waviness significantly affects the measurement value whereby a variation in the overall flatness of the surface causes a deviation between the initial and final position of the centreline. As a result, the measured deviations between the actual surface profile and the centreline are somewhat distorted compared to readings taken on a totally flat surface. The difficulty in positioning the sample absolutely flat in the vice, within a tolerance range of the surface roughness, parallel to the stylus further compounded this problem. Furthermore,

as described in Chapter 2, the rate of electropolishing is faster at elevated locations and edges on the surface. Hence, as a result of more rapid dissolution at these edges, the polished surface curved towards the edges, exacerbating the problem.

Secondly, isolated extremities on the surface in the form of tiny scratches or inclusions have a significant impact on the final R_a value. As these surface irregularities would not be representative of the entire surface, the measured value leads to inaccuracies in the overall representation of the surface roughness.

In an attempt to overcome these shortfalls, the stylus-based measurement was modified as follows:

- The variations in the signal from the transducer representing the surface topography were amplified and logged to a PC by converting the signal to a number ranging between 0 and 255.
- This data was plotted to obtain a graphical representation of the surface profile for that particular measurement as shown in Figure 4.6, which was obtained for an arbitrarily chosen polished sample, labelled sample A3. Sample A3 will be used throughout this chapter to illustrate aspects of the various measurement techniques as well as in comparing the relative accuracy of the different techniques in describing the surface roughness.

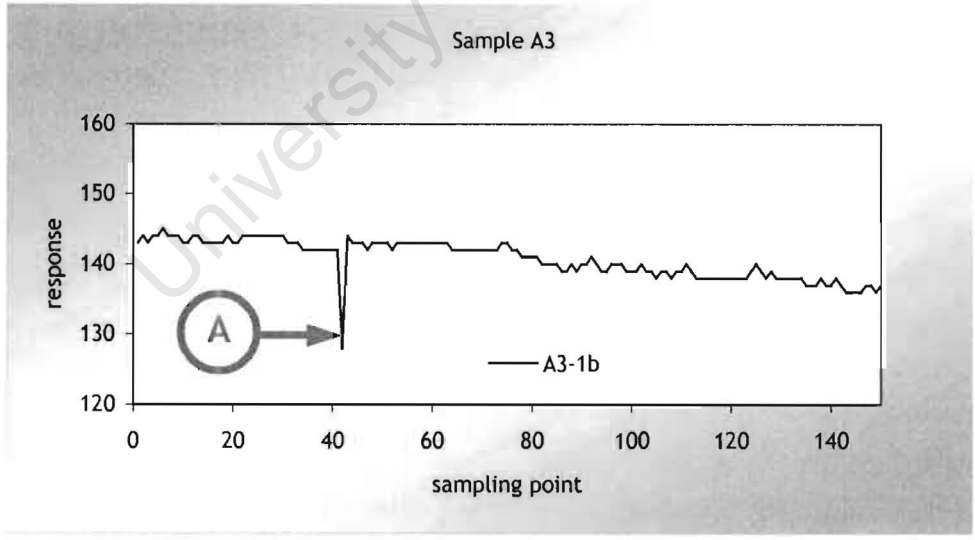

Figure 4.6: 2-dimensional surface profile of sample A3

With a two-dimensional visual representation of the surface profile based on the data from each trace, any inconsistent variations in the form of scratches and inclusions could be identified and excluded from the analysis. Thus, the data representing features such as that labelled A in Figure 4.6, which clearly would not be caused as a result of the experimental

conditions, could be removed from the analysis, giving a modified two-dimensional surface profile shown in Figure 4.7:

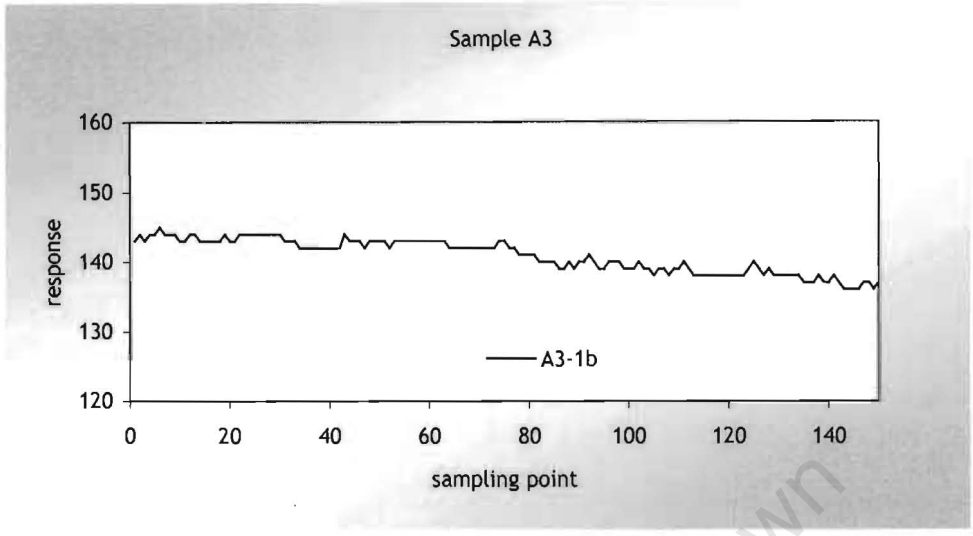

Figure 4.7: Sample A3 modified 2-dimensional surface profile

Having dealt with the effect of inconsistent surface variations in the surface roughness measurement, the next step was account for the waviness or overall flatness of the surface. This phenomenon can be clearly seen in Figures 4.6 and 4.7, where the surface profile slopes downward as the number of sampling points increases. With the quality of the surface polish being measured as a function of its micro roughness rather than its macro roughness, the waviness of the surface was negated by fitting a third order polynomial equation to the data for each measurement and measuring the variation of the actual data points from the fitted equation. In other words, the fitted equation represented a perfectly smooth surface with an identical macro roughness (waviness) to the actual surface profile as shown in Figure 4.8, allowing the micro roughness relative to a perfect finish to be determined.

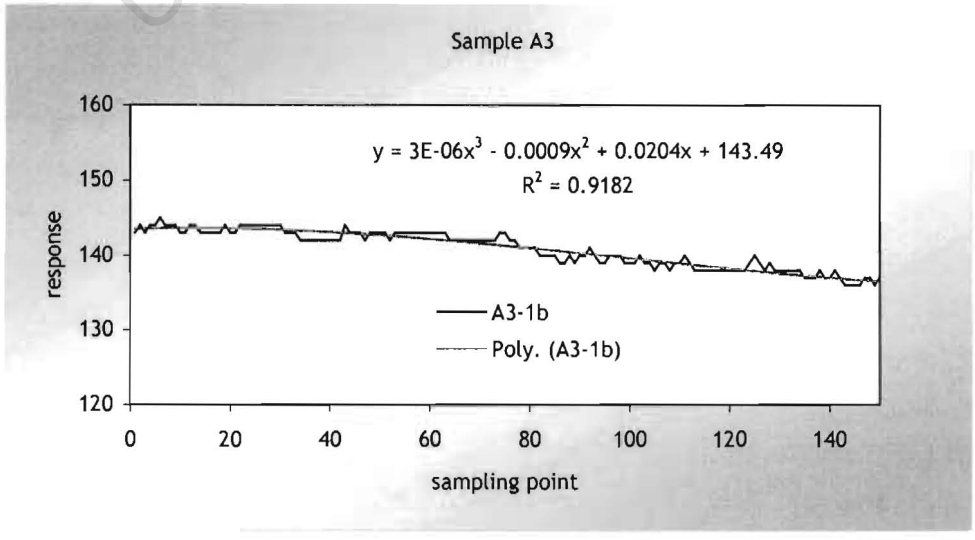

Figure 4.8: Sample A3 modified 2-dimensional surface profile with fitted polynomial

The mathematical function based on the R-squared value and the variance, derived and validated by a statistician, to measure the variation in the actual surface profile (measured data) to that of the perfectly smooth surface (fitted equation) is shown below:

$$\text{Stylus Roughness Index (SRI)} = \sqrt{(1 - R^2) * \text{var iance}} \qquad \text{(Equation 4.1)}$$

In essence, the SRI measured:

- The standard deviation of the deviations from the fitted polynomial. This could be obtained indirectly from $(1\text{-}R^2)$, which is equal to the sum of squares of the deviations divided by the sum of squares of the response variable.
- The variance of the response variable, which is equal to the sum of squares of the response variable divided by total number of measurements minus one.

Thus the square root of the product of these two produced Equation 4.1.

When taking a surface roughness reading, each surface underwent three traces using the stylus and the average of the three SRI values was reported as the final surface roughness measurement.

4.2.3 Comparison of surface roughness measurements based on the conventional stylus measurement and SRI measurement

The measurements and percentage variances for surface roughness measurements obtained using the conventional stylus measurement (derived from the average of the three R_a values read off the stylus) and the modified SRI measurement technique are shown in Table 4.1:

Table 4.1: Comparison of surface roughness measurements obtained for sample A3

	Conventional stylus measurement [μm]	SRI measurement [-]
Trace 1	0.58	0.761
Trace 2	0.75	0.711
Trace 3	0.29	0.961
Average roughness	0.54	0.811
% Variance	13%	2.2%

From Table 4.1, it is clear from the percentage variance in the three measurements for each of the techniques that the SRI measurement provides a significantly more consistent

measurement in terms of the surface roughness. Consequently, the SRI measurement technique was used for the most part of this research to measure surface roughness until the superior image processing technique described in section 4.3 was developed.

The major disadvantage of the SRI measurement was that despite having reduced the inaccuracies as a result of isolated inconsistencies on the surface as well as the surface waviness, it still only provided a two-dimensional representation of the surface topography. The three individual profiles obtained at different locations on the work piece lacked a comprehensive representation of the surface. Moreover, the measurement process and data analysis was extremely costly in terms of time, which lead to the continued exploration into devising a more efficient method.

4.3 Digital image processing based roughness measurement

As expressed in the previous section, both forms of the stylus-based measurements were limited to providing a two-dimensional profile of three isolated traces on the surface, which was not entirely representative of the surface. The development of a non-contact surface roughness measurement based on digital image processing of a microscopic image of the metal surface provided a measurement based on areas on the surface rather than just profiles. This fundamentally provided a significantly better three-dimensional representation of the surface topography and consequent characterisation of the surface roughness.

4.3.1 Some basics about digital image processing

The human eye is capable of distinguishing less than one hundred shades of grey whilst black and white film is typically capable of reproducing in the region of fifty shades of grey. Digital image systems on the other hand, are capable of acquiring imagery representing several thousand shades of grey, consequently enabling a single digital image to present a vast amount of information in a compact, easily interpretable form (Green, 1998).

The three main elements of an image processing system are:

1. Image acquisition
2. Image processing
3. Image display

Image Acquisition

This involves translation of the picture to a digital representation that can be processed by a digital computer. A digital image can be viewed as a matrix of numbers, with each point within the digital representation corresponding to an area in object space. Each point in the digital image is called a picture element or pixel, with the digital value assigned to it representative of the intensity of that area in object space. A simple example of a digital image is shown in Figure 4.9:

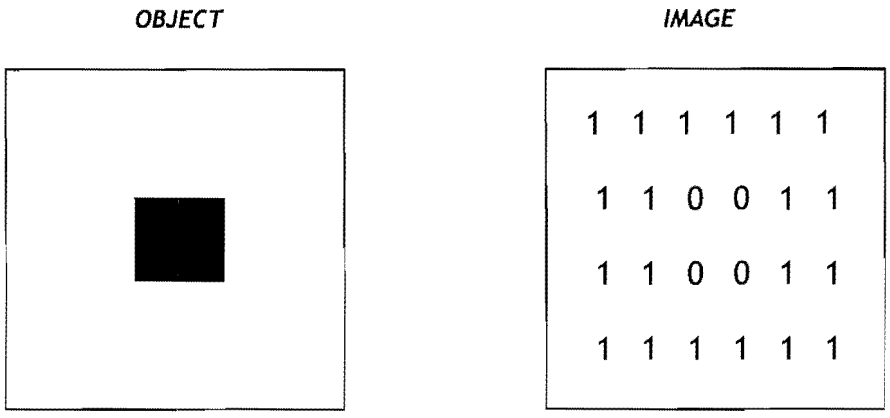

Figure 4.9: Digital image example (Green, 1998)

In the example above, a single bit is used to represent the intensity at each sampled position, with the black square intensity represented by the value 0 and the white background intensity represented by the value 1. Clearly, a higher sampling frequency would result in more matrix elements representing the square thus providing sharper definition and a more accurate digital representation of the image. The different levels of grey scale or colour are obtained by increasing the range of digital intensity values assigned to each pixel, within a range of 0 to 255, with 0 representing black and 255 representing white.

Image processing

This phase involves digital processing of the acquired image in order to produce the desired result, be it a measurement of a certain aspect of the image or an enhancement in the quality of the image.

A large number of mathematical algorithms have been developed to extract specific information from the digital images. For this research, those required for obtaining information with regards to the Fast Fourier Transform (FFT) based high, medium and low frequencies, the variance, mean absolute difference, skewness, inter quartile range and kurtosis of the metal surface microscopic image were used. In addition, flat fielding algorithms were employed to overcome similar problems associated with regards to the surface waviness that were encountered using the stylus-based measurement.

Image display

This component of the image processing system is associated with the generation of an output product that can be seen by an observer or an instrument, which uses the information to perform a subsequent task.

The following section describes the specific characteristics of these three principle elements of an image processing system, used in this project to obtain a measurement for the surface roughness.

4.3.2 Digital image acquisition of the metal surface topography

The input to this digital image processing method, developed to measure the surface roughness, was the acquisition of a microscopic digital image of the metal surface viewed through a Nomarski differential interference contrast (DIC) microscope. Each polished sample was rinsed with methanol and dried prior to being analysed for its surface topography using a Leica MeF4 Nomarski microscope.

Figure 4.10 shows a schematic diagram of the optical layout of a Normarski microscope (Wyant, 2003).

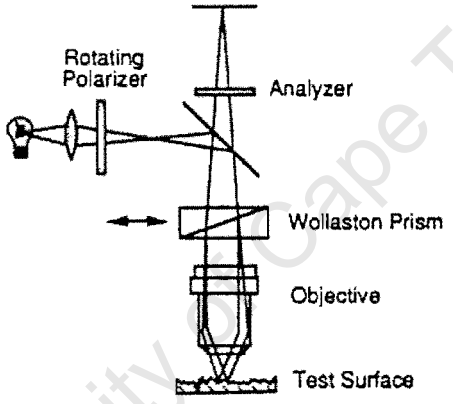

Figure 4.10: Schematic diagram of Nomarski microscope (Wyant, 2003)

A polariser placed subsequent to the white light source sets the angle of the polarised light incident upon a Wollaston prism. The prism splits the light into two beams, having orthogonal polarisation, sheared with respect to each other. The prism then recombines the beams after reflection off the surface being tested. An analyser placed after the Wollaston prism transmits like components of the two beams, generating an interference pattern, which results in an image showing the difference between two closely spaced points on the test surface. Consequently, the image displays slope changes, producing the effect of the surface being illuminated from one side thus clearly revealing the surface topography (Wyant, 2003).

A five times magnification was used for all the analyses during this project. The image of the surface topography was then captured in digital form using a digital camera and stored in a compact JPEG form. Figure 4.11 shows a digital image of sample A3's surface topography.

Figure 4.11: Digital image of sample A3 viewed under a Nomarski microscope (X5 magnification)

Whereas each data point in the stylus measurement technique represents the relative height of the surface at that point, in the digital image, the data points or pixels with their corresponding intensity values are representative of the level of greyscale at that particular position on the image. Consequently, with elevated points on the surface exhibiting a lighter greyscale than lower points, the level of greyscale can be directly related to the height of the surface at each point, allowing a three-dimensional representation of the surface topography to be analysed.

4.3.3 Image processing

This phase of the analysis involved extracting information from the digital image that could be used to quantify the surface roughness. The digital image was processed in MATLAB® version 6.1 using its image processing toolbox for which an algorithm was developed and coded into the software. The programming code written for this task can be found in Appendix 4. The first step was to convert the colour digital image into one of greyscale.

Analogous to the problems encountered using the stylus measurement with curving of the surface as result of more rapid dissolution at the edges or in not being able to place the sample absolutely flat for analysis; the digital image often displayed dark patches at the edges of the image. This phenomenon is clearly visible on the top right hand corner of Figure 4.11. To correct this, a flat fielding algorithm, which divides all the images by a flat field that has been normalised to unity was used. Thus the dark patches at the edges were removed without losing any vital information with regards to the surface roughness. Figure 4.12 shows an image of sample A3 before and after flat fielding.

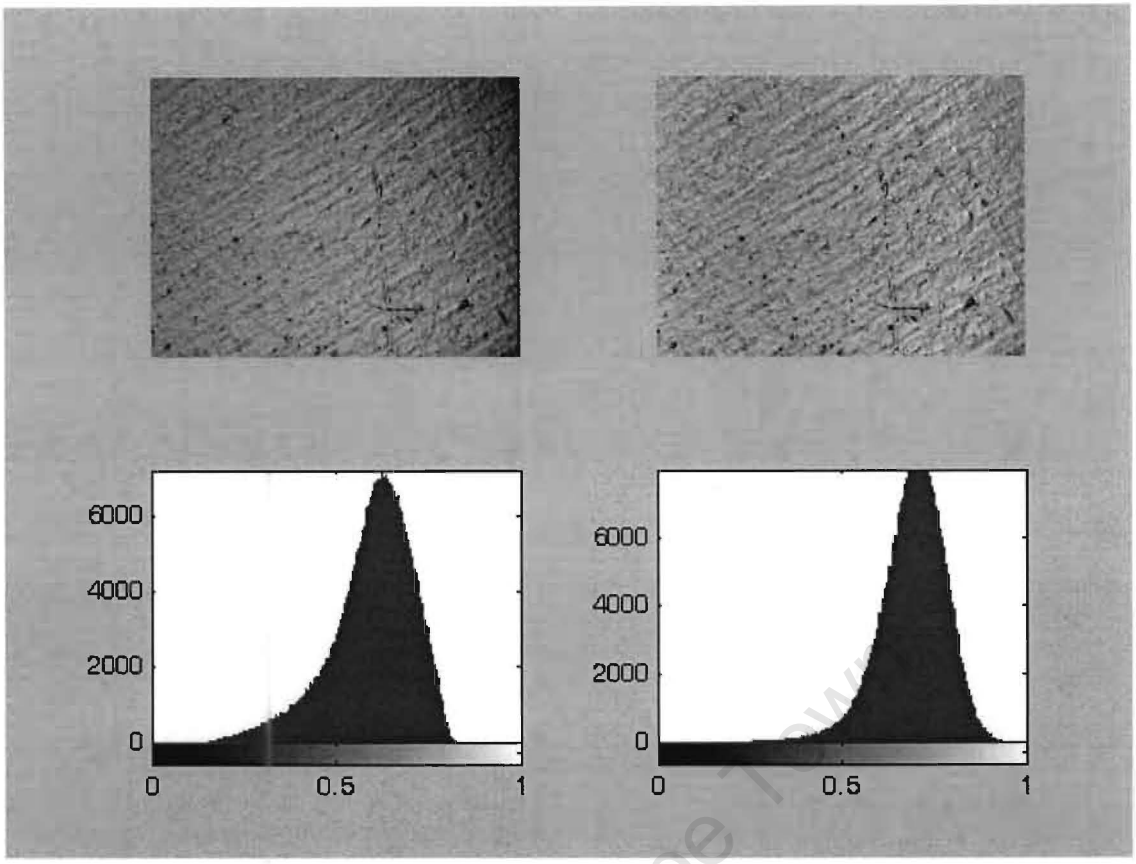

Figure 4.12: Images of sample A3 before and after flat fielding

Having corrected the image for the curved edges of the analysed sample, the next step was to establish which parameters of the image provided useful information with respect to describing the surface roughness. The imaging software analysed each surface's digital image by segmenting it into 760 horizontal and 580 vertical sectors, providing vastly more information compared to the SRI technique. Parameters surveyed included the Fast Fourier Transform (FFT) based high, medium and low frequencies, variance, mean absolute difference, skewness, inter quartile range and kurtosis of the metal surfaces microscopic digital image. This data was then exported to Microsoft Excel for further analysis.

By establishing the relative variations in these parameters with variations in the images of the surface topography, the most influential parameters were determined. In developing this relationship, data from fifty-two polished metal specimens from the electrolyte optimisation experiments, described in Chapter 7, was used.

The most influential parameters in describing the variation in surface topography were found to be the variance, mean absolute difference and FFT based high frequency. These are analogous to the parameters rooted in the SRI measurement. The importance of the FFT based high frequency as opposed to the medium and low frequencies is expected as the surface micro roughness falls well within the high frequency range.

Each of the chosen parameters underwent a dual normalisation process, firstly in terms of the range of data for each parameter and secondly a normalisation of each parameter with respect to the other parameters. This was carried out due to differences in magnitude of each of the three chosen parameters.

The normalisation within each parameter was accomplished by subtracting 0.0143768, 0.09115075 and -9.71735 respectively from the variance, mean absolute difference and FFT based high frequency. These values were chosen from the corresponding values for electrolyte 12 described in Chapter 7, based on it giving the worst surface finish of all the electrolytes that polished and thus marked a zero level in terms of the quality of polished surfaces without pitting.

Conversely, the normalisation of each of the three chosen parameters with respect to each other, due to their differences in magnitude, was achieved by dividing each parameter by its corresponding maximum value from the entire pool of data. Thus the variance, mean absolute difference and FFT based high frequency parameters were divided by 0.0091379, 0.03709675 and 1.67005 respectively.

Having normalised the chosen parameters, an impact-weighted formula for measuring the surface roughness, incorporating these parameters was developed. The variance, mean absolute difference and FFT based high frequency were multiplied by an impact weighting of 0.4, 0.4 and 0.2 towards the final roughness measurement. This relationship called the Smoothness Index (SI) from this point onwards is shown below:

$$SI = -\left[\frac{0.4}{0.0091379}(variance - 0.0143768) + \frac{0.4}{0.03709675}(mean\_abs\_diff - 0.09115075) + \frac{0.2}{1.67005}(FFT_{high} + 9.71735)\right]$$

Based on the SI formula, when comparing the relative surface roughness of any two or more samples, a larger SI value represents a lower surface roughness and consequently smoother surface finish than a lower SI value.

Figure 4.13 shows typical values of SI obtained for surfaces with different roughness profiles:

Figure 4.13: Typical values of SI obtained for surfaces with different roughness profiles

Each SI value reported throughout this research is an average based on the analysis of two digital images acquired at different locations on the sample being analysed.

4.3.4 Comparison of surface roughness measurements based on the image processing and SRI measurement

The measurements and percentage variances for surface roughness measurements obtained using the SRI measurement and the image processing techniques are shown in Table 4.2:

Table 4.2: Comparison of surface roughness measurements obtained for sample A3

	SRI Measurement [-]	SI Measurement [-]
Trace 1	0.761	0.5613
Trace 2	0.711	0.5931
Trace 3	0.961	-
Average roughness	0.811	0.5772
% Variance	2.2%	8.7%

As imaging software analysed each surface's digital image by segmenting it into 760 horizontal and 580 vertical sectors, it takes into consideration vastly more information compared to the SRI technique which is only based on three traces. Hence, despite the fact that the percentage variation for the image processing technique is greater than that of the SRI method, it intuitively provides a better overall representation of the surface roughness. On this principle basis as well the shorter analysis turnover time using the image processing technique, all the surface roughness results presented in this research are based on this method of analysis.

Incidentally, as the development of the image processing method was only completed after the electrolyte optimisation experiments described in Chapter 7 were performed, the SRI method was initially used in the analysis of the surface roughness. These results are however not included in this report, as the surfaces for all the experimental results presented were re-analysed using the image processing technique, which provided more accurate results in terms of its overall representation of the metal surfaces.

4.4 Conclusions on the development of techniques and instrumentation for measuring surface roughness

Of the three methods explored, the image processing method was chosen as the best technique for the measurement of surface roughness based on its sufficiently accurate, overall three-dimensional representation of the surface topography.

The modified stylus measurement technique (SRI method) was found to provide significantly more consistent measurements compared to the conventional stylus measurement. However, both these methods were limited in their overall representation of the surface due to their two-dimensional profiles of three isolated traces at different positions on the surface.

The SRI method could be greatly improved by increasing the number of traces on the surface. Theoretically, by carrying out traces over the entire surface, a three-dimensional map of the surface topography could be generated. However, without automating the tracing process, this process would be excruciatingly time consuming.

In hindsight, the accuracy of the results for all three methods would have been improved by grinding each metal specimen to the same surface roughness prior to electropolishing. This way, differences in the surface roughness could be predominantly attributed to experimental conditions and less to variations in the initial surface roughness due to manufacturing process of the specimen.

Chapter 5

Experimental apparatus and procedure

5.1 *The experimental apparatus*

Figure 5.1 shows a schematic diagram of the experimental set up used to perform the experiments.

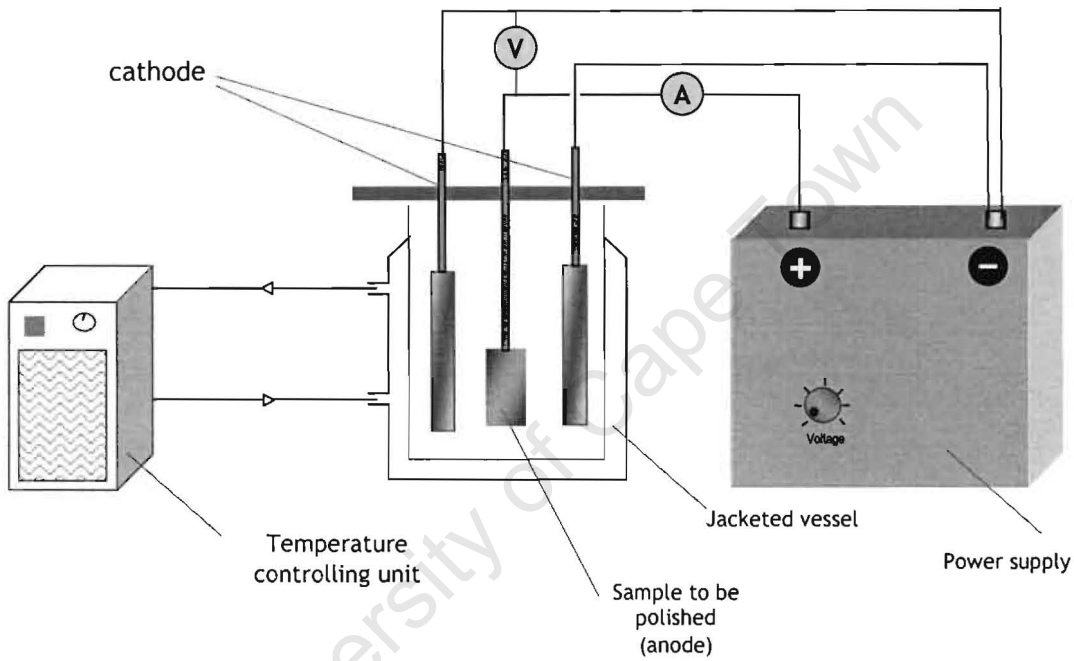

Figure 5.1: Schematic diagram of experimental apparatus

5.1.1 Electropolishing bath and temperature control mechanism

The experimental set up consisted of a one litre jacketed glass vessel. The temperature within the vessel was controlled by continuously circulating ethylene glycol through the outer wall of the vessel after being passed through a Grant LT D6G temperature-controlling unit. The unit acted as a heat source or heat sink depending on the thermal requirement of the system. Figure 5.2 shows a photograph of electropolishing bath and temperature control system:

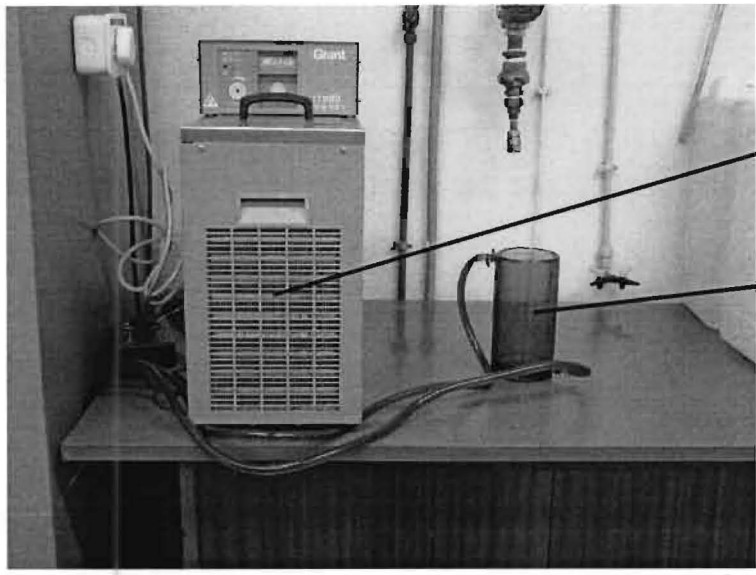

Figure 5.2: Photograph of electropolishing vessel and temperature controlling unit

5.1.2 The electrical circuit

The electrical circuit consisted of a Struers-Polipower direct current variable power supply capable of delivering up to 30V, connected in series with a Fluke ammeter and the electropolishing cell. A Fluke voltmeter was connected in parallel with the cell to measure its voltage. As the driving force for electropolishing is the current density, this parameter was kept constant during each experiment by varying the voltage. Figure 5.3 shows the electrical components of the electropolishing set up:

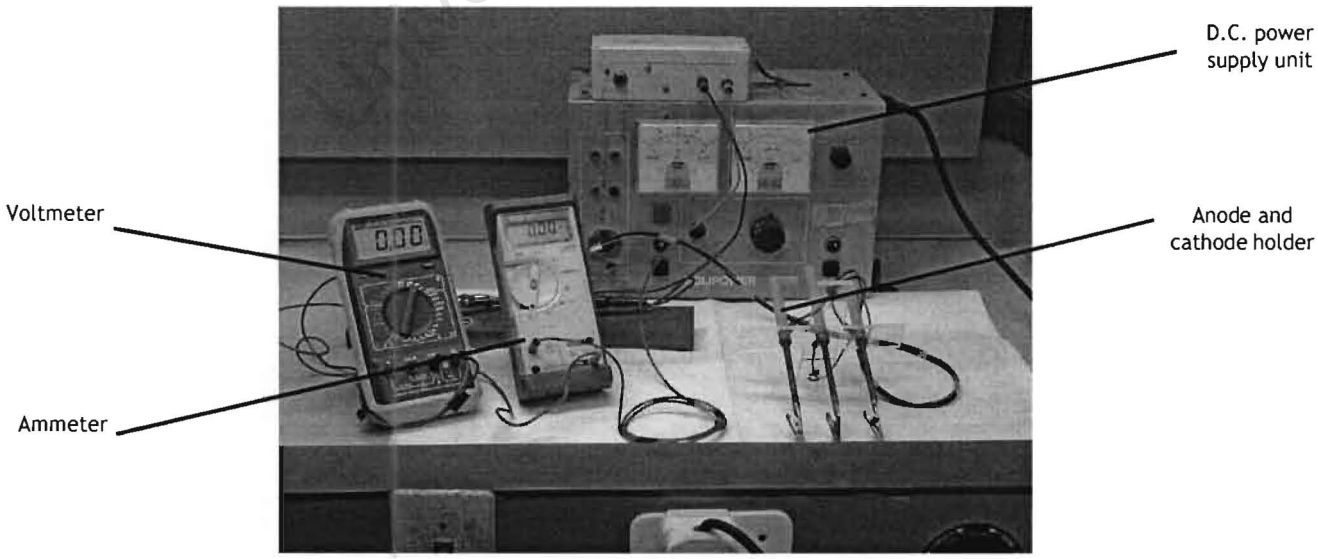

Figure 5.3: Photograph of electrical circuit

5.1.3 The anode and cathode

Two lead cathodes of dimensions 20mm x 50mm x 2mm with an active cathode height of 30mm were positioned on either side of the stainless steel anode. The anode had dimensions 13mm x 45mm x 1mm with an active anode height adjusted by insulating the rest of the anode with teflon tape on the inactive part such that the total surface area for polishing was $3cm^2$. Both anode and cathode were held in a fixed position using a piece of apparatus that was specifically constructed for this purpose. Figure 5.4 shows a photograph of this set up:

Figure 5.5 shows the a photograph of the assembled electropolishing apparatus:

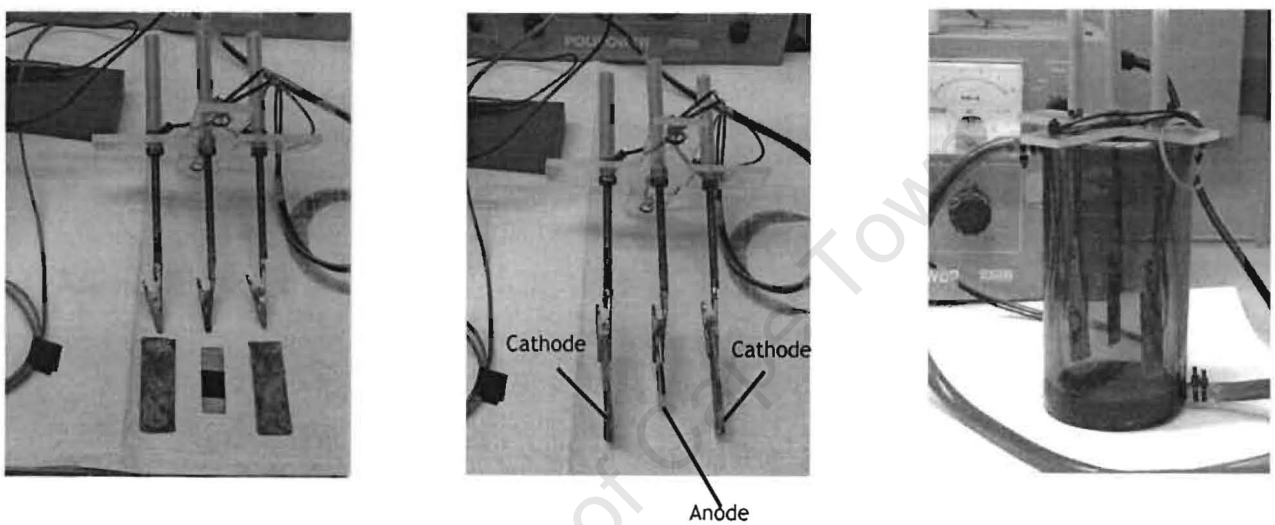

Figure 5.4: Anode and cathode set up

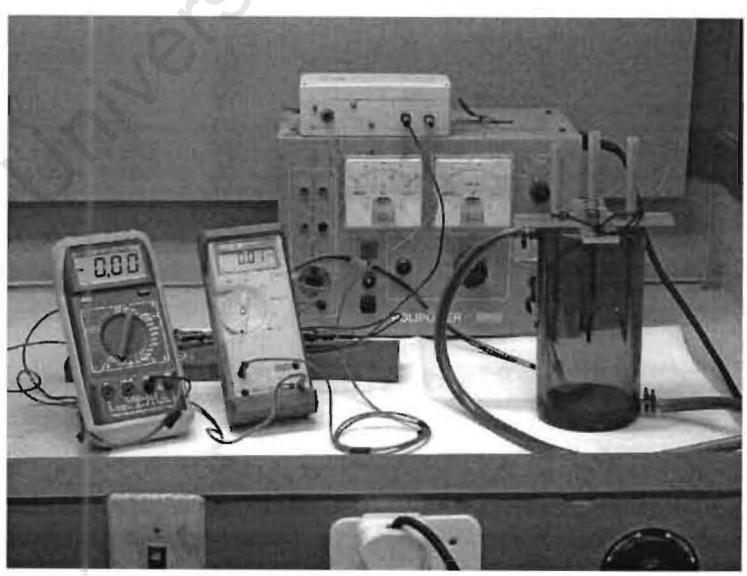

Figure 5.5: Photograph of assembled experimental apparatus

5.2 Electrolyte preparation

The electrolytes for each experiment, differing in the compositions of H_2SO_4, H_3PO_4 and G, were prepared using analytical grade Merck chemicals. The concentrations of the H_2SO_4 and H_3PO_4 were 98% and 85% respectively.

The electrolytes were prepared in a 500ml glass beaker whose contents were constantly stirred by means of an overhead stirrer. The required amount of H_3PO_4 was added first to the beaker, followed by the H_2SO_4 and finally the diol (G).

Once prepared, the electrolytes were stored in 500ml Schott bottles.

5.3 Experimental Procedure

Before starting each experiment, 200ml of electrolyte was placed in the jacketed electropolishing vessel and brought up to the correct operating temperature. While the electrolyte was being heated to the required temperature, the 304 stainless steel sample (anode) to be polished was cleaned by rinsing it with deionised water, followed by ethanol after which the sample was dried using a stream of hot air. An identification number was engraved at the top of each sample and the sample was weighed. The active height of the anode was then adjusted by measuring $3cm^2$ of exposed surface area for polishing and insulating the rest of the sample with Teflon tape.

Once the electrolyte had stabilised at the correct operating temperature, the anode and cathode apparatus was lowered into the vessel. The power supply was set to the required operating current and switched on. Each experiment was carried out for a fixed polishing time that was monitored with a stopwatch. Throughout the duration of each experiment, the current was monitored and maintained at the required level by a dynamic voltage adjustment whilst the temperature was kept constant by the temperature control unit.

After polishing the sample for the required time, the current was switched off and the anode-cathode apparatus was removed from the vessel. After removing the Teflon tape, the polished sample was rinsed in deionised water and ethanol, dried and weighed. A microscopic digital image of the metal surface, using a Nomarski DIC microscope was then acquired and the image processed in MATLAB® to obtain its SI value.

Chapter 6

Mapping & optimising the performance of PS electrolyte

6.1 Introduction

This phase of the project was carried out to establish the operating conditions for optimal performance of the PS electrolyte in terms of polishing quality (SI), fastest polishing rate and shortest polishing time.

Once established, these findings would enable recommendations to be made in terms of improving the polishing process using the PS electrolyte whilst at the same time setting a standard of polishing performance against which any new electrolyte compositions could be compared.

The tasks performed included establishing the voltage-current density relationship for the PS electrolyte-304 stainless steel system with the intention of identifying the plateau region in which polishing takes place, as depicted by point P2 in Figure 3.2 reproduced below:

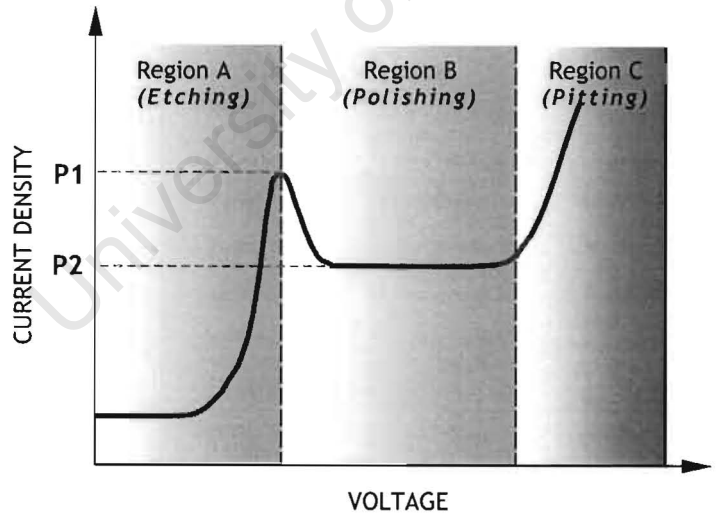

Figure 3.2: Typical current density-voltage relationship for an electropolishing process

After establishing the optimal operating current density, the shortest polishing time at this current density was determined for the PS electrolyte.

6.2 *Voltage-Current density relationship for PS electrolyte - 304 stainless steel system*

6.2.1 Materials and experimental methods

In determining the voltage-current density relationship for the PS electrolyte-304 stainless steel system, the experimental set up and procedure outlined in chapter 5 was employed. The PS electrolyte used for these tests was obtained directly from the plant's new electrolyte stock. 3cm^2 of active surface area for polishing was used at an operating temperature of 80°C. This temperature was chosen as it marks the upper temperature limit to which the PS electrolyte system is operated in industry. As the voltage was increased from 0 - 12V in steps of 0.5V, the corresponding current, which was measured by the ammeter, was recorded.

6.2.2 Results and discussion

The relationship between voltage and current density for the PS electrolyte - 304 stainless steel system is shown in Figure 6.1:

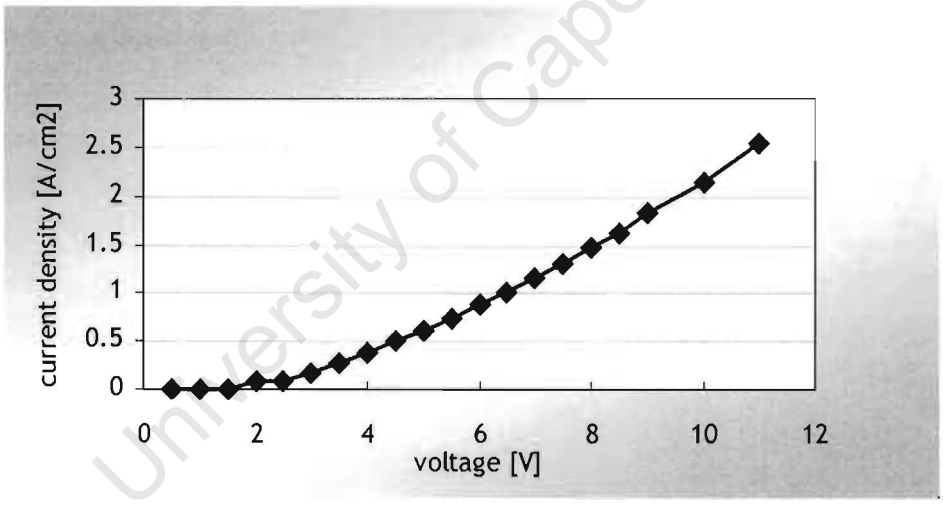

Figure 6.1: PS electrolyte's voltage - current density relationship

The PS electrolyte system did not exhibit a theoretical electropolishing plateau region as shown in Figure 3.2. The ambiguity of the plateau region for the iron - phosphoric acid systems is consistent with the results of Hoare and co-workers (1981), who concluded that, experimentally, predominantly salt solutions exhibit a well-defined limiting current region unlike concentrated acid solutions (the exception being the copper - phosphoric acid system).

An alternative explanation for absence of significant plateau is the possibility that the 0.5 Volt step size between each subsequent voltage level was larger than the entire plateau

region, therefore masking its presence. Regrettably, due to the limitations of the power supply available for these experiments, it was impossible to use smaller step sizes.

6.3 *Establishing the optimum operating current density for PS electrolyte*

6.3.1 Introduction

Being unable to establish the optimum operating current density based on a voltage - current density plot for this system, a more direct approach was adopted. This method entailed polishing specimens at increasing current densities and measuring the polishing quality and rate.

6.3.2 Materials and experimental methods

Following the experimental procedure outlined in Chapter 5, the polishing quality and rate when operating at current densities in the range between 0.5 - 3A/cm^2 were measured. Each specimen had a 3cm^2 active surface area for polishing and was polished for an arbitrarily chosen three minutes. The operating temperature was 80°C.

6.3.3 Results and discussion

Figure 6.2 indicates that the best polishing quality (SI) was achieved when operating at a current density between 1 - 2A/cm^2. This range is in agreement with the findings of Hocheng and co-workers (2001).

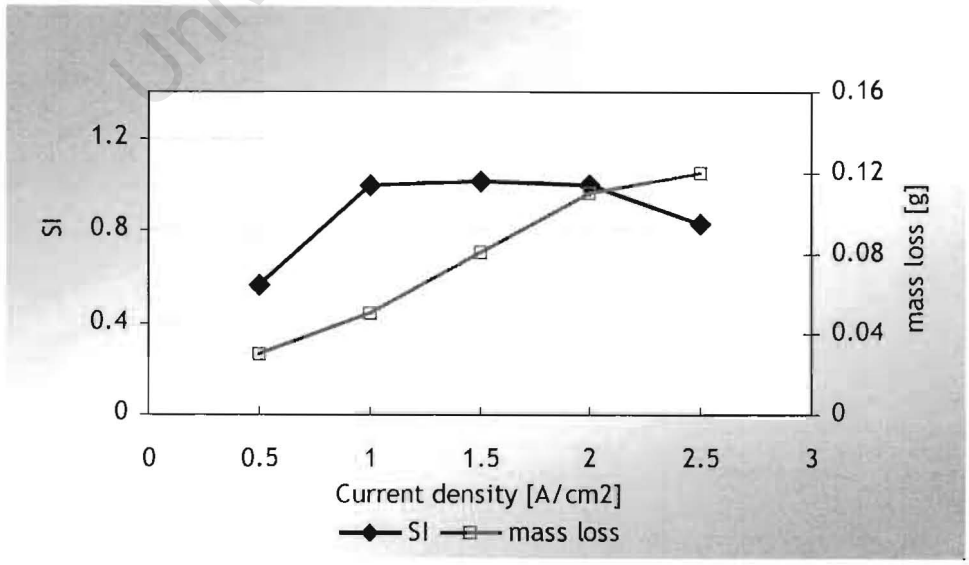

Figure 6.2: PS electrolyte's current density-SI relationship

As expected, based on Faraday's Law, operating at higher current densities results in higher mass loss from the surface (Twidwell *et al.*, 1992). Furthermore, as a higher mass loss implies faster surface levelling, up until a current density of $2A/cm^2$, the higher the operating current density, the faster the levelling.

Consequently, the ideal operating current density for the PS electrolyte - 304 stainless steel system is $2A/cm^2$ in terms of obtaining the best surface finish (SI) at the fastest rate (mass loss).

These results also show that the polishing quality (SI) decreases at current densities greater than $2A/cm^2$, indicating the transition from the electropolishing region to the pitting region. At this point the anode layer begins to destabilise on account of the excess energy input, exposing locations on the metal surface that would normally be protected by the anode layer (Hoare *et al.*, 1981). This causes the premature metal dissolution at these compromised points on the surface, forming troughs, which are more commonly known as pits.

Based on the results shown above, operating current densities of 1.5 and 2 A/cm^2 were chosen as the most favourable, both in terms of polishing quality and rate. Consequently these two current density levels were used in the electrolyte composition optimisation experiments, which are discussed in Chapter 7.

6.4 Shortest polishing time for PS electrolyte at the optimum current density

6.4.1 Introduction

Having determined the optimal operating current density for this system, the next phase of the study focussed on determining the shortest possible polishing time for the PS electrolyte when operating at this optimal current density level.

6.4.2 Materials and experimental methods

In order to determine the shortest polishing time, seven specimens, each with an active surface area for polishing of $3cm^2$, were polished at a current density of $2A/cm^2$ for incremental time periods, ranging between 30 seconds and 5 minutes. The operating temperature was maintained at 80°C.

6.4.3 Results and discussion

The results of this study are shown in Figure 6.3:

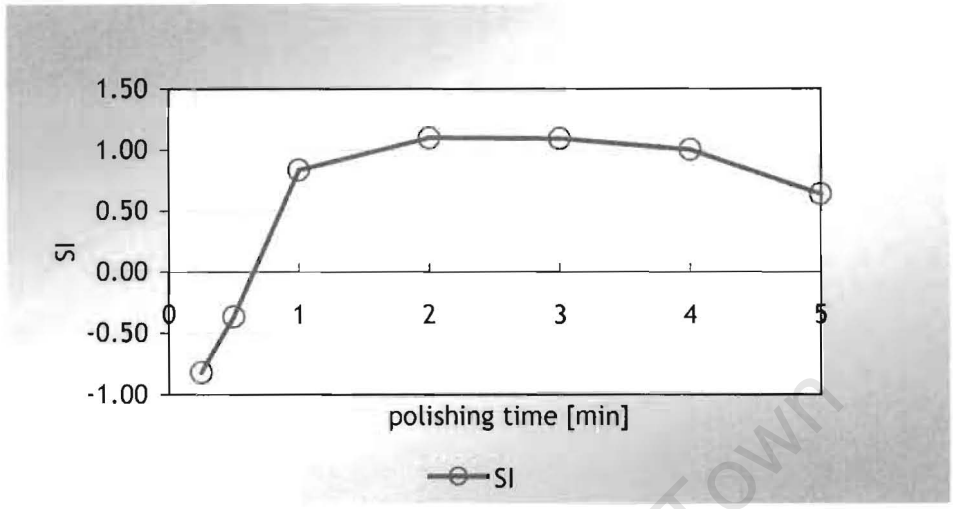

Figure 6.3: Effect of polishing time on quality of surface finish (SI)

The results show that the SI value increased with an increase in the polishing time and reached a maximum after three minutes of polishing. This was a dramatic improvement in the polishing time compared to shortest polishing time of 10 minutes that was previously found to be possible with the current PS electrolyte at plant scale operation. As the current density is not dependent on the scale of the operation, but rather on a unit surface area being polished, it can be concluded that the polishing time at plant scale can theoretically be reduced to three minutes by operating at a current density of $2A/cm^2$.

The fact that the longer polishing time at plant scale was as a result of operating below the ideal current density was confirmed by plant data, which showed that when operating under the same conditions of voltage and temperature, the polishing time was shorter than 10 minutes when polishing a smaller total surface area in the form of smaller quantity of articles in the bath. This finding therefore forms one of the most significant outcomes of this project; that the full potential of the PS electrolyte is not currently being exploited. By increasing the operating current density to as close to $2A/cm^2$ as possible, based on the limitations of the power supply, a reduction in polishing time can easily be achieved.

It is interesting to note that the SI value starts to decrease with polishing times greater than three minutes. A possible explanation for this is that after three minutes of polishing; all the prominent surface asperities have been levelled. Hence, continuing to provide a current beyond three minutes causes the loss of metal ions at locations where there is the slightest

difference in the anode layer thickness. Once exposed, these locations continue to be attacked until such time that their surrounding locations are significantly higher relative to them or the anode layer is regenerated. At this point, based on the thickness of the anode layer, the surroundings become exposed and surface levelling resumes.

If the current were supplied indefinitely, this cyclic increase and subsequent decrease in the SI value would be expected to continue until complete dissolution of the metal piece.

Further experimentation would however need to be carried out to validate the above explanation. This would involve a continuation of the experiment to determine the effect of polishing time on SI value for polishing times greater than five minutes. A confirmation of this hypothesis would be the prevalence of the cyclic variation in the SI value.

6.5 *Conclusions on mapping and optimising the performance of the PS electrolyte*

The results of this research in terms of the ambiguous polishing region for the PS electrolyte - 304 stainless steel system are in agreement with the findings of Hoare and co-workers (1981) who established that the phosphoric acid - iron system does not exhibit a clear cut plateau region.

Consequently, in trying to establish the optimum operating current density, the final polishing quality (SI) was measured at various operating current densities. The most favourable range was found to be between 1 - 2A/cm^2, with 2A/cm^2 selected to be the best, based on its higher rate of mass loss and therefore more rapid surface levelling. It must taken into consideration that this choice excludes economic factors such as increased electricity costs of operating at a higher current density.

The system also showed a decrease in polishing quality when operating at current densities higher than 2A/cm^2, signifying the transition into the pitting region.

The shortest polishing time for the PS electrolyte was found to be three minutes when operating at the optimum current density. This is a substantial reduction in polishing time compared to the shortest time of 10 minutes that was previously achieved at plant scale. Plant operating data confirmed that the polishing process was being run below the optimum operating current density. Theoretically, a plant scale polishing time of three minutes is feasible by increasing the operating current density to 2A/cm^2.

Chapter 7

Optimisation of electrolyte composition

7.1 Introduction

In the preceding chapter it was established that increasing the plant operating current density towards the optimum value of $2A/cm^2$ could significantly decrease the polishing time for the PS electrolyte to three minutes. Following on from this, this phase of the research focussed on finding an optimum electrolyte composition that could further enhance the polishing performance. This involved:

1. Determining the relative impact of the ratio of H_2SO_4, H_3PO_4 and the diol, G, as well as the temperature and current density on the quality and rate of polishing based on Response Surface Methodology (RSM).
2. Developing a mathematical model describing the quality and rate response as a function of the concentration of the three components, the current density and the operating temperature.
3. Predicting new electrolyte compositions that could potentially enhance the polishing performance based on the mathematical model.
4. Comparing the performance of the proposed new electrolytes to that of the PS electrolyte before making recommendations towards implementing their use.

7.2 Materials and experimental methods

7.2.1 Experimental design - Electrolyte compositions investigated

With the electrolyte being a three-component system (H_2SO_4, H_3PO_4 and G), all possible combinations of the three components can be described by means of a ternary diagram. However, due to time and financial constraints it would be impractical to measure the polishing performance of all possible electrolyte combinations and therefore certain confines were laid out upfront for this experimental design. These included:

1. Excluding all electrolytes with G concentrations exceeding 20 volume percent. This was based on the fact that G is only added to the electrolyte in order to enhance the polishing quality owing to its stabilising effect on the anode layer. Being incapable of electropolishing alone, its presence in higher concentrations is at the expense of the other two components and would therefore significantly reduce the rate of polishing.

2. The step size between each of the different electrolyte mixtures was based on compromise between the required resolution detail of the response surface generated from the results and keeping the number of experiments to a minimum. A suite of 13 electrolyte mixtures comprising the boundary points, midway points and a centroid point on the G constrained ternary diagram were selected. The location of these points on the ternary diagram are shown in Figure 7.1, whilst the specific compositions are shown in Table 7.1:

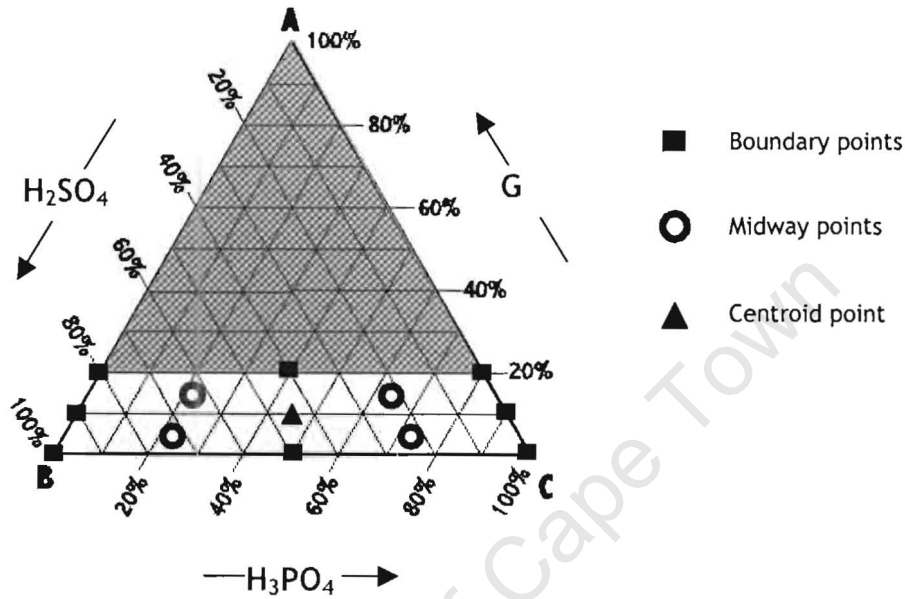

Figure 7.1: Ternary diagram showing the different combinations of H_2SO_4, H_3PO_4 and G electrolyte mixtures investigated

Table 7.1: Compositions of electrolyte mixtures investigated

Electrolyte Number	G [volume %]	H_3PO_4 [volume %]	H_2SO_4 [volume %]
1	0	100	0
2	10	90	0
3	20	80	0
4	20	40	40
5	20	0	80
6	10	0	90
7	0	0	100
8	0	50	50
9	9.45	45.275	45.275
10	14.72	62.64	22.64
11	14.72	22.64	62.64
12	4.72	22.64	72.64
13	4.72	72.64	22.64

7.2.2 Experimental design - Factors varied and responses measured

The factors varied for this experimental design were:

1. The electrolyte composition according to the 13 electrolyte compositions described in section 7.1.1.
2. The current density at the two levels of 1.5 and 2A/cm^2 that were found to be the two best operating current densities for this system as described in Chapter 6.
3. The temperature at two levels, 70°C and 80°C. This factor was investigated to determine the advantages in terms of the polishing quality and rate of operating either at an elevated or decreased temperature.

52 experiments (13 electrolyte compositions x 2 levels of current density x 2 levels of temperature) were performed in searching for an electrolyte composition with superior polishing performance to that of the PS electrolyte. In addition to this, these experiments would also shed light on the impact of temperature and operating current densities on the overall polishing performance of each of these electrolytes.

The responses measured were:

1. The SI value, indicative of the quality of the surface finish;
2. The mass loss percentage, indicative of the rate at which metal atoms leave the surface and is therefore a measure of the rate the electropolishing process.

7.2.3 Experimental design - Data analysis methodology

In analysing the results of the polishing quality and rate for each of the 13 electrolytes at two levels of current density and temperature, a regression approach to the analysis of variance was adopted. The regression modelling facilitated the prediction of the response as a function of the quantitative independent variables while the analysis of variance modelling performed significance tests on multiple population means (Walpole *et al.*, 1985).

For the simple linear regression model $Y = \beta_0 + \beta_1 x + \varepsilon$, the analysis process involved:

1. Determining which dependent variables relate to the response;
2. Determining the form of the relationship;
3. Determining the best fitting regression model;
4. Estimating the parameters β_0 and β_1 and ε of the regression function;
5. Testing the hypotheses about the estimated parameters of the regression function;
6. Predicting Y at values of $x_1, x_2, \ldots, x_k$, whether these were observed or not;
7. Establishing the strength of the correlation between Y and the x's based on the P-value. A P-value less than 0.05 indicates a significant impact of that parameter, with at least 95% confidence, on the response variable.

Statistical analyses of the results were performed using the Statistica (Version 6) software. Once developed, the mathematical models were used to find the optimal performance region in terms of the polishing quality and rate responses. This was carried out using the Solver tool in Microsoft Excel.

7.2.4 Experimental design - PS electrolyte preparation

The PS electrolyte for this phase of the work was prepared in the laboratory. This was unlike the experiments performed to determine the optimum operating conditions for the PS electrolyte discussed in Chapter 6, which were carried out using PS electrolyte obtained directly from the plant's new electrolyte stock. The principle reason for this difference being that the "new" plant electrolyte already contains 8.3 $g.l^{-1}$ of dissolved iron ions, which are added to increase the conductivity. This minimises the time taken for the electrolyte performance to reach its best level, which requires the presence of some dissolved metal ions.

To standardise the performance of the PS electrolyte with respect to the other electrolytes tested during this phase of the work, the PS electrolyte was prepared in the laboratory to the exact H_3PO_4, H_2SO_4 and G ratio but without the dissolved iron.

Alternatively, 8.3 $g.l^{-1}$ of iron ions could have been added to all of the other electrolytes to standardise their performance relative to the PS electrolyte obtained directly from the plant's new electrolyte stock. Even though the former method was preferred due to its ease of implementation, it can be assumed that both methods would yield the same final results in terms of determining and comparing the optimum electrolytes' performance to that of the PS electrolyte.

The exact ratios in which the three components are mixed in the PS electrolyte are not presented in this report for proprietary reasons.

7.3 Preliminary experiments

7.3.1 Introduction and rationale

In determining the optimum electrolyte composition founded on the two levels each for the current density and temperature, four experiments were required per electrolyte composition. In line with this, preliminary experiments were performed to determine whether the same electrolyte could be used to carry out these four experiments without having a significant effect on the polishing quality and rate with each subsequent polish.

7.3.2 Materials and experimental methods

This task was performed by electropolishing five metal samples each with an active surface area for polishing of $3cm^2$ for 3 minutes at 80°C, in line with the experimental procedures outlined in chapter 5. The electrolyte used for this test was the laboratory prepared PS electrolyte.

7.3.3 Results and discussion

The results of this analysis are shown in Figure 7.2 below:

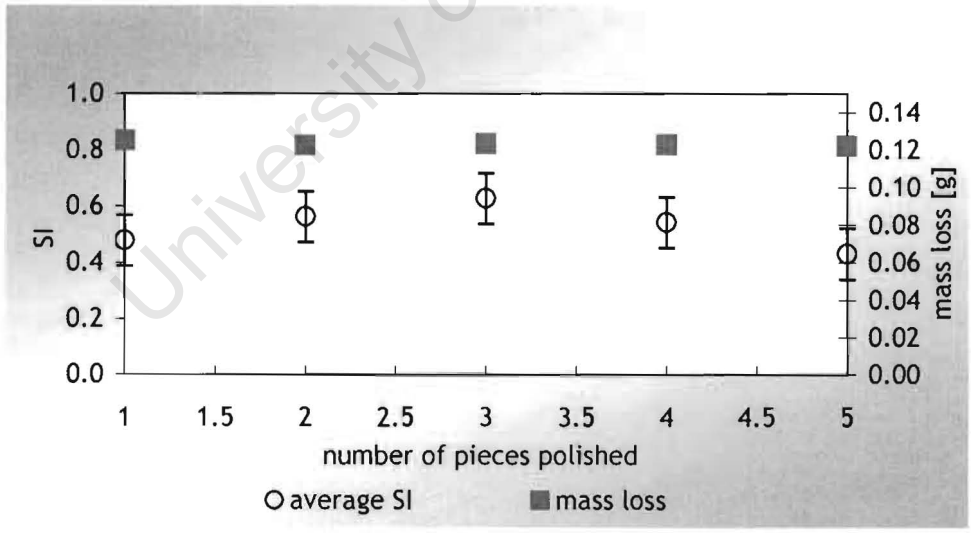

Figure 7.2: PS electrolyte's polishing performance trend with an increase in the number of pieces polished

Referring to Figure 7.2, the mass loss and SI results show that the impact of polishing five samples for three minutes was negligible with respect to a change in the rate and quality of polishing. The fact that the difference in mass loss is not significant with each additional specimen polished can be attributed to relatively insignificant amount of metal ions added to

the electrolyte. The total mass of metal ions added to the electrolyte is 0.31g.l^{-1} compared to the typical total dissolved metal ion content of 83.4g.l^{-1} for the spent electrolyte (discussed in Chapter 8). Consequently, the four experiments per electrolyte were performed on the same electrolyte for the electrolyte optimisation experiments.

The error bars shown on the SI values represent the variations, not primarily as a result of the measurement technique, but rather, due to slight surface differences in the individual metal pieces polished. These differences were in the form of microscopic surface scratches and irregularities, characteristic of metals prepared by rolling.

This exposed a weakness in the image processing technique developed for measuring the surface roughness in that although it was designed to look past this macro roughness and measure the micro roughness on the surface, there are inevitably regions where the differentiation between transition from one level of roughness to the other is indistinct.

In hindsight, grinding each metal sample to the same surface roughness prior to each experiment would have minimised the variations in the SI value as a result of the surface dissimilarities caused during preparation of the metal. Alternatively, by measuring the surface topography for each sample before and after polishing, the final response could be normalised with respect to the initial surface topography.

7.4 Results of electrolyte optimisation study

As described earlier in this chapter, this section of the research focussed on establishing the relative impact of the ratio of H_2SO_4, H_3PO_4 and G as well as the temperature and current density on the quality and rate of polishing. Once established, these results were used to predict and test new electrolyte compositions that could potentially enhance the polishing performance.

7.4.1 The effect of electrolyte composition & operating conditions on polishing quality (SI) and rate of polishing (% mass loss)

The model fitted to both the SI and percent mass loss data was:

$$\text{Response} = \beta_1x_1 + \beta_2x_2 + \beta_3x_3 + \beta_{12}x_1x_2 + \beta_{13}x_1x_3 + \beta_{23}x_2x_3 + (\beta_1x_1 + \beta_2x_2 + \beta_3x_3 + \beta_{12}x_1x_2 + \beta_{13}x_1x_3 + \beta_{23}x_2x_3)\text{*Density} + (\beta_1x_1 + \beta_2x_2 + \beta_3x_3 + \beta_{12}x_1x_2 + \beta_{13}x_1x_3 + \beta_{23}x_2x_3)\text{*Temperature} + \varepsilon$$

where x_1, x_2 and x_3 represent G, H_3PO_4 and H_2SO_4 while β_{xy} represents the corresponding parameter estimates based on the analysis of variance.

The significance of operating temperature and current density on the surface finish and the rate of electropolishing of 304 Stainless Steel

Statistical analysis of variance on the data showed that based on the P-values (Appendix 3), both the current density and temperature at the two levels of 1.5 and 2A/cm^2 and 70°C and 80°C respectively, had a much smaller influence on the polishing quality (SI) when compared to the electrolyte composition. Furthermore, investigation into the interactions involving current density and temperature indicate that, based on the relative magnitudes of the P-values, the temperature interactions had a more significant effect on the SI value than the current density interactions. This could be attributed to the destabilisation of the anode layer at elevated temperatures and the consequent negative impact on the SI value (Hoare *et al.*, 1981).

In terms of the percent mass loss, the statistical analysis showed the H_3PO_4 - H_2SO_4 - current density interaction, with a P-value of 0.0423, to be more significant than any of the temperature-electrolyte composition interactions. In the final analysis, all the insignificant interaction terms were dropped, leaving the current density - electrolyte composition interactions. The analysis showed that the extent of the current density - interaction was different at the two densities investigated. As expected, in conformity with Faraday's Law of a higher mass loss at a higher current density, the interaction at the higher of the two current densities resulted in a greater mass loss percentage than that at the lower current density (Twidwell *et al.*, 1992). Despite that, the H_3PO_4 - H_2SO_4 interaction was still found to be the most significant factor influencing the rate of mass loss.

Although the influence of the electrolyte composition was expected to play a more important role with respect to polishing quality and rate, compared to the temperature and current density, the extent of the insignificance of the other two parameters investigated could be attributed to the relatively small range between the levels at which each were investigated.

In hindsight, although the current density range for this phase of the work was appropriate, having been based on the optimum current density range as described in Chapter 6, the range between the two levels of temperature could have been greater. This would have provided more valuable information with regards to the influence of temperature on the polishing quality and rate.

As a consequence of the insignificant effect of the variations in the temperature and current density on the polishing quality and rate, the results for each of the four experiments per electrolyte were averaged. This approach enabled the overall robustness of each electrolyte within the investigated limits of current density and temperature to be established. In addition, it ensured four test repeats on each electrolyte.

To obtain a clearer picture in terms of the relative influence of the G, H_3PO_4 and H_2SO_4 on the two measured responses, the experimental data was fitted to the model of the form: Response = $\beta_1 G + \beta_2 P + \beta_3 S + \beta_{12} GP + \beta_{13} GS + \beta_{23} PS + \beta_{123} GPS + \varepsilon$, resulting in the following parameter estimates describing the response surface of SI and percent mass loss as a function of the electrolyte composition (G, P and S correspond to the G, H_3PO_4 and H_2SO_4 respectively:

SI response:

Table 7.3: Parameter estimates for SI response surface

Variable	Parameter estimate	Standard Error	P-value
G	-0.630291	0.221460	0.0067
P	-0.006237	0.003941	0.1207
S	-0.038737	0.003941	0.0001
GP	0.007922	0.002773	0.0065
GS	0.007328	0.002773	0.0113
PS	0.003105	0.001351	0.0263
GPS	7.8705E-5	0.000018	0.0001

% Mass loss response:

Table 7.4: Parameter estimates for % mass loss response surface

Variable	Parameter estimate	Standard Error	P-value
G	-0.045769	0.120150	0.7050
P	0.010399	0.002138	0.0001
S	0.001948	0.002138	0.3672
GP	0.000825	0.001504	0.5863
GS	0.000567	0.001504	0.7082
PS	0.000738	0.000100	0.0001
GPS	-2.875E-6	0.000009	0.7641

Figure 7.3 below shows the results of the combined average of the SI values and mass loss percentages achieved for each of the 13 electrolytes. For the purpose of comparison, the values achieved by the PS electrolyte under the same conditions are also included in the Figure 7.3:

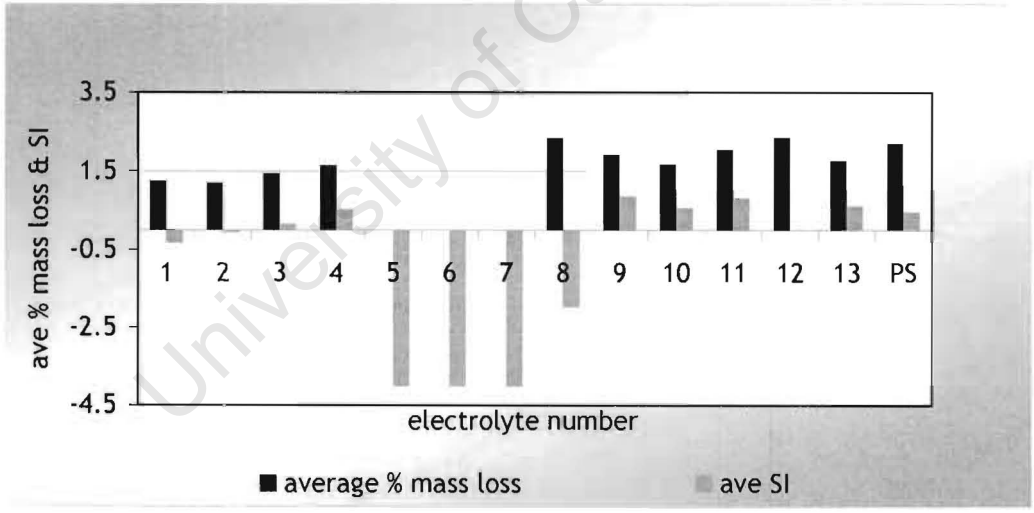

Figure 7.3: Average SI and % mass loss results for the 13 electrolytes investigated

Electrolytes 9, 10, 11 and 13 all yielded superior SI values compared to that of the PS electrolyte. For visual comparison, microscopic images with a five times magnification of the surface profiles of these four electrolytes as well that of the PS electrolyte are shown in Figure 7.4:

Figure 7.4: Microscopic images (x5 magnification) of the surface topography for electrolytes 9, 10, 11, 13 & PS electrolyte

The significance of H_3PO_4 in terms of the surface finish and rate of electropolishing of 304 Stainless Steel

The electrolytes that did not contain any H_3PO_4, namely, Electrolytes 5, 6 and 7, did not electropolish at all, indicated by a 0 Amps current reading on the ammeter as well as no mass loss. Hence, they were assigned SI values of -4, which is lower than the lowest of the average SI values for electrolytes that did electropolish. The inert behaviour of these H_3PO_4 free electrolytes towards electropolishing persisted even when the electric potential was progressively ramped up to the 30 Volt limit on the power supply. Conversely, the electrolytes that contained even as little as 22% by volume of H_3PO_4 resulted in electropolishing.

This phenomenon could be explained by the passive behaviour of stainless steel, even towards H_2SO_4, that is attributed to its largely inert chromium oxide surface layer. Despite the aggressive oxidation potential of H_2SO_4 towards metals, it is only when the inert chromium oxide surface layer is removed by the H_3PO_4 in the electrolyte, that the pure metal atoms are exposed to the H_2SO_4. Hence, although H_2SO_4 is a stronger oxidising agent than H_3PO_4, the electropolishing reaction can only take place in the presence of the stronger reducing agent, namely, H_3PO_4.

In terms of the rate of polishing, by comparing the percentage mass loss between Electrolytes 1 and 13, it is apparent that although H_3PO_4 is capable of electropolishing on its own, the presence of H_2SO_4 greatly enhances the rate of mass loss. This result is in agreement with the findings of Hocheng and co-workers (2001). The explanation for this observation is discussed further on in this report under the significance of H_2SO_4 in terms of the surface finish and rate of electropolishing.

The significance of G in terms of the surface finish and rate of electropolishing of 304 Stainless Steel

G on its own is incapable of electropolishing and as such, its increased concentration in the electrolyte is at the expense of the other two oxidising components. This fact is confirmed by the negative parameter estimate of -0.045769 for G in the percentage mass loss response. Consequently, the amount of G added needs to be a compromise between the quality of the surface finish and the rate of polishing. Included among the properties of good electropolishing electrolytes, described previously in Chapter 2, are that (Metals Handbook, 1998):

- The electrolytes must be fairly viscous to promote stability within the anode layer;
- The electrolytes should contain in combination with large ions such as PO_4^{3-}, SO_4^{2-} or ClO_4^-, large organic molecules, which improve electrolyte performance.

G's organic nature and its viscous characteristics satisfy both the criteria above. This is clearly illustrated in Figure 7.3 when comparing the electropolishing results of electrolytes 8 and 9. Due to the instability within the anode layer in the absence of G (Electrolyte 8), the acids indiscriminately attack the metal surface, rather than predominantly attacking the elevated surface asperities, resulting in pitting and consequently a poor SI value of -2.35. Conversely, Electrolyte 9, which has a similar make up to that of Electrolyte 8 in terms of H_2SO_4 and H_3PO_4 except with 9.45% G by volume, resulted in the best surface finish of all the electrolytes with a SI value of 0.86. This is similar to the findings of Hocheng and co-workers (2001), who used glycerine rather than G. Digital microscopic images with a five times magnification of the surface topography obtained using electrolytes 9 and 8 are shown below in Figures 7.5 and 7.6 respectively:

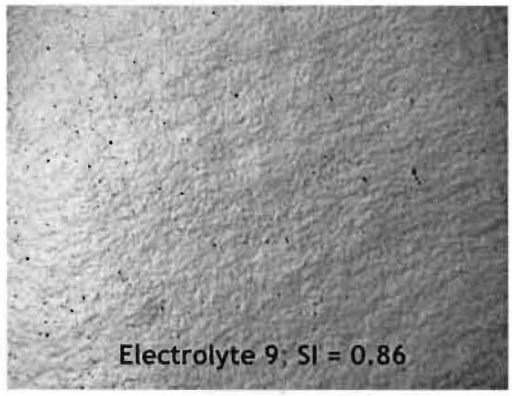

Figure 7.5: Microscopic image (x5 magnification) of the surface topography for electrolyte 9

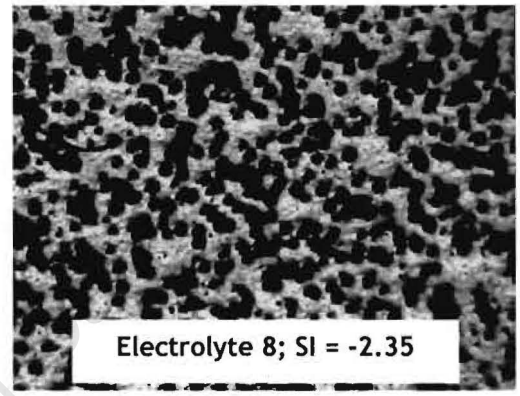

Figure 7.6: Microscopic image (x5 magnification) of the surface topography for electrolyte 8

The significance of H_2SO_4 in terms of the surface finish and rate of electropolishing of 304 Stainless Steel

The results of electrolyte 11, which yielded the second best SI value of 0.76, show that H_2SO_4 plays a vital role in attaining a good surface finish. However, the value of the H_2SO_4 is in its interaction with the other two components as the reaction only occurs provided that some H_3PO_4 is present to initially remove the chromium oxide layer and if there is sufficient G to dampen the aggressive metal dissolution characteristics of H_2SO_4. The electropolishing reaction then progresses rapidly as indicated by the increased rate of mass loss from the surface, smoothing the surface asperities to yield a good surface finish. This explanation is consistent with the results of Electrolytes 10 and 11, which show a marked improvement in SI values from 0.59 to 0.76 and percentage mass losses from 1.9% to 2.5% respectively.

The significance of H_3PO_4 - H_2SO_4 - G interactions in terms of the surface finish and rate of electropolishing of 304 Stainless Steel

The relative significance of these interactions in terms of the polishing quality is revealed by the P-values of 0.0075, 0.0116 and 0.001 for the G - H_3PO_4, G - H_2SO_4 and the H_3PO_4 - H_2SO_4 interactions respectively (Appendix 7A). The H_3PO_4 - H_2SO_4 interaction clearly has the most significant influence on the polishing quality of all the interaction terms. Furthermore, as expected due to their anode layer stabilising capability, the G - acid interactions also play a significant role in the surface finish.

In terms of the rate of polishing, the relative significance of these interactions is dominated by the H_3PO_4 - H_2SO_4 interaction (P-value = 0.0001). The absence of any significant G - H_3PO_4 - H_2SO_4 interaction was to be expected due to G's inability to electropolish on its own.

The relationship between the SI value and the percentage mass loss

From the results of Electrolyte 8, it is clear that the percentage mass loss independently as a response is an insufficient measure of good polishing. Electrolyte 8 achieves the highest mass loss of all the electrolytes with an average of 2.78% whilst simultaneously achieving the worst surface finish (SI value = -2.35) of all the electrolytes that did polish. This indicates that a faster rate of mass loss does not necessarily imply faster surface levelling and consequently a better surface finish. Rather, the SI value should be used as the primary selection criterion when comparing the performance of electrolytes, followed by a comparison of rate of mass loss as the secondary selection criterion.

This order of the selection criterion is typical for electropolishing processes where the surface finish is of more importance than the mass loss, as opposed to a chemical machining processes where initially the rate of mass loss is more critical.

7.4.2 Finding the optimum electrolyte composition based on the experimental design results

From the preceding discussion on the significance of the effect of the three components on the surface finish and the rate of electropolishing of 304 stainless steel, it is evident that a balance needs to be reached with respect to the amount of each component in the electrolyte.

At the forefront, the presence of H_3PO_4 is critical to the initiation of the electropolishing reaction, removing the passive chromium oxide surface layer, after which, regardless of the presence or absence of H_2SO_4 and G, it continues with the dissolution of the metal surface. However, the presence of H_2SO_4, which is a stronger oxidising agent than H_3PO_4, speeds up

the metal dissolution process achieving a good surface finish, provided that there is sufficient G.

In order to identify the region of optimal electrolyte composition in terms of the best surface finish and mass loss, the response surfaces were plotted. These are shown in Figures 7.7 and 7.8. For each response, the view of the surface from each of the axes as well as a contour plot of the surface profile is shown. The corresponding standard errors for each parameter estimates are shown in parenthesis under the response surface function.

$$SI = -0.630291G - 0.006237P - 0.038737S + 0.007922GP + 0.007328GS + 0.003105PS + 7.8705E\text{-}5GPS$$
$$(0.221460)\quad (0.003941)\quad (0.003941)\quad (0.002773)\quad (0.002773)\quad (0.001351)\quad (0.000018)$$

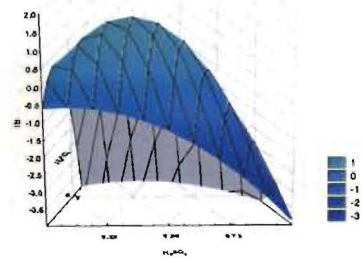

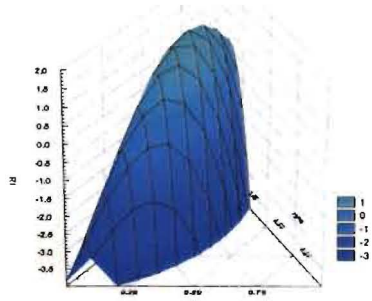

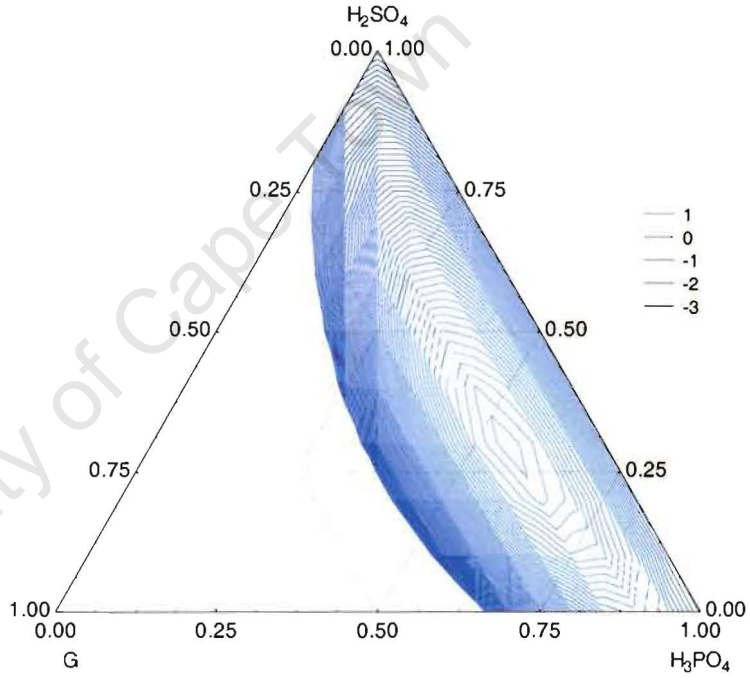

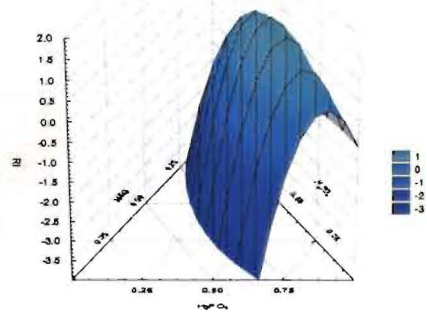

Figure 7.7: SI response surface as a function of the electrolyte composition

$$\%\ mass\ loss = -0.045769G + 0.010399P + 0.001948S + 0.000825GP + 0.000567GS + 0.000738PS - 2.875E\text{-}6GPS$$
$$(0.120150)\quad (0.002138)\quad (0.002138)\quad (0.002138)\quad (0.001504)\quad (0.000100)\quad (9.000E\text{-}6)$$

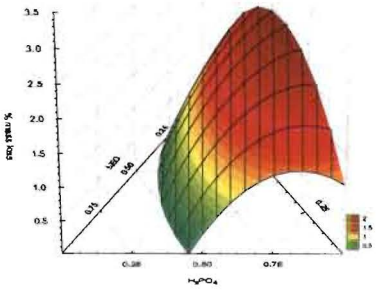

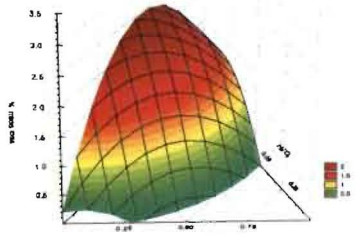

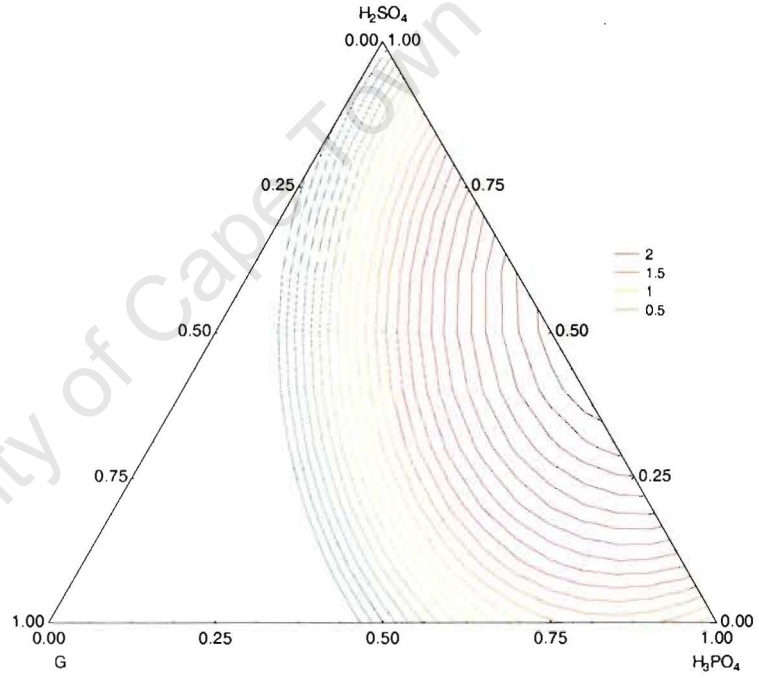

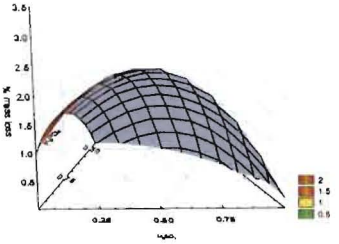

Figure 7.8: % mass loss response surface as a function of the electrolyte composition

Figure 7.7 shows that the region of optimum electrolyte compositions for an improved surface finish tends towards electrolytes with higher concentrations of H_3PO_4 and relatively moderate quantities of G.

Figure 7.8 on the other hand, shows that the region of optimum electrolyte compositions for the highest mass loss tends towards approximately equal concentrations of H_2SO_4 and H_3PO_4 without any G. However, the optimum region for highest mass loss is skewed towards a higher concentration of H_3PO_4 than one would expect. This is due to the fact that electrolytes 5, 6 and 7, which contained H_2SO_4 concentrations in excess of 80 volume percent but without any H_3PO_4, did not polish. Consequently, to accommodate this sudden drop in the response variable at the higher H_2SO_4 concentrations, the mathematical model tends to pull the response surface down prematurely. This therefore forecasts an optimum region biased towards a higher H_3PO_4 concentration compared to what would be expected based on the fact that H_2SO_4 is considerably more aggressive than H_3PO_4. Hence, for highest mass loss, the electrolyte should contain predominantly H_2SO_4 and just enough H_3PO_4 to initiate the electropolishing process. This is confirmed by the high mass loss achieved by electrolyte 12. In hindsight, the results for electrolytes 5, 6 and 7 could have been left out the analysis to achieve a more accurate picture of the response surface's optimum region, bearing in mind that electrolytes without H_3PO_4 do not electropolish.

With the response surfaces for SI and percent mass loss having an optimum region in different locations on their respective ternary diagrams, the two models were combined to form an SI + percent mass loss function so as to simultaneously optimise their response surfaces.

To avoid the overshadowing of one of the responses by the other due to variations in the range of each of the responses, each corresponding response was normalised by dividing it by the highest SI or percent mass loss value obtained for the initial experimental design. Hence, the SI response was divided by 0.86 whilst the percent mass loss response was divided by 2.5%. The normalised, combined function was then maximised using Microsoft Excel's Solver tool by iteratively varying the three electrolyte compositions subject to the constraint of G's concentration not exceeding 20 volume percent.

The optimum electrolyte using the technique described above was found to have the following composition:

Table 7.5: Optimum electrolyte composition based on combined SI + % mass loss response surface

Component	Volume %
G	14.24
H_3PO_4	55.66
H_2SO_4	30.00

The predicted SI and percent mass loss were 1.33 and 2.05% respectively, for this optimised electrolyte referred to as Electrolyte EO0 from this point onwards.

The performance of Electrolyte EO0 together with the Electrolytes 9 and 11, which achieved the best polishing results up to this point of the research, were then tested against that of the PS electrolyte. Two additional electrolyte compositions that were within the optimum region depicted in Figures 7.6 and 7.7 were also added to the final performance comparison experiments with the PS electrolyte. This work is described in more detail in the following section.

7.4.3 Performance comparison of the experimental design predicted electrolytes against the PS electrolyte

Selecting the two best electrolyte compositions

This marked the final phase in terms of the research into the possibility of enhancing quality and the rate of polishing based on the composition of the electrolyte. The electropolishing performances of the two best electrolytes (9 and 11) from the preceding experimental design together with the predicted optimal electrolyte EO0 and two additional electrolytes in the optimum region, EO1 and EO2 were compared to that of the PS electrolyte.

The compositions of the different electrolytes tested against the PS electrolyte in this phase of the work are shown in Table 7.6:

Table 7.6: Compositions of electrolytes used in performance comparison experiments

Electrolyte Number	G [volume %]	H_3PO_4 [volume %]	H_2SO_4 [volume %]
9	9.45	45.28	45.28
11	14.72	22.64	62.64
EO0	14.24	55.66	30.00
EO1	10	65	25
EO2	10	35	55

Identical polishing conditions of $2A/cm^2$, 80°C, $3cm^2$ of active polishing surface and 3 minutes polishing time were used for these experiments. The SI and mass loss results obtained using these electrolytes are shown in Figure 7.9:

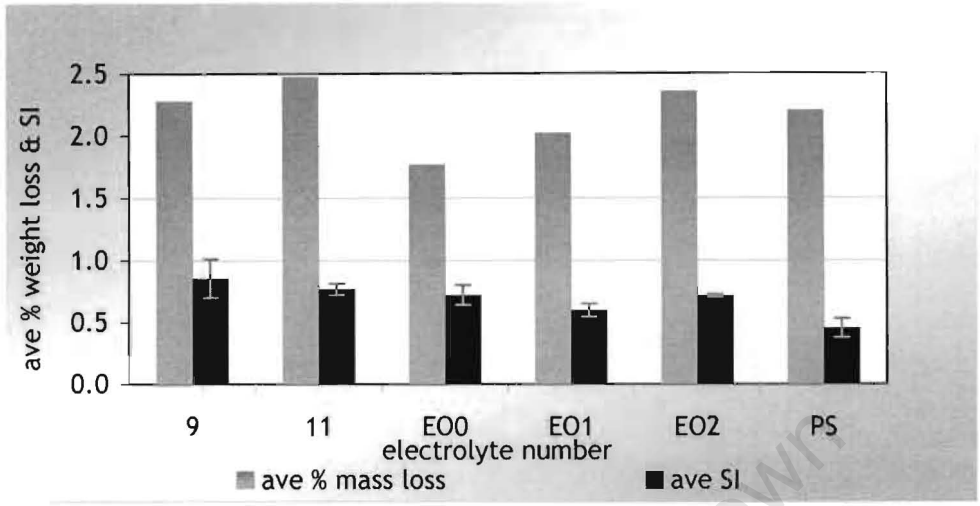

Figure 7.9: Performance comparison of new electrolytes against PS electrolyte

The results above show that all of the new electrolytes exhibit significantly enhanced performance over the PS electrolyte in terms of the SI value. With regard to the percent mass loss, all the new electrolytes apart from electrolytes EO0 and EO1 exhibit higher mass losses.

Electrolyte EO0, predicted to be the optimal electrolyte composition gave the third highest SI value after electrolytes 9 and 11 respectively. Its deviation from the predicted SI value of 1.33 can be attributed to the limitations of the mathematical model especially with respect to its inability to accurately model the sudden halt in polishing in the absence of H_3PO_4. To accommodate this sudden fall off in polishing performance, as discussed previously in this chapter, the model tends to pull the surface down prematurely, consequently predicting the optimum electrolyte composition at a higher H_3PO_4 concentration than it should.

With the electrolyte being optimised for an electropolishing process rather than a chemical machining one, the primary criterion for determining whether a specimen is polished or not is its visual appearance and not the amount of mass loss. Consequently, in determining the two potential successors to the PS electrolyte for any further pilot scale research, only the two electrolytes with the highest SI values were selected. Based on this selection criterion, electrolytes 9 and 11 were once again found to perform the best.

The fact that the two best electrolytes, 9 and 11, which although having the same G composition, differ quite significantly in terms of their H_2SO_4 and H_3PO_4 compositions, brings to light the need to perform further tests within this region of the ternary diagram to increase

the resolution of the response surface topography. This would provide a clearer picture in terms of the effect of the electrolyte composition on polishing performance and consequently facilitate a more accurate prediction of an optimum electrolyte.

It is important to note that, if a definite minimum polishing quality criterion in the form of an SI value is specified, the electrolyte that meets this minimum level of polishing with the lowest mass loss would be the preferred choice. The primary advantage of a lower mass loss is a longer electrolyte life due to a slower increase in the concentration of dissolved metal ions, which plays an increasingly significant role in the rate of polishing as the electrolyte ages.

Determining the shortest polishing time for electrolytes 9,11 and PS

In this phase of the work, tests were performed to determine the shortest polishing time for electrolytes 9 and 11 and these results were compared to that of the PS electrolyte.

Specimens were polished with each electrolyte for 0.5, 1 and 2 minutes. Both SI and the percent mass losses were measured. In line with the preceding experiments, the experimental conditions used were $2A/cm^2$, 80°C and $3cm^2$ of active polishing surface.

The results of the SI values achieved by these electrolytes with increasing polishing times are presented in Figure 7.10:

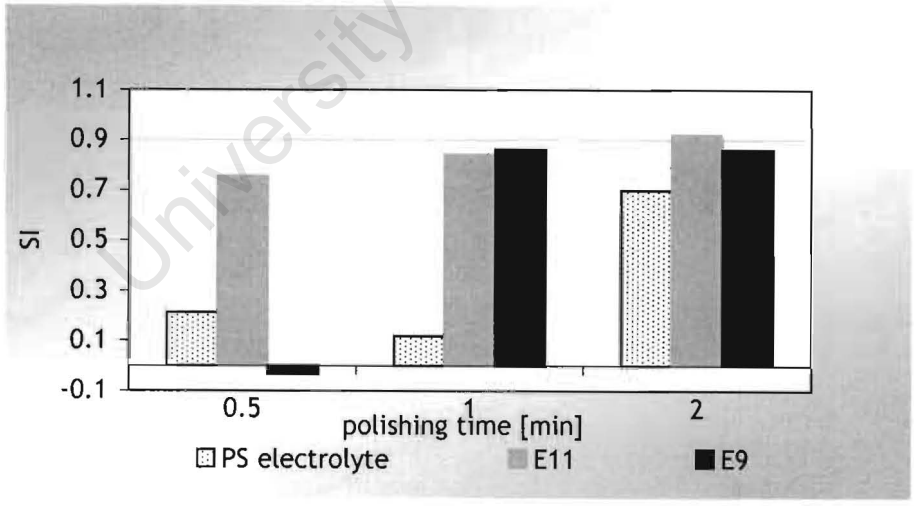

Figure 7.10: Change in SI with increasing polishing time for electrolytes 9, 11 & PS

The results above show that after one minute of polishing, both electrolytes 9 and 11 achieved SI values higher than that of the PS electrolyte. Moreover, the SI value achieved by electrolyte 11 after half a minute of polishing was higher even than that of the PS electrolyte after two minutes of polishing. The SI value for the PS electrolyte after one minute of

polishing is marginally lower than the value after 0.5 minutes of polishing. A possible explanation may be set in the surface irregularities on the metal surface prior to it being polished.

Nonetheless, electrolytes 9 and 11 clearly demonstrate their superiority in terms of the quality of the surface finish under laboratory scale conditions over the PS electrolyte.

In addition, these results highlight the significant improvement in polishing time over the PS electrolyte, as they are capable of achieving SI values in excess of 0.8 after only one minute of polishing.

The determination of the mass loss at this stage of the research was primarily to establish which electrolyte would potentially have a longer polishing life based on lower metal dissolution characteristics. The percent mass loss results with increasing polishing times are shown in Figure 7.11:

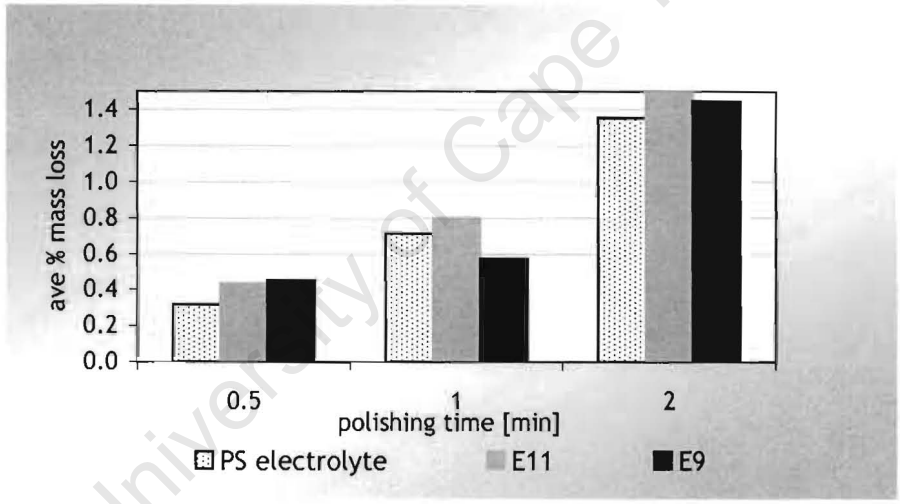

Figure 7.11: Change in % mass loss with increasing polishing time for electrolytes 9, 11 & PS

The graph above shows that after two minutes of polishing, the percent mass loss for both electrolytes 9 and 11 are marginally higher than that of the PS electrolyte. Of the two new electrolytes, electrolyte 9 appears to exhibit characteristics of a longer operating electrolyte life based on its lower mass loss.

The effect of the concentration of dissolved metal ions in the electrolyte on polishing performance

As a final test before deciding on a the best electrolyte composition, an additional set of experiments to determine the performance characteristics of electrolytes 9 and 11 with increasing dissolved metal ions were performed and compared to that of the PS electrolyte.

For this study, electrolyte mixtures corresponding to electrolytes 9, 11 and PS with dissolved metal ions ranging from 0 - 30g/l were prepared. This was achieved by adding the required amount of dissolved metal ions using spent industrial PS electrolyte and subsequently adding the corrected ratios of the three components so as to achieve each electrolyte's characteristic relative ratio of the three components. Each experiment was performed at $2A/cm^2$, an active polishing surface of $3cm^2$ and a total polishing time of 3 minutes at 80°C. The SI value and mass loss results of this study are shown below in Figures 7.12 and 7.13 respectively:

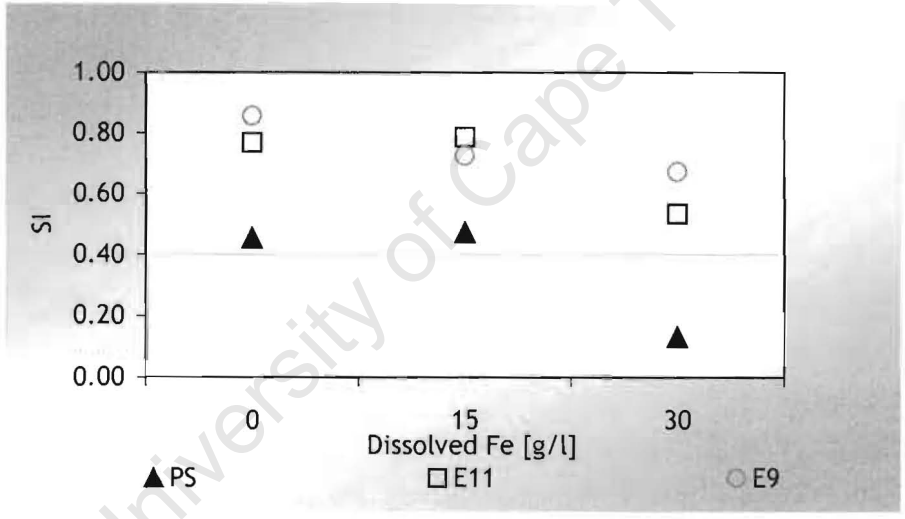

Figure 7.12: Effect of increased dissolved metal ions on SI

In terms of the surface finishing quality, the SI values show that both electrolytes 9 and 11 continue to exhibit their superiority over the PS electrolyte. The fact that the SI values for both electrolytes 9 and 11 at 30g/l are higher than that of PS without any dissolved metal ions, further substantiates this point. The results also show the similarity in performance between electrolytes 9 and 11, with an additional selection criterion such as the mass loss - electrolyte life relationship necessary to decide on the better of the two.

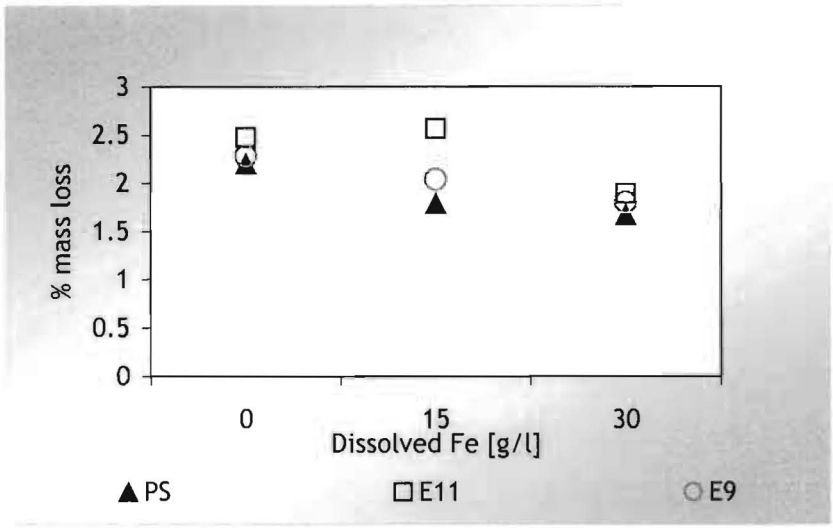

Figure 7.13: Effect of increased dissolved metal ions on % average mass loss

From Figure 7.13 above, it is evident that in terms of the decrease in percent mass loss with increasing dissolved metal ions in solution; electrolyte 9 shows a similar trend in the drop in performance when compared to the PS electrolyte. Electrolyte 11 maintains its initial performance even after a dissolved metal ion concentration of 15g/l. This can be attributed to its higher metal oxidising potential as a result of it having a higher H_2SO_4 concentration than either the PS electrolyte or electrolyte 9. However, the higher mass loss characteristics exhibited by electrolyte 11 mean that this electrolyte will reach its saturation limit in terms of dissolved metal ions more rapidly than either of electrolytes 9 or the PS electrolyte and would therefore need to replaced sooner.

7.5 Conclusions on optimisation of electrolyte composition

Based on the findings presented throughout this chapter, electrolytes 9 and 11 have shown the best electropolishing characteristics in terms of polishing quality and shortest polishing time. Electrolyte 11 with its lower H_3PO_4 concentration would be cheaper to produce than electrolyte 9. However, its higher mass loss characteristics imply that it would need to be replaced sooner and therefore offset its lower cost. Therefore based on overall performance, electrolyte 9, containing 9.45% G, 45.275% H_2SO_4 and 45.275% H_3PO_4 by volume, was determined to be the optimum electrolyte composition for the polishing of 304 stainless steel.

Chapter 8

Determining the metal ion speciation characteristics of the PS electrolyte

8.1 Introduction

The objective of this phase of the work was to establish the metal ion speciation characteristics of the PS electrolyte. This was to identify the predominant species in the spent electrolyte and to investigate the possibility of precipitating this species, consequently reducing the dissolved metal ion concentration in the electrolyte. This would reduce the slowing down of metal dissolution caused by a decrease in the driving force for dissolution as the electrolyte approaches saturation with respect to the dissolved metal ions.

8.2 Thermodynamic modelling

Metal ion speciation in an aqueous system is usually determined thermodynamically and presented in the form of a Pourbaix diagram. OLI Systems Inc. (2003) software, which provides a predictive thermodynamic framework for calculating the physical and chemical properties of multi-phase, aqueous-based systems, was used. Specifically, OLI systems Corrosion Analyser (version 1.2) aqueous modelling software was used to generate the relevant Pourbaix diagrams.

As with all aqueous modelling tools there is a limitation in terms of the minimum water requirement and the OLI software requires a minimum water content of 60 mole percent. Due to the highly acidic nature of the electrolyte and particularly low water content, this research was primarily aimed at determining the dominating species rather than their exact solubility in the electrolyte. Therefore, the modelling was carried out with the following simplification. The system was modelled using the minimum water content (60 mole %) required to solve the speciation thermodynamics whilst maintaining the exact ratio of the components making up the electrolyte.

The implications of this simplification were that the pH of the system was slightly raised and hence the position of the dominating species in terms of the pH would shift marginally to the left of the Pourbaix diagram. Notwithstanding this, the Pourbaix diagram would still identify the form of the dominant species, which was essentially of primary interest.

8.3 Interpreting a Pourbaix diagram

8.3.1 What the solid lines represent

The solid lines on a Pourbaix diagram represent (Vieler, 2002):

1. The boundaries between stability areas of a solid and an aqueous species or two aqueous species
2. The boundary between an aqueous and solid species where a solid starts to precipitate or dissolve in an aqueous phase
3. The boundary between two aqueous species.

8.3.2 What the dashed lines represent

The dashed lines are only found within the stability ranges of solids and represent the boundaries between stability areas of two aqueous species that coexist with at least one solid phase.

8.3.3 What the areas delimited by the solid lines represent

These represent the stability fields of solid or aqueous species. When conditions are within the stability field of a solid, the solid is stable and usually coexists with an aqueous phase. On the other hand, if the conditions are within the stability field of an aqueous species, a solid cannot be stable and consequently, that species is predominantly in the solution.

8.3.4 What the areas delimited by the dashed lines represent

These present stability fields of predominant aqueous species that coexist with one or more solid phases. Moreover, the dashed lines can only be found within the stability fields of solid species. In the Pourbaix diagrams shown in Figures 8.1 and 8.2, the names of aqueous species that are predominant only in the presence of a solid phase and not in a homogeneous solution are represented with small characters.

8.3.5 What the line denoted by "a" and "b" represents

This line denoted by "a" represents the equilibrium state between H^+ and H_2O, with the oxidised form (H^+) stable above this line and the reduced form (H_2O) stable below it. The line denoted by "b" represents the equilibrium state between O_2 and O^{2-}, with the oxidised form (O_2) stable above this line and the reduced form (O^{2-}) stable below it. Water, being a combination of H^+ and O^{2-}, is stable between "a" and "b" (Vieler, 2002).

8.4 Chemical analysis of spent PS electrolyte

This analysis was performed to establish the concentration of dissolved metal ions in the spent PS electrolyte so that a Pourbaix diagram based on those conditions could be generated. In addition, the pH and redox potential were determined in order to identify the current operating region of the PS electrolyte within the generated Pourbaix diagram.

A sample of spent PS electrolyte obtained from the industrial plant was analysed using atomic absorption to determine the relative quantities of dissolved iron, chromium and nickel ions in solution. The pH and redox potential were also determined. The results of this analysis are shown in Table 8.1:

Table 8.1: Analysis results of spent PS electrolyte

[Fe]	62580 ppm
[Cr]	16620 ppm
[Ni]	4244 ppm
pH	-1.65
Redox potential	506 mV

8.5 Pourbaix diagram for spent PS electrolyte

Using the electrolyte characteristics shown in Table 8.1, Pourbaix diagrams for the iron, which is the predominant metal in stainless steel as well as the Pourbaix diagram for 304 stainless steel were generated. These are shown in Figures 8.1 and 8.2 below:

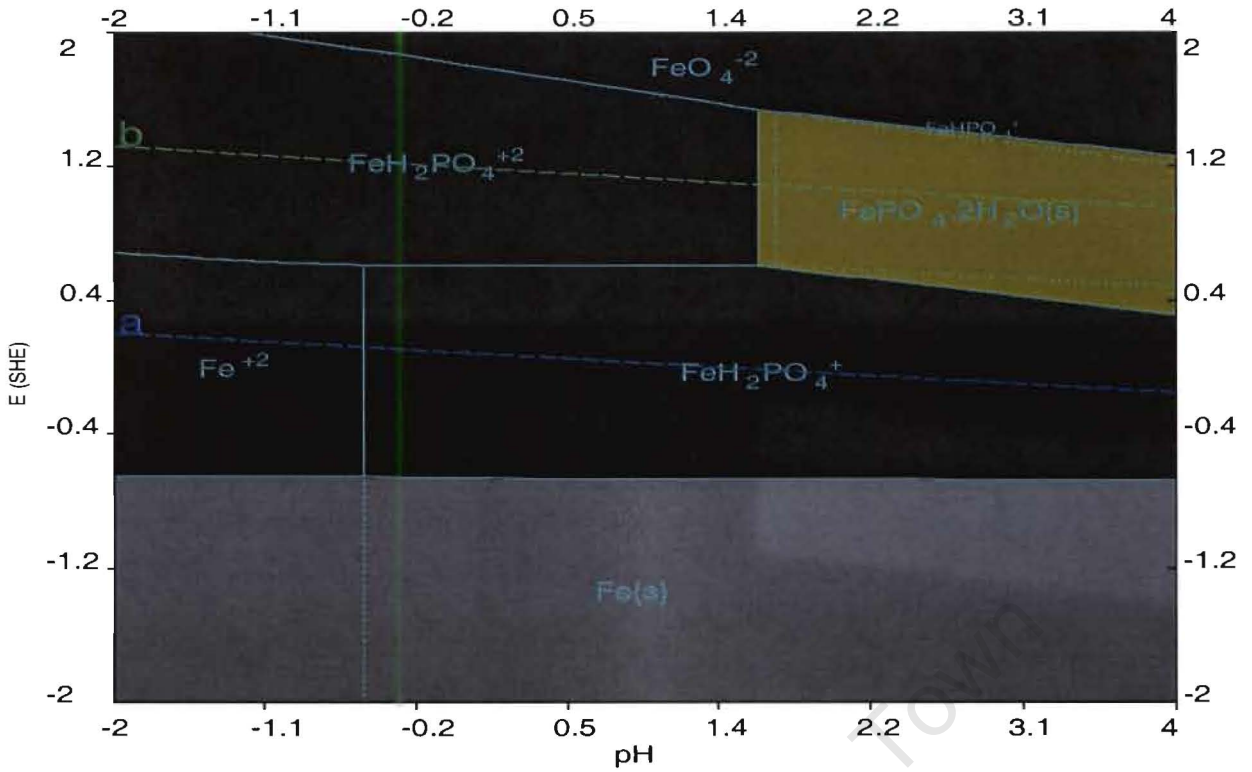

Figure 8.1: Pourbaix diagram for iron at PS electrolyte composition

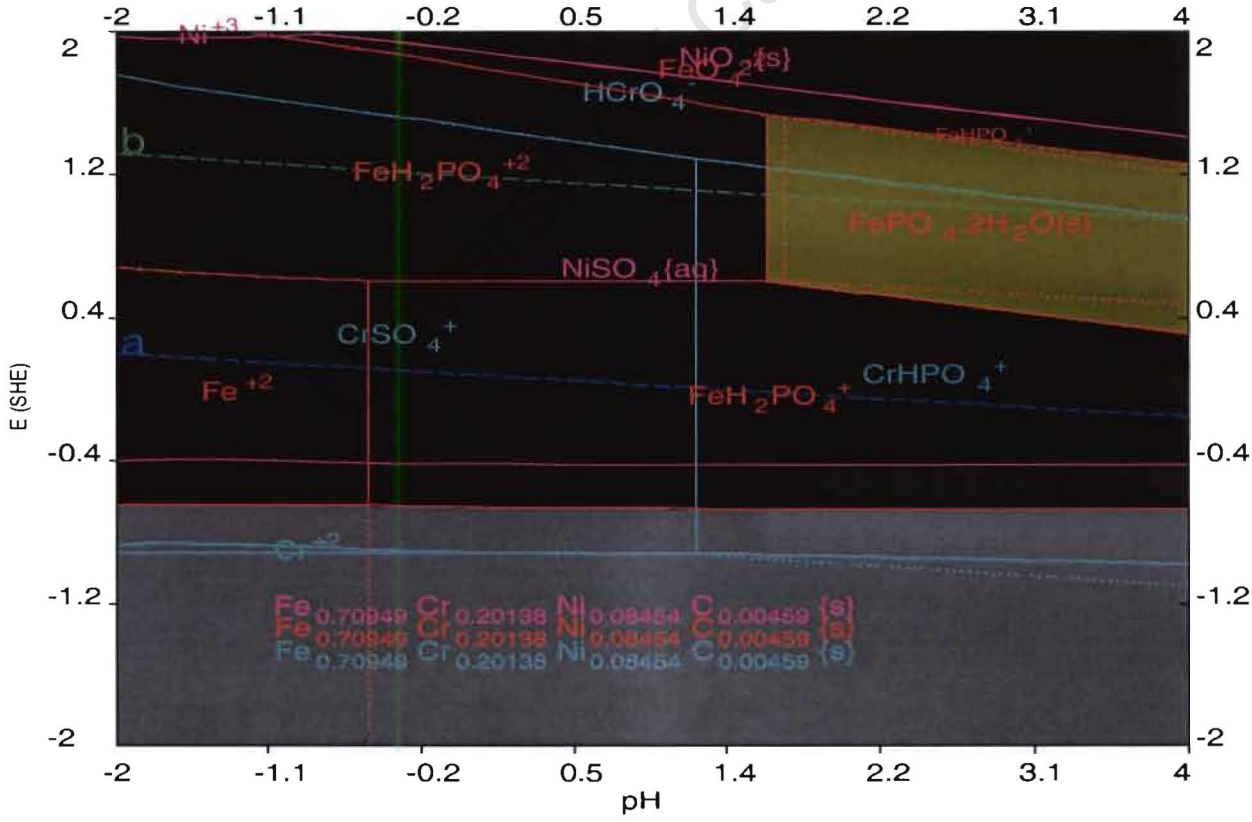

Figure 8.2: Pourbaix diagram for 304 stainless steel at PS electrolyte composition

Based on the Pourbaix diagrams shown above, the dominant species in the range of the PS electrolyte redox potential shown in Table 8.1 is $FeH_2PO_4^+$. However, to precipitate this species out, the pH of the electrolyte will need to be significantly raised, consequently altering the composition of the electrolyte and impacting on its polishing performance. Alternatively, the solubility of the iron in the electrolyte could be reduced to cause the iron species to precipitate at dissolved iron concentrations lower than the present level of 62g/l. Referring to Figure 8.3, this could be carried out by increasing the phosphate concentration from P1 to P2, which would serve to move the system down the solubility curve from point A towards point B as depicted in the solubility diagram shown below:

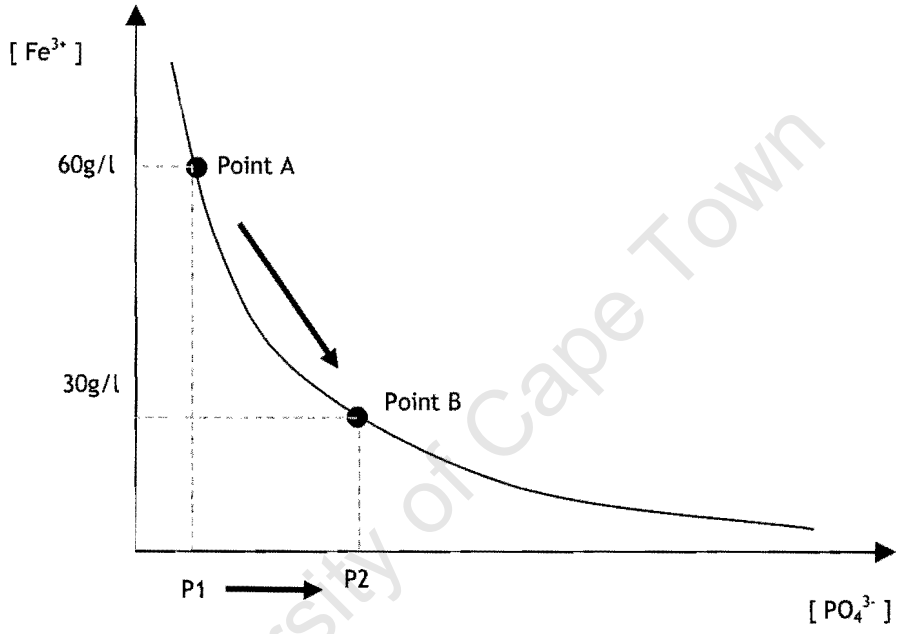

Figure 8.3: Generic solubility curve for Fe^{3+}: PO_4^{3-} system for illustration purposes

However, the addition of phosphate species in the form of phosphoric acid to carry out this process would also alter the composition of the electrolyte, affecting its performance excluding this as a viable option to extending the electrolytes performance life.

Removing the sludge formed and topping the bath up with fresh electrolyte after the electrolyte ages and reaches its metal ion solubility limit appears to be the easiest way of improving the driving force for metal dissolution, consequently extending the operating life of the electrolyte.

Chapter 9

Conclusions and recommendations

Having initially set out to reduce the electropolishing time for 304 stainless steel, the following conclusions can be drawn with respect to the degree of success to which this goal was achieved, as well as, the understanding acquired with regards to the effect of operating parameters on the quality and rate of electropolishing.

Pertaining to the performance of the currently used electrolyte (PS electrolyte):

- The PS electrolyte - 304 stainless steel system, as with most phosphoric acid - iron systems, does not exhibit a clear polishing plateau region on the voltage - current density plot. A recommendation for future work with respect to this is to refine this relationship using a smaller voltage step size;

- By measuring the polishing quality (SI) at increasing operating current densities, the optimal current density operating range was found to be between 1 and 2A/cm^2. It must taken into consideration that this choice excludes economic factors such as increased electricity costs of operating at a higher current density;

- When operating at 2A/cm^2, a polishing time of three minutes was achieved. This substantial reduction in polishing time, compared to the current plant polishing time of 10 minutes, can primarily be attributed to the plant operating at a current density well below the optimum range. Thus operating the plant at a current density as close to 2A/cm^2 as possible, based on limitations of the power supply, forms one of the most important recommendations to come out of this research;

With regards to finding the optimum electrolyte composition and operating conditions:

- The effect of varying the current density and temperature within the ranges investigated showed insignificant impact on the polishing quality and rate when compared to impact of varying electrolyte composition. In light of this, future tests at a wider temperature range need to be performed to determine the impact of temperature on polishing performance;

- Electrolytes without H_3PO_4 did not undergo electropolishing;

- The H_3PO_4 - H_2SO_4 interaction was found to play the most significant role in terms of the rate of electropolishing while the interaction of increasing amounts of the diol G with the two acids was found to have a positive influence on the polishing quality.

Based on RSM, the relationship between the polishing quality (SI) and rate (% mass loss) to the compositions of the components making up the electrolyte was found to be (standard errors for each of the parameter estimates are shown in parenthesis):

$$SI = -0.630291G - 0.006237P - 0.038737S + 0.007922GP + 0.007328GS + 0.003105PS + 7.8705E\text{-}5GPS$$
$$(0.221460)\quad (0.003941)\quad (0.003941)\quad (0.002773)\quad (0.002773)\quad (0.001351)\quad (0.000018)$$

$$\%\ mass\ loss = -0.045769G + 0.010399P + 0.001948S + 0.000825GP + 0.000567GS + 0.000738PS - 2.875E\text{-}6GPS$$
$$(0.120150)\quad (0.002138)\quad (0.002138)\quad (0.001504)\quad (0.001504)\quad (0.000100)\quad (9.000E\text{-}6)$$

- The optimum electrolyte composition predicted by the simultaneous optimisation of the SI and percentage mass loss responses was found to be one with 14.24% G, 55.66% H_3PO_4 and 30% H_2SO_4 by volume;

- Reanalysing the experimental design data without the data for electrolytes 5, 6 and 7 should provide a more refined prediction of the optimum electrolyte composition;

- After an exhaustive selection process for determining the best electrolyte, an electrolyte containing 9.45% G, 45.275% H_3PO_4 and 45.275% H_2SO_4 by volume was found to be the optimum for the electropolishing of 304 stainless steel.

The metal ion speciation characteristics of the spent PS electrolyte based on thermodynamic modelling were established. It was found that the precipitation of dissolved metal ions from solution in order to increase the rate of polishing and the electrolyte life could not be achieved without drastically changing the electrolytes composition and therefore the electrolytes polishing performance. Consequently, decanting a portion of the spent bath and topping it up with fresh electrolyte appears to be the easiest method of maintaining the driving force for electropolishing and extending the overall electrolyte life.

Of the three methods investigated for measuring surface roughness, the image processing of a Nomarski microscope acquired digital image appears to give the most accurate results in terms of the overall representation of the surface roughness. However, there is still considerable room for improvement in this technique especially in terms of the weaknesses exposed in distinguishing between macro roughness in the form of manufacturing defects and the micro roughness characteristics as a result of the electropolishing process. Thus when performing any future work, all the metal specimens should be ground to the same

surface roughness prior to polishing. This will significantly improve the accuracy and reproducibility of the results.

Further recommendations for future work include:

- Establishing a fundamental understanding of the role played by the electrical conductivity, viscosity and diffusivity on the electropolishing performance. Establishing mathematical relationships between these parameters could potentially lay the foundation for developing simulation capabilities for this process;

- Investigating the effect of the distance between the anode and cathode on the polishing performance;

- Initiating pilot scale studies using the key results from this work before implementing the findings at industrial scale.

Chapter 10

References & Bibliography

10.1 References

ASME B46.1-1995, (1996). Surface Texture (Surface Roughness, Waviness, and Lay). An American National Standard, American Society of Mechanical Engineers, ISBN 0 7918 2356 3.

Betova, I., Bojinov, M., Tzvetkoff, T., (2003). Role of surface reactions in the transpassive dissolution of ferrous alloys in concentrated H_3PO_4. *Applied Surface Science*, (article in press)

Datta, M., Vega, L., Romankiw, L., Duby, P., (1992). Mass transport effects during electropolishing of iron in phosphoric-sulphuric acid. *Electrochimica Acta,* **37**, p2469-2475.

Delayen, J., Mammosser, J., Phillips, L., Wu, A., (2001). Alternate electrolyte composition for electropolishing of niobium surfaces. *Proceedings of the 10th Workshop on RF superconductivity*; Tsukuba City, Japan; September 6-11, 2001.

Electropolishing, A user's guide to applications, quality standards and specifications, 8th edition, (1998). *Delstar Corporation.*

Faust, C.L., (1976). Heat treating, cleaning and finishing. *Metals handbook*, 8th Edition, p484-488.

Green, W., (1998). Digital Image Processing, A systems approach. p1-23.

Hensel, K., (2003). Electropolishing. *Surface treatments*, www.ep-systems.com; 8/04/2003

Hoare, J.P., Laboda, M.A., (1981). Electrochemical machining. In: Bockris, J., Conway, B., Yeager, E., White, R., (1981). Electrochemical Processing. *Comprehensive Treatise of Electrochemistry*, **2**, p399-520.

Hocheng, H., Kao, P., Chen, Y., (2001). Electropolishing of 316L stainless steel for anticorrosion passivation. *Journal of materials engineering and performance*, **10(4)**.

Kish, J.R., Ives, M.B., Rodda, J.R., (2003). Anodic behaviour of stainless steel S43000 in concentrated solutions of sulphuric acid. *Corrosion Science*, **45**, p1571-1594.

Landolt, D., (1986). Fundamental aspects of electropolishing. *Electrochimica Acta*, **32**, p1-11.

Metals Handbook, 2nd edition, (1998). ASM International; p1367-1370.

Taylor-Hobson, (1995). Surtronic 3P operating instructions manual. Taylor-Hobson

Twidwell, L., O'Keefe, J., Ettel, V., Robinson, J., (1992). Unit processes in extractive metallurgy. *Electrometallurgy*.

Vieler, A., (2002). Aqueous systems modelling course notes, OLI Systems Inc. Modelling course and workshop; University of Cape Town, 14 - 15th January, 2002

Walpole, R.E., Myers, R.H., (1985). *Probability and Statistics for Engineers and Scientists*; 3rd Edition; Macmillan Publishing Company.

Wyant, J., (2003). Optics course notes, University of Arizona; http://www.optics.arizona.edu/jcwyant/Short_Courses/SIRA/4-MeasurementOfSurfaceQuality.pdf, 11/08/03

Younis, M., (1998). Online surface roughness measurements using image processing towards adaptive control. *Computers ind. Engng*, **35**, p49-52.

10.2 Bibliography

Chappard, D., Degasne, I., Hure, G., Legrand, E., Audran, M., Basle, M., (2002). Image analysis measurements of roughness by texture and fractal analysis correlate with contact profilometry. *Biomaterials*, **24**, p1399-1407.

Datta, M., Landolt, D., (1999). Fundamental aspects and applications of electrochemical microfabrication. *Electrochimica Acta*, **45**, p2535-2558.

Datta, M., Vega, L., Romankiw, L., Duby, P., (1992). Mass transport effects during electropolishing of iron in phosphoric-sulphuric acids. *Electrochimica Acta*, **37**, p2496-2475.

Drazic, D., Popic, J., (2002). Dissolution of chromium in sulphuric acid. *J. Serb. Chem. Soc.*, **67(11)**, p777-782

Hocheng, H., Pa, P.S., (1998). Electropolishing and electrobrightening of holes using different feeding electrodes. *Journal of materials processing technology*, **89-90**, p440-446

Juttner, K., Galla, U., Schmieder, H., (1999). Electrochemical approaches to environmental problems in the process industry. *Electrochimica Acta*, **45**, p2575-2594.

Murali, S., Ramachandra, M., Murthy, K.S.S., Raman, K.S., (1997). Electropolishing of Al-7Si-0.3Mg cast alloy by using perchloric and nitric acid electrolytes. *Materials characterization*, **38**, p273-286.

Piotrowski, O., Madore, C., Landolt, D., (1998). Electropolishing of tantalum in sulphuric acid-methanol electrolytes. *Electrochimica Acta*, **44**, p3389-3399.

Sazou, D., (1997). Current oscillations and mass transport control during electrodissolution of iron in phosphoric acid solutions. *Electrochimica Acta*, **42**, p627-637.

Sedahmed, G., Abdo, M.S., Kamal, M.A., Fadaly, O.A., Osman, H.M., (2001). A mass transfer study of the electropolishing of metals in mechanically agitated vessels. *Int. Comm. Heat Mass Transfer*, **28(2)**, p257-265.

Sedahmed, G., Abdo, M.S., Kamal, M.A., Fadaly, O.A., Osman, H.M., (2000). Effect of gas sparging on the rate of mass transfer during electropolishing of vertical plates. *Chemical engineering and processing*, **40**, p195-200.

Singh, V.B., Upadhyay, B.N., (1998). The electrochemical behaviour of (Cr-1Mo steel in concentrated acid solution mixtures. *Corrosion Science*, **40**, p705-713

Smithells, C.L., (1967). Metals reference book, **1**, 4th Edition, Butterworths, London

Zhou, X., Thompson, G.E., Habazaki, H., Shimizu, K., Skeldon, P., Wood, G.C., (1997). Copper enrichment in Al-Cu alloys due to electropolishing and anodic oxidation. *Thin solid films*, **293**, p327-332.

Appendices

Appendix 1: Experimental data - Mapping and optimising the performance of PS electrolyte

Appendix 2: Experimental data - Optimising electrolyte composition

Appendix 3: Statistical analysis - Optimising electrolyte composition

Appendix 4: MATLAB® script file for measuring SI

Appendix 1

Experimental data - Mapping & optimising the performance of PS electrolyte

Experiment I.D.	A1
Aim of experiment	To establish PS electrolyte-304 SS voltage-current density relationship, limiting current & optimum operating current density
Exposed surface area	3cm^2
Temperature	80°C

Results:

Voltage	*current*	*current density*
[V]	*[A]*	*[A/cm^2]*
0.5	0	0.000
1	0	0.000
1.5	0.02	0.007
2	0.25	0.083
2.5	0.26	0.087
3	0.53	0.177
3.5	0.81	0.270
4	1.14	0.380
4.5	1.5	0.500
5	1.83	0.610
5.5	2.2	0.733
6	2.62	0.873
6.5	3	1.000
7	3.46	1.153
7.5	3.9	1.300
8	4.4	1.467
8.5	4.85	1.617
9	5.45	1.817
10	6.44	2.147
11	7.6	2.533

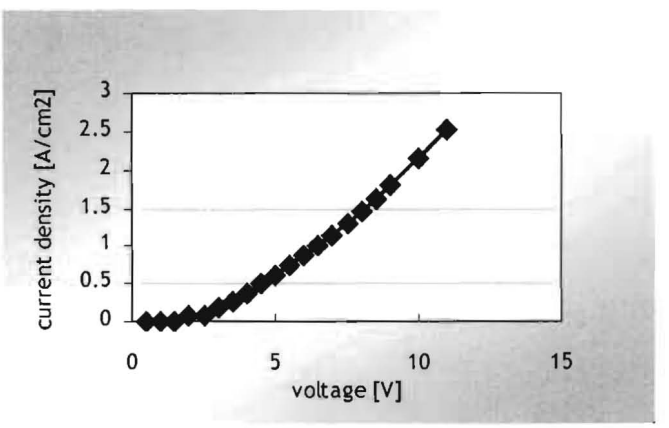

Experiment I.D.	A3
Aim of experiment	Establishing the optimum operating current for PS electrolyte based on polishing quality achieved at increasing current densities
Exposed surface area	$3cm^2$
Temperature	80°C

Results:

sample no.	*polishing time*	*current density*	*initial weight*	*final weight*	*weight loss*	*average SI*
	[mins]	*[A/cm²]*	*[g]*	*[g]*	*[g]*	
A3-1	3	0.5	5.350	5.320	0.030	0.561
A3-2	3	1	5.460	5.410	0.050	0.995
A3-3	3	1.5	5.630	5.550	0.080	1.009
A3-4	3	2	5.420	5.310	0.110	0.994
A3-5	3	2.5	5.450	5.330	0.120	0.828

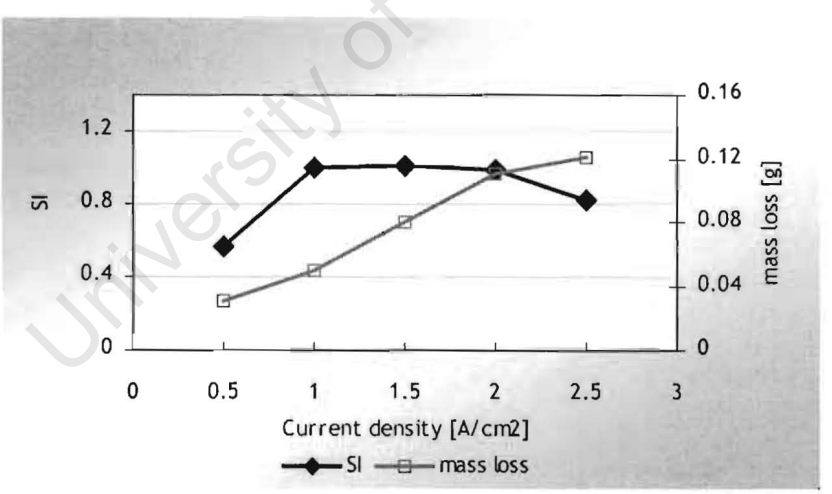

Experiment I.D.	A2
Aim of experiment	Determining shortest possible polishing time for PS electrolyte
Exposed surface area	$3cm^2$
Temperature	80°C

Results:

sample no.	*polishing time*	*initial weight*	*final weight*	*weight loss*	*SI*
	[mins]	*[g]*	*[g]*	*[g]*	
AA2-0	0.25	5.650	5.640	0.010	-0.821
AA2-1	0.5	5.580	5.570	0.010	-0.369
AA2-2	1	5.550	5.530	0.020	0.836
AA2-3	2	5.490	5.430	0.060	1.098
AA2-4	3	5.730	5.630	0.100	1.095
AA2-5	4	5.730	5.610	0.120	1.001
AA2-6	5	5.360	5.200	0.160	0.638

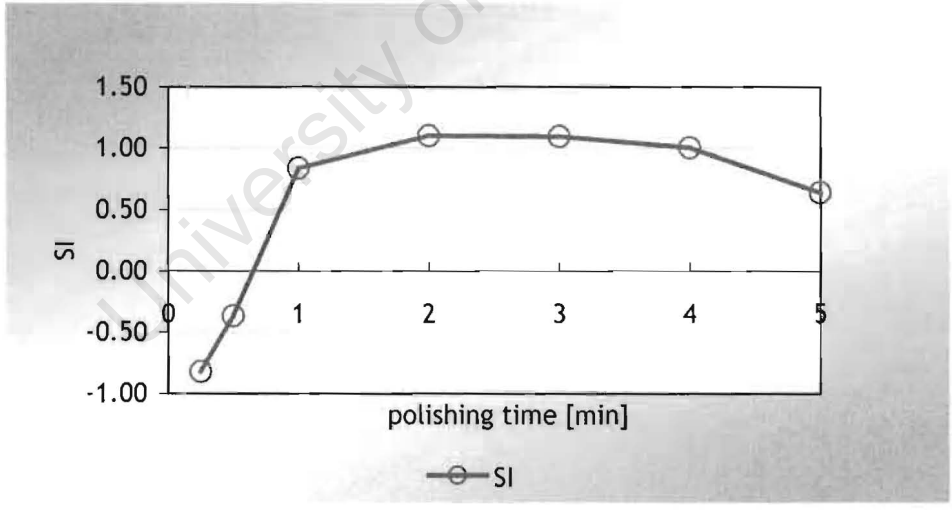

Appendix 2

Experimental data - Optimisation of electrolyte composition

Experiment I.D.	PS expt
Aim of experiment	To establish the effect of polishing 5 samples on the polishing performance of PS electrolyte - to determine if the same electrolyte can be used to perform all 4 optimisation expts.
Exposed surface area	$3cm^2$
Temperature	80°C

Results:

sample no.	*polishing time*	*current density*	*initial weight*	*final weight*	*weight loss*	*%weight loss*	*Average SI*
	[mins]	*[A/cm²]*	*[g]*	*[g]*	*[g]*	*[%]*	
PS1	3	2	5.605	5.480	0.125	2.232	0.478
PS2	3	2	5.701	5.579	0.123	2.150	0.564
PS3	3	2	5.478	5.355	0.123	2.252	0.627
PS4	3	2	5.541	5.418	0.123	2.216	0.543
PS5	3	2	5.675	5.553	0.122	2.151	0.431

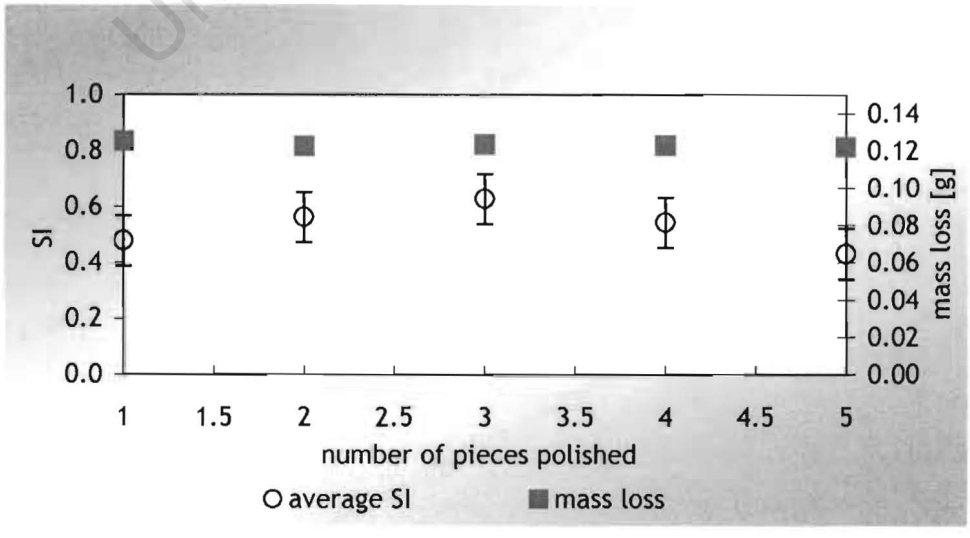

Experiment I.D.	B expts
Aim of experiment	Optimisation of electrolyte composition.
Exposed surface area	$3cm^2$
Temperature	70 & 80°C

Results:

Raw data for B expt

Electrolyte	*G*	*H3PO4*	*H2SO4*	*Current density*	*Temperature*	*mass loss*	*Ave SI*
no	*%*	*%*	*%*	*[A/cm²]*	*[°C]*	*%*	
1	0	100	0	1.5	70	1.058	-0.154
1	0	100	0	2	70	1.439	-0.792
1	0	100	0	1.5	80	1.111	-0.359
1	0	100	0	2	80	1.384	0.021
2	10	90	0	1.5	70	1.119	-0.359
2	10	90	0	2	70	1.408	0.099
2	10	90	0	1.5	80	0.919	-0.229
2	10	90	0	2	80	1.401	0.247
3	20	80	0	1.5	70	1.257	-0.417
3	20	80	0	2	70	1.521	-0.035
3	20	80	0	1.5	80	1.308	0.888
3	20	80	0	2	80	1.685	0.159
4	20	40	40	1.5	70	1.316	0.449
4	20	40	40	2	70	2.015	0.294
4	20	40	40	1.5	80	1.473	0.850
4	20	40	40	2	80	1.808	0.494
5	20	0	80	1.5	70	0.000	-4.000
5	20	0	80	2	70	0.000	-4.000
5	20	0	80	1.5	80	0.000	-4.000
5	20	0	80	2	80	0.000	-4.000
6	10	0	90	1.5	70	0.000	-4.000
6	10	0	90	2	70	0.000	-4.000
6	10	0	90	1.5	80	0.000	-4.000
6	10	0	90	2	80	0.000	-4.000
7	0	0	100	1.5	70	0.000	-4.000
7	0	0	100	2	70	0.000	-4.000
7	0	0	100	1.5	80	0.000	-4.000
7	0	0	100	2	80	0.000	-4.000
8	0	50	50	1.5	70	1.855	0.333
8	0	50	50	2	70	2.693	-1.303
8	0	50	50	1.5	80	1.968	-3.515

8	0	50	50	2	80	2.878	-3.402
9	9.45	45.275	45.275	1.5	70	1.465	0.954
9	9.45	45.275	45.275	2	70	2.116	0.746
9	9.45	45.275	45.275	1.5	80	1.633	0.774
9	9.45	45.275	45.275	2	80	2.448	0.967
10	14.72	62.64	22.64	1.5	70	1.439	0.526
10	14.72	62.64	22.64	2	70	1.795	0.780
10	14.72	62.64	22.64	1.5	80	1.457	0.499
10	14.72	62.64	22.64	2	80	2.015	0.402
11	14.72	22.64	62.64	1.5	70	1.416	0.714
11	14.72	22.64	62.64	2	70	2.465	0.800
11	14.72	22.64	62.64	1.5	80	1.842	0.918
11	14.72	22.64	62.64	2	80	2.491	0.736
12	4.72	22.64	72.64	1.5	70	1.954	0.444
12	4.72	22.64	72.64	2	70	2.867	0.029
12	4.72	22.64	72.64	1.5	80	2.026	0.038
12	4.72	22.64	72.64	2	80	2.564	-0.511
13	4.72	72.64	22.64	1.5	70	1.504	0.403
13	4.72	72.64	22.64	2	70	2.075	0.924
13	4.72	72.64	22.64	1.5	80	1.465	0.684
13	4.72	72.64	22.64	2	80	2.007	0.389

Experiement ID :	B expt
Aim :	Optimisation of electrolyte composition

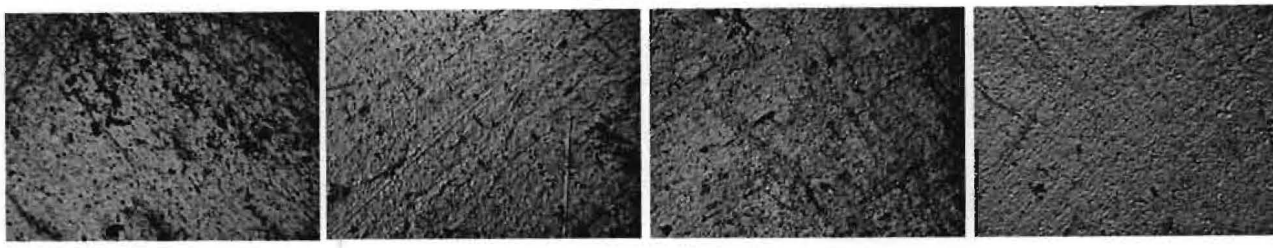

Electrolyte 1 1.5A/cm2; 70oC 2A/cm2; 70oC 1.5A/cm2; 80oC 2A/cm2; 80oC

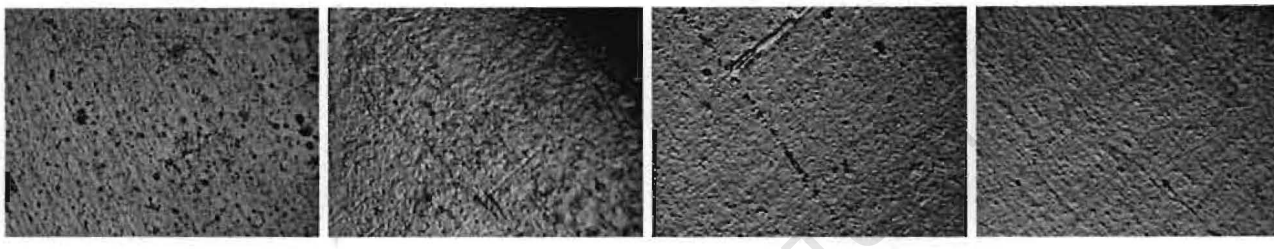

Electrolyte 2 1.5A/cm2; 70oC 2A/cm2; 70oC 1.5A/cm2; 80oC 2A/cm2; 80oC

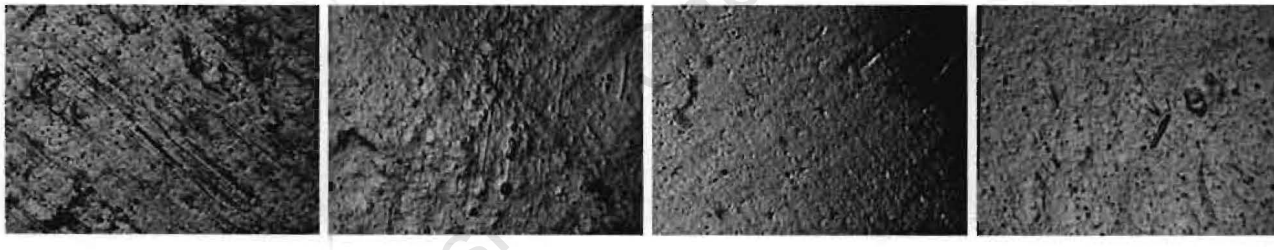

Electrolyte 3 1.5A/cm2; 70oC 2A/cm2; 70oC 1.5A/cm2; 80oC 2A/cm2; 80oC

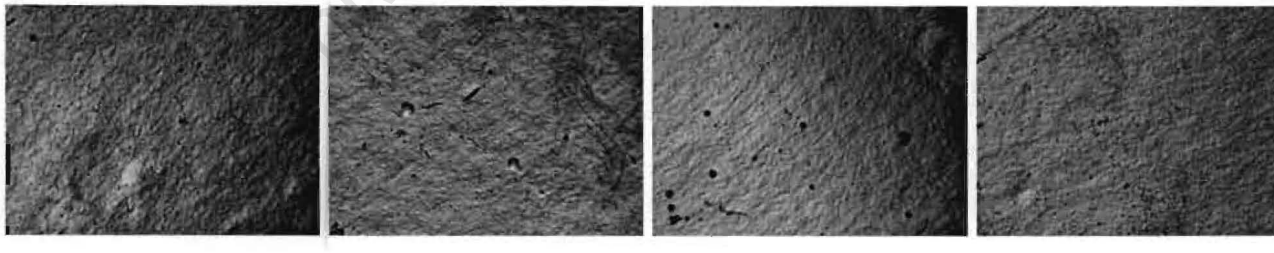

Electrolyte 4 1.5A/cm2; 70oC 2A/cm2; 70oC 1.5A/cm2; 80oC 2A/cm2; 80oC

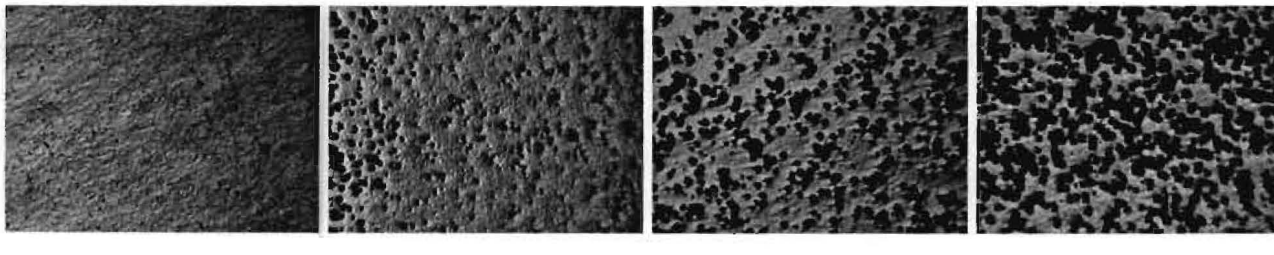

Electrolyte 8 1.5A/cm2; 70oC 2A/cm2; 70oC 1.5A/cm2; 80oC 2A/cm2; 80oC

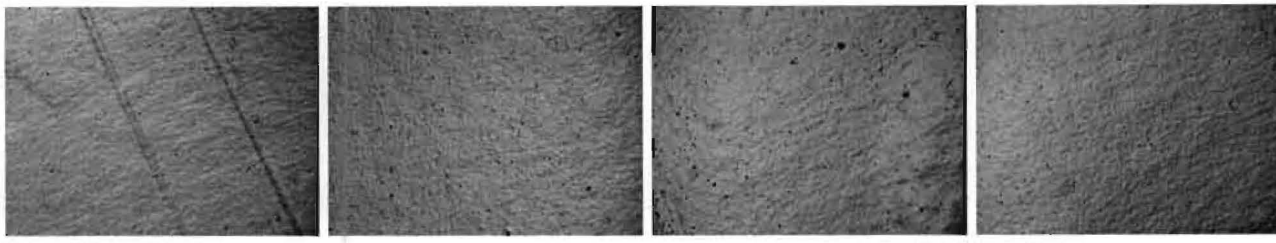

Electrolyte 9 1.5A/cm2; 70oC 2A/cm2; 70oC 1.5A/cm2; 80oC 2A/cm2; 80oC

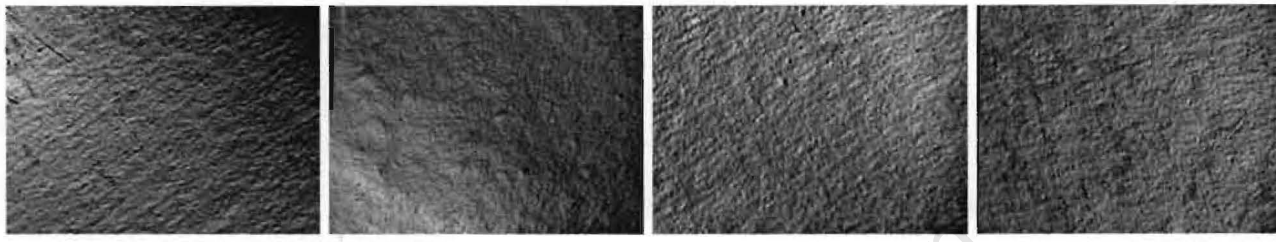

Electrolyte 10 1.5A/cm2; 70oC 2A/cm2; 70oC 1.5A/cm2; 80oC 2A/cm2; 80oC

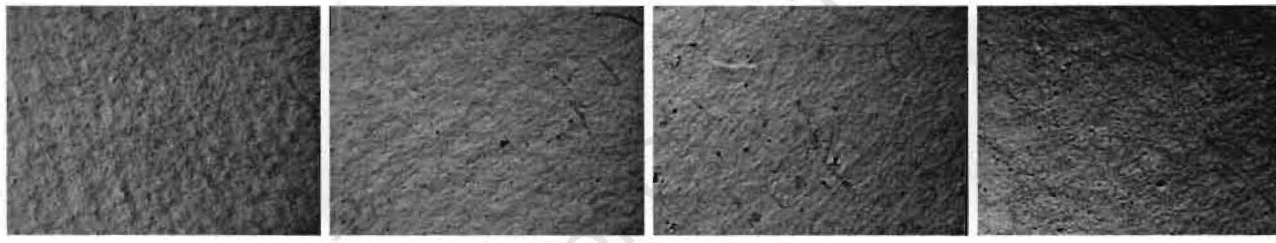

Electrolyte 11 1.5A/cm2; 70oC 2A/cm2; 70oC 1.5A/cm2; 80oC 2A/cm2; 80oC

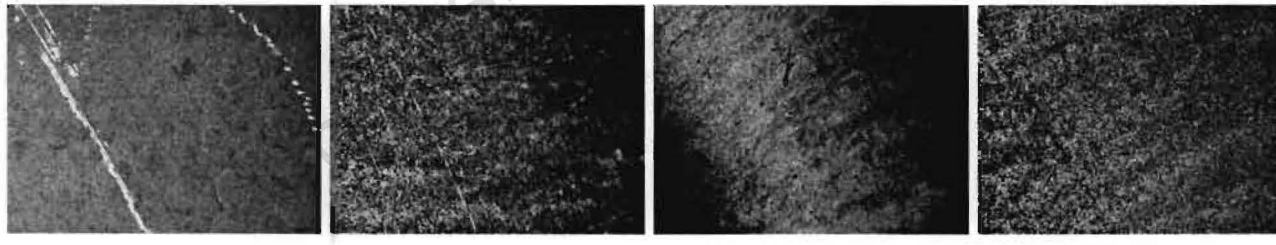

Electrolyte 12 1.5A/cm2; 70oC 2A/cm2; 70oC 1.5A/cm2; 80oC 2A/cm2; 80oC

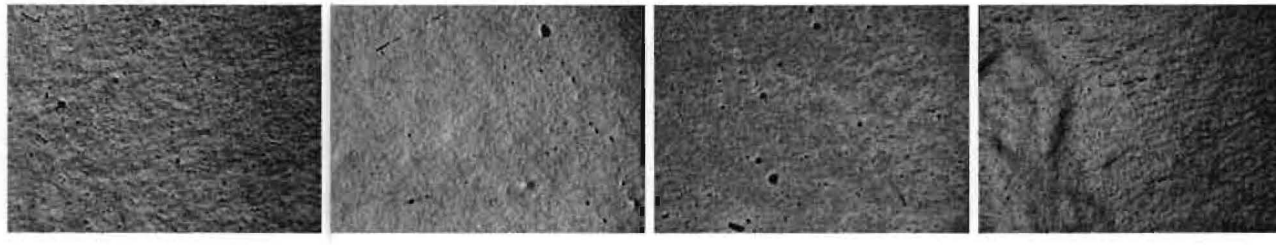

Electrolyte 13 1.5A/cm2; 70oC 2A/cm2; 70oC 1.5A/cm2; 80oC 2A/cm2; 80oC

Experiment I.D.	B expts
Aim of experiment	Optimisation of electrolyte composition.
Exposed surface area	$3cm^2$
Temperature	Average of 70 & 80°C

Results:

Electrolyte number	G vol %	H3PO4 vol %	H2SO4 vol %	average SI	mass loss [%]
1	0	100	0	-0.321	1.248
2	10	90	0	-0.0605	1.21175
3	20	80	0	0.14875	1.44275
4	20	40	40	0.52175	1.653
5	20	0	80	-4	0
6	10	0	90	-4	0
7	0	0	100	-4	0
8	0	50	50	-1.97175	2.3485
9	9.45	45.275	45.275	0.86025	1.9155
10	14.72	62.64	22.64	0.55175	1.6765
11	14.72	22.64	62.64	0.792	2.0535
12	4.72	22.64	72.64	0	2.35275
13	4.72	72.64	22.64	0.6	1.76275
PS	7.7	51.2	40.81	0.4532	2.201

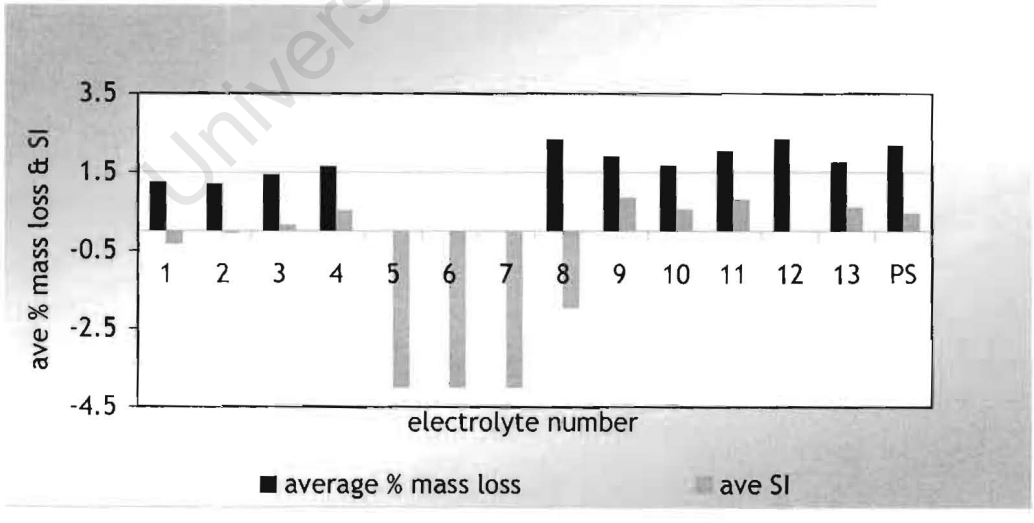

Experiment I.D.	EO expts
Aim of experiment	Performance comparison of new electrolytes vs PS electrolyte.
Exposed surface area	$3cm^2$
Temperature	80^oC

Results:

sample no.	*polishing time [mins]*	*Polished area [cm2]*	*Current density [A/cm2]*	*ave % mass loss [%]*	*Average SI*
9	3	3	2	2.282	0.856
11	3	3	2	2.478	0.768
EO0	3	3	2	1.766	0.720
EO1	3	3	2	2.025	0.596
EO2	3	3	2	2.358	0.714
PS	3	3	2	2.201	0.453

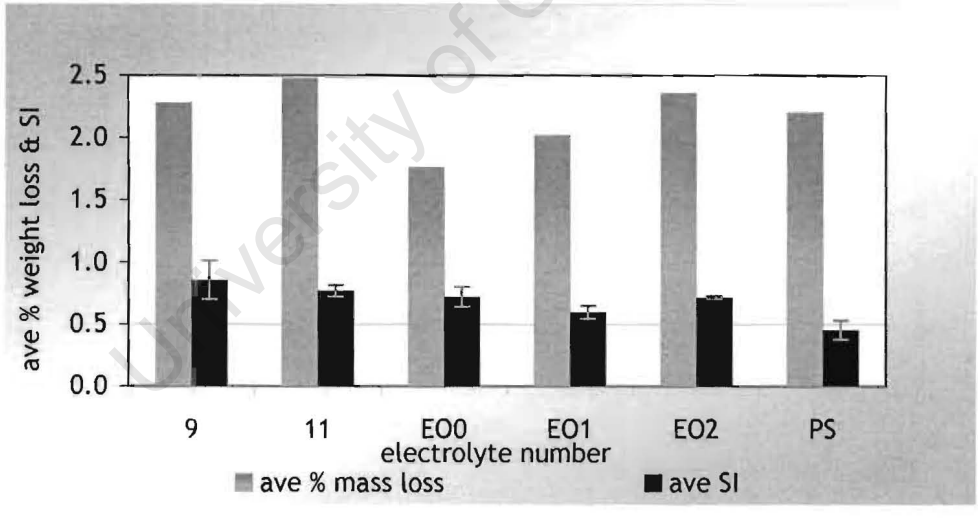

Experiment I.D.	X expts
Aim of experiment	To determine shortest polishing time for electrolytes PS, 11 & 9.
Exposed surface area	$3cm^2$
Temperature	80^oC

Results:

electrolyte	*sample no*	*polishing time [min]*	*initial mass [g]*	*final mass [g]*	*mass loss [g]*	*% mass loss*	*SI*
PS	X1-1	0.5	5.351	5.334	0.017	0.318	0.214
PS	X1-2	1	5.188	5.151	0.037	0.713	0.119
PS	X1-3	2	5.687	5.61	0.077	1.354	0.699
E11	X2-1	0.5	5.759	5.734	0.025	0.434	0.757
E11	X2-2	1	5.367	5.324	0.043	0.801	0.844
E11	X2-3	2	5.683	5.598	0.085	1.496	0.920
E9	X3-1	0.5	5.09	5.067	0.023	0.452	-0.032
E9	X3-2	1	5.591	5.559	0.032	0.572	0.863
E9	X3-3	2	5.386	5.308	0.078	1.448	0.860

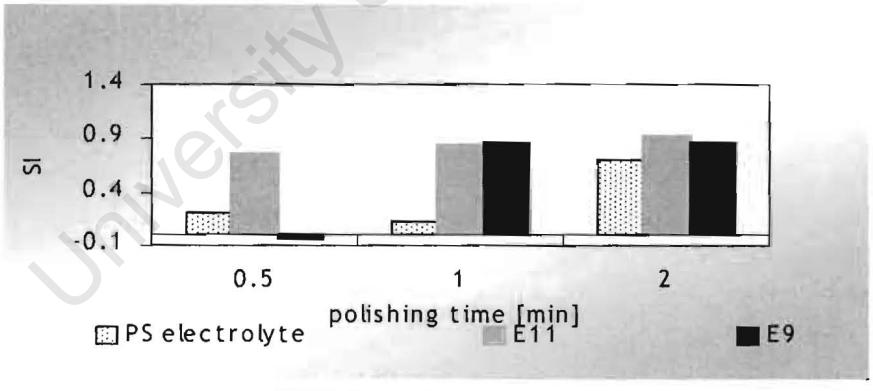

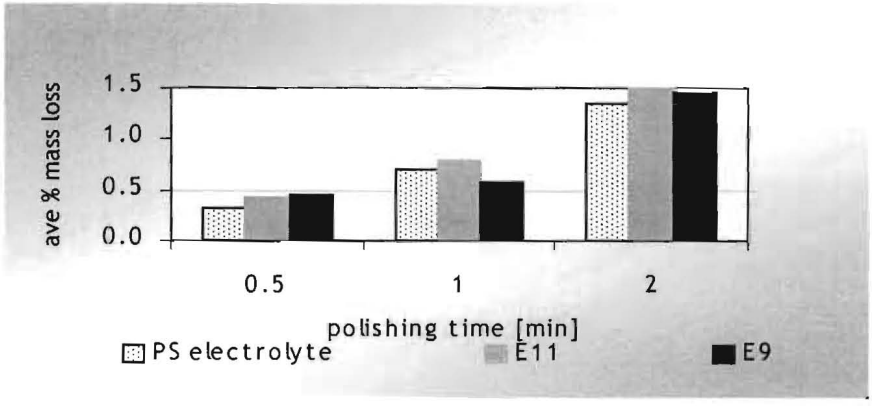

Experiment I.D.	Y expts
Aim of experiment	To determine the effect to of increased dissolved metal ions on polishing performance of electrolytes PS, 11 & 9.
Exposed surface area	$3cm^2$
Temperature	80°C

Results:

electrolyte	*sample no*	*[Fe]*	*initial mass*	*final mass*	*mass loss*	*mass loss*	*SI*
		[g/l]				*%*	
E9		0				2.282	0.856
E9	Y1-1	15	5.547	5.434	0.113	2.037	0.724
E9	Y1-2	30	5.396	5.299	0.097	1.798	0.671
E11		0				2.478	0.768
E11	Y2-1	15	5.499	5.358	0.141	2.564	0.787
E11	Y2-2	30	5.447	5.344	0.103	1.891	0.533
PS		0				2.201	0.453
PS	Y3-1	15	5.533	5.434	0.099	1.789	0.473
PS	Y3-2	30	5.507	5.415	0.092	1.671	0.132

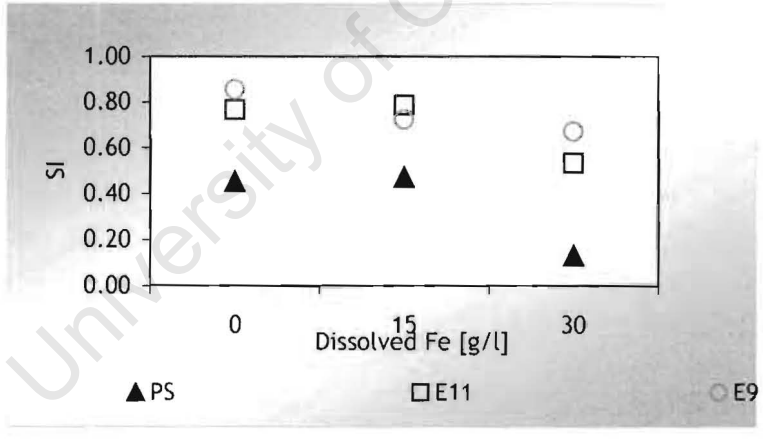

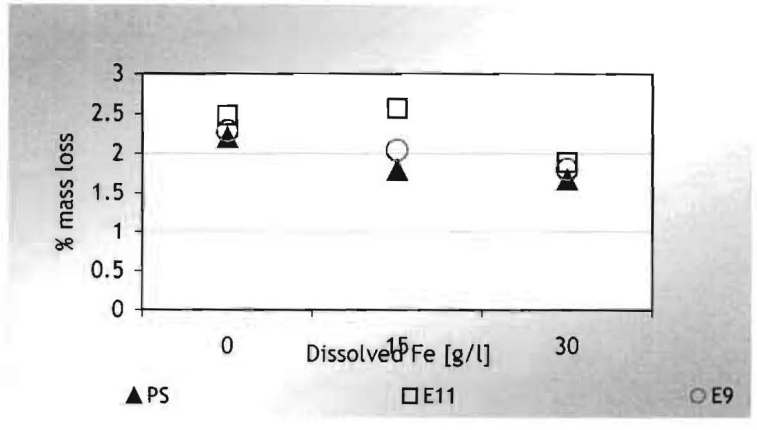

Appendix 3

Statistical Analysis - Optimisation of electrolyte composition

Analysis I.D.	B expt SI statistical analysis
Aim of experiment	Optimisation of electrolyte composition.
Exposed surface area	$3cm^2$
Temperature	Average of 70 & 80°C

The model to be fitted to all the data is

$$\text{Response} = \beta_1x_1 + \beta_2x_2 + \beta_3x_3 + \beta_{12}x_1x_2 + \beta_{13}x_1x_3 + \beta_{23}x_2x_3$$

$$+ (\beta_1x_1 + \beta_2x_2 + \beta_3x_3 + \beta_{12}x_1x_2 + \beta_{13}x_1x_3 + \beta_{23}x_2x_3)\text{*Density}$$

$$+ (\beta_1x_1 + \beta_2x_2 + \beta_3x_3 + \beta_{12}x_1x_2 + \beta_{13}x_1x_3 + \beta_{23}x_2x_3)\text{*Temperature}$$

$$+ (\beta_1x_1 + \beta_2x_2 + \beta_3x_3 + \beta_{12}x_1x_2 + \beta_{13}x_1x_3 + \beta_{23}x_2x_3)\text{*Density*Temperature} + \varepsilon.$$

This is a model which combines a quadratic model in the mixture variables (for which there is evidence) with a model with both main effects and two-factor interaction in the process variables.
This is the model with which I started and this full model produced the following analysis:

NOTE: No intercept in model. R-square is redefined.
Dependent Variable: SI

Analysis of Variance

Source	DF	Sum of Squares	Mean Square	F Value	Prob>F
Model	24	188.98244	7.87427	5.383	0.0001
Error	28	40.95763	1.46277		
U Total	52	229.94007			

Root MSE	1.20945	R-square	0.8219
Dep Mean	-0.83683	Adj R-sq	0.6692
C.V.	-144.52825		

Parameter Estimates

Variable	DF	Parameter Estimate	Standard Error	T for H0: Parameter=0	Prob > |T|
G	1	10.568738	33.53555501	0.315	0.7550
H3P04	1	0.264310	0.56777398	0.466	0.6452
H2S04	1	0.040575	0.56777398	0.071	0.9435
GP	1	-0.165424	0.41709366	-0.397	0.6947
GS	1	-0.137107	0.41709366	-0.329	0.7448
PS	1	0.010304	0.02007200	0.513	0.6117
GD	1	-5.037274	18.97057469	-0.266	0.7925
GT	1	-0.136440	0.44615039	-0.306	0.7620
GDT	1	0.059093	0.25238077	0.234	0.8166
PD	1	-0.148357	0.32118147	-0.462	0.6477
PT	1	-0.003662	0.00755355	-0.485	0.6316
PDT	1	0.001966	0.00427293	0.460	0.6490

SD	1	-0.029486	0.32118147	-0.092	0.9275
ST	1	-0.001014	0.00755355	-0.134	0.8942
SDT	1	0.000325	0.00427293	0.076	0.9399
GPD	1	0.079696	0.23594380	0.338	0.7381
GPT	1	0.002158	0.00554893	0.389	0.7003
GPDT	1	-0.000961	0.00313895	-0.306	0.7618
GSD	1	0.063968	0.23594380	0.271	0.7883
GST	1	0.001770	0.00554893	0.319	0.7521
GSDT	1	-0.000750	0.00313895	-0.239	0.8129
PSD	1	-0.003003	0.01135444	-0.264	0.7934
PST	1	-0.000115	0.00026703	-0.432	0.6689
PSDT	1	0.000034993	0.00015106	0.232	0.8185

Clearly no effects are significant, and the next step was to delete all the four factor terms. This produced the following analysis:

NOTE: No intercept in model. R-square is redefined.
Dependent Variable: REFLECTIVITY

Analysis of Variance

Source	DF	Sum of Squares	Mean Square	F Value	Prob>F
Model	21	188.58968	8.98046	6.733	0.0001
Error	31	41.35039	1.33388		
U Total	52	229.94007			

Root MSE	1.15494	R-square	0.8202
Dep Mean	-0.83683	Adj R-sq	0.6983
C.V.	-138.01405		

Parameter Estimates

Variable	DF	Parameter Estimate	Standard Error	T for H0: Parameter=0	Prob > |T|
G	1	1.505741	5.40833118	0.278	0.7825
H3P04	1	0.145738	0.38840855	0.375	0.7101
H2S04	1	0.158398	0.38840855	0.408	0.6862
GP	1	-0.039323	0.06213428	-0.633	0.5315
GS	1	-0.038674	0.06213428	-0.622	0.5382
PS	1	0.005711	0.00299012	1.910	0.0654
GD	1	0.141581	1.68927176	0.084	0.9337
GT	1	-0.015600	0.06628191	-0.235	0.8155
GDT	1	-0.009959	0.01578494	-0.631	0.5327
PD	1	-0.080602	0.21757997	-0.370	0.7136
PT	1	-0.002081	0.00515641	-0.404	0.6893
PDT	1	0.001063	0.00288828	0.368	0.7154
SD	1	-0.096813	0.21757997	-0.445	0.6594
ST	1	-0.002585	0.00515641	-0.501	0.6197
SDT	1	0.001223	0.00288828	0.423	0.6750
GPD	1	0.007638	0.01498735	0.510	0.6139
GPT	1	0.000476	0.00074937	0.636	0.5297
GSD	1	0.007721	0.01498735	0.515	0.6101
GST	1	0.000458	0.00074937	0.611	0.5457
PSD	1	-0.000378	0.00072124	-0.525	0.6035
PST	1	-0.000054174	0.00003606	-1.502	0.1432

The next step was to delete all the three factor terms, and the resultant analysis is as follows:

NOTE: No intercept in model. R-square is redefined.
Dependent Variable: REFLECTIVITY

Analysis of Variance

Source	DF	Sum of Squares	Mean Square	F Value	Prob>F
Model	12	184.23492	15.35291	13.436	0.0001

```
Error            40      45.70515       1.14263
U Total          52     229.94007

    Root MSE        1.06894     R-square       0.8012
    Dep Mean       -0.83683     Adj R-sq       0.7416
    C.V.         -127.73707

Parameter Estimates

                  Parameter       Standard    T for H0:
Variable  DF       Estimate          Error   Parameter=0    Prob > |T|

G          1     -1.117930     0.41124363        -2.718        0.0097
H3P04      1      0.031514     0.05551302         0.568        0.5734
H2S04      1      0.033795     0.05551302         0.609        0.5461
GP         1      0.009764     0.00346784         2.816        0.0075
GS         1      0.009169     0.00346784         2.644        0.0116
PS         1      0.000986     0.00016688         5.908        0.0001
GD         1      0.015033     0.07304769         0.206        0.8380
GT         1      0.004907     0.00365238         1.344        0.1867
PD         1     -0.001942     0.01336607        -0.145        0.8852
PT         1     -0.000534     0.00066830        -0.798        0.4294
SD         1     -0.005443     0.01336607        -0.407        0.6860
ST         1     -0.000916     0.00066830        -1.370        0.1783
```

A clearer picture is now emerging. If we look at the interactions involving Density and Temperature, the p values indicate that the Temperature interactions are having a greater effect on reflectivity than the Density interactions (with p values of 0.8380, 0.8852 and 0.6860). This led to the fitted model in the report and my comment that Density had a negligible effect. In my report I took the analysis further by adding back into the model the three factor terms involving temperature but these were not significant. The interaction terms involving Temperature in the table above are not significant, although with smaller p values than those for Density. This led to my final paragraph, that there is no clearcut (or strong) evidence for a Temperature effect.
This is the same conclusion at the end of your section 5.

SECTIONS 4.1 AND 4.2

The analyses at the two temperatures are similar except for the PS effect which is significant at Temperature 70 but not significant at Temperature 80. I have now fitted the same model for the combined temperature data but including the PST term. In the first analysis below there is no GPS term, and in the second analysis the GPS term is included.

```
NOTE: No intercept in model. R-square is redefined.
Dependent Variable: REFLECTIVITY

Analysis of Variance

                          Sum of          Mean
Source           DF      Squares        Square      F Value       Prob>F

Model             7    184.13225      26.30461       25.841       0.0001
Error            45     45.80783       1.01795
U Total          52    229.94007

    Root MSE        1.00894     R-square       0.8008
    Dep Mean       -0.83683     Adj R-sq       0.7698
    C.V.         -120.56686

Parameter Estimates

                  Parameter       Standard    T for H0:
Variable  DF       Estimate          Error   Parameter=0    Prob > |T|

G          1     -0.723588     0.26317307        -2.749        0.0086
H3P04      1     -0.011901     0.00445565        -2.671        0.0105
H2S04      1     -0.044402     0.00445565        -9.965        0.0001
GP         1      0.009764     0.00327318         2.983        0.0046
GS         1      0.009169     0.00327318         2.801        0.0075
PS         1      0.003688     0.00160503         2.298        0.0263
PST        1  -0.000036027     0.00002130        -1.692        0.0976


Analysis of Variance

                          Sum of          Mean
Source           DF      Squares        Square      F Value       Prob>F
```

Model	8	198.50320	24.81290	34.729	0.0001
Error	44	31.43687	0.71447		
U Total	52	229.94007			

Root MSE	0.84527	R-square	0.8633
Dep Mean	-0.83683	Adj R-sq	0.8384
C.V.	-101.00844		

Parameter Estimates

Variable	DF	Parameter Estimate	Standard Error	T for H0: Parameter=0	Prob > |T|
G	1	-0.630291	0.22146021	-2.846	0.0067
H3P04	1	-0.006237	0.00394074	-1.583	0.1207
H2S04	1	-0.038737	0.00394074	-9.830	0.0001
GP	1	0.007922	0.00277278	2.857	0.0065
GS	1	0.007328	0.00277278	2.643	0.0113
PS	1	0.003105	0.00135091	2.299	0.0263
GPS	1	0.000078705	0.00001755	4.485	0.0001

Analysis I.D.	B expt % mass loss statistical analysis
Aim of experiment	Optimisation of electrolyte composition.
Exposed surface area	$3cm^2$
Temperature	Average of 70 & 80°C

The model to be fitted to all the data is

$$\text{Response} = \beta_1x_1 + \beta_2x_2 + \beta_3x_3 + \beta_{12}x_1x_2 + \beta_{13}x_1x_3 + \beta_{23}x_2x_3$$

$$+ (\beta_1x_1 + \beta_2x_2 + \beta_3x_3 + \beta_{12}x_1x_2 + \beta_{13}x_1x_3 + \beta_{23}x_2x_3)\text{*Density}$$

$$+ (\beta_1x_1 + \beta_2x_2 + \beta_3x_3 + \beta_{12}x_1x_2 + \beta_{13}x_1x_3 + \beta_{23}x_2x_3)\text{*Temperature}$$

$$+ (\beta_1x_1 + \beta_2x_2 + \beta_3x_3 + \beta_{12}x_1x_2 + \beta_{13}x_1x_3 + \beta_{23}x_2x_3)\text{*Density*Temperature} + \varepsilon.$$

This is a model which combines a quadratic model in the mixture variables (for which there is evidence) with a model with both main effects and two-factor interaction in the process variables.
This is the model with which I started and this full model produced the following analysis:

NOTE: No intercept in model. R-square is redefined.
Dependent Variable: % WEIGHT LOSS

Analysis of Variance

Source	DF	Sum of Squares	Mean Square	F Value	Prob>F
Model	24	128.91402	5.37142	25.502	0.0001
Error	28	5.89758	0.21063		
U Total	52	134.81161			

Root MSE	0.45894	R-square	0.9563
Dep Mean	1.35890	Adj R-sq	0.9188
C.V.	33.77295		

Parameter Estimates

Variable	DF	Parameter Estimate	Standard Error	T for H0: Parameter=0	Prob > |T|
G	1	-1.798624	12.72550899	-0.141	0.8886
H3P04	1	0.010859	0.21544933	0.050	0.9602
H2S04	1	-0.003421	0.21544933	-0.016	0.9874
GP	1	0.023769	0.15827169	0.150	0.8817
GS	1	0.019005	0.15827169	0.120	0.9053
PS	1	-0.002160	0.00761659	-0.284	0.7788
GD	1	0.969246	7.19863496	0.135	0.8939
GT	1	0.025527	0.16929765	0.151	0.8812
PD	1	0.002258	0.12187655	0.019	0.9853
PT	1	-0.000135	0.00286630	-0.047	0.9628
SD	1	0.004254	0.12187655	0.035	0.9724
ST	1	0.000054971	0.00286630	0.019	0.9848
GPD	1	-0.012950	0.08953199	-0.145	0.8860
GPT	1	-0.000334	0.00210562	-0.159	0.8752
GPDT	1	0.000188	0.00119112	0.158	0.8757
GSD	1	-0.010253	0.08953199	-0.115	0.9096
GST	1	-0.000274	0.00210562	-0.130	0.8975
GSDT	1	0.000152	0.00119112	0.128	0.8993
PSD	1	0.001413	0.00430859	0.328	0.7453
PST	1	0.000025515	0.00010133	0.252	0.8030
PSDT	1	-0.000011506	0.00005732	-0.201	0.8424
GDT	1	-0.014129	0.09576921	-0.148	0.8838
PDT	1	0.000045112	0.00162142	0.028	0.9780
SDT	1	-0.000045653	0.00162142	-0.028	0.9777

In the next step the four factor terms were omitted to produce the following:

NOTE: No intercept in model. R-square is redefined.
Dependent Variable: PERCMASS

Analysis of Variance

Source	DF	Sum of Squares	Mean Square	F Value	Prob>F
Model	18	128.87622	7.15979	41.014	0.0001
Error	34	5.93539	0.17457		
U Total	52	134.81161			

Root MSE	0.41782	R-square	0.9560
Dep Mean	1.35890	Adj R-sq	0.9327
C.V.	30.74653		

Parameter Estimates

Variable	DF	Parameter Estimate	Standard Error	T for H0: Parameter=0	Prob > |T|
G	1	0.055786	1.80729607	0.031	0.9756
H3P04	1	0.004938	0.03059844	0.161	0.8728
H2S04	1	0.002571	0.03059844	0.084	0.9335
GP	1	-0.000914	0.02247799	-0.041	0.9678
GS	1	-0.000958	0.02247799	-0.043	0.9663
PS	1	-0.000650	0.00108172	-0.601	0.5518
GD	1	-0.090417	0.43593621	-0.207	0.8369
GT	1	0.000801	0.02179681	0.037	0.9709
PD	1	0.005642	0.00738062	0.764	0.4499
PT	1	-0.000056057	0.00036903	-0.152	0.8802
SD	1	0.000830	0.00738062	0.112	0.9111
ST	1	-0.000024921	0.00036903	-0.068	0.9466
GPD	1	0.001155	0.00542189	0.213	0.8326
GPT	1	-0.000004661	0.00027109	-0.017	0.9864
GSD	1	0.001154	0.00542189	0.213	0.8327
GST	1	-0.000007501	0.00027109	-0.028	0.9781
PSD	1	0.000551	0.00026092	2.110	0.0423
PST	1	0.000005380	0.00001305	0.412	0.6827

The PSD interaction is significant, but no other interaction turns out to be significant except for PS. The other interaction terms were dropped and the final analysis is shown under the heading Testing for the effect of Density in the previous report. The conclusion is that there is a PS interaction but this interaction is not the same at each Density. The analyses for each Density, in the previous report, show that the PS interaction causes a greater % weight loss at Density 2 (parameter value 0.000863) than at Density 1 (parameter value 0.000582). There was no evidence of a Temperature effect, and the analyses for the separate Temperatures show that the PS interaction is much the same in each case.

ELECTROPOLISHING : % MASS LOSS ALL DATA : FINAL ANALYSIS

% WEIGHT LOSS

NOTE: No intercept in model. R-square is redefined.
Dependent Variable: % WEIGHT LOSS

Analysis of Variance

Source	DF	Sum of Squares	Mean Square	F Value	Prob>F
Model	7	125.34796	17.90685	85.148	0.0001
Error	45	9.46365	0.21030		
U Total	52	134.81161			

Root MSE	0.45859	R-square	0.9298
Dep Mean	1.35890	Adj R-sq	0.9189
C.V.	33.74692		

Parameter Estimates

Variable	DF	Parameter Estimate	Standard Error	T for H0: Parameter=0	Prob > |T|
G	1	-0.045769	0.12015048	-0.381	0.7050
H3P04	1	0.010399	0.00213800	4.864	0.0001
H2S04	1	0.001948	0.00213800	0.911	0.3672
GP	1	0.000825	0.00150433	0.548	0.5863
GS	1	0.000567	0.00150433	0.377	0.7082
PS	1	0.000738	0.00010045	7.347	0.0001
GPS	1	-0.000002875	0.00000952	-0.302	0.7641

Appendix 4

MATLAB® Script file for measuring SI

```
format compact
format long
cd('c:\Jeeten\ri lab\')
wordstruct1 = dir('*.jpg');
num_ims = length(wordstruct1);

[filenames1{1:num_ims,1}] = deal(wordstruct1.name);

for im_num = 1:num_ims
tic

clear im1_sm im1 mask mask2 disc
filename1 = char(filenames1(im_num));

iptsetpref('ImshowBorder', 'tight')
iptsetpref('TruesizeWarning','off')

im1 = (rgb2gray(im2double(imread(filename1))));
disp(filename1)

[rows cols] = size(im1);

% Fitting a surface to the picture for flatfielding (normalising with respect to lighting)

rowvec = (1:rows)-rows./2;
%rowvec = (1:rows);
rowmat = rowvec(ones(1,cols),:);
colvec = transpose(1:cols)-cols./2;
%colvec = transpose(1:cols);
colmat = colvec(:,ones(1,rows));

fulrowvec = reshape(rowmat,rows.*cols,1);
fulcolvec = reshape(colmat,rows.*cols,1);

rv = fulrowvec;
cv = fulcolvec;


%E = [ones(rows.*cols,1) rv rv.^2 rv.^3 rv.^4 rv.^5 rv.^6 rv.^7 rv.^8 rv.^9 rv.^10 cv cv.^2cv.^3 cv.^4
cv.^5 cv.^6 cv.^7 cv.^8 cv.^9 cv.^10];
%E = [ones(rows.*cols,1) rv rv.^2 rv.*cv cv cv.^2]; % edges sometimes funny
E = [ones(rows.*cols,1) rv rv.^2  rv.*cv  (rv.^2).*cv rv.*(cv.^2) cv cv.^2 ]; % edges sometimes funny
%E = [ones(rows.*cols,1) rv log(rv) cv log(cv)];

im3 = transpose(im1);
y = reshape(im3,rows.*cols,1);

c = E\y;

surface1 = E*c;
surface = transpose(reshape(surface1,cols,rows));
```

```
corrs = corrcoef(surface1,y);
spread(im_num) = ((1-corrs(1,2).^2)*var(y)).^0.5;

im2 = mat2gray(im1-surface);

% End flatfielding

%FFT data to get freq info
data = reshape(im2,(rows.*cols),1);
datafft = data-mean(data);

%figure(1)
%hold on
[p,w] = pyulear(datafft,100,1000);
%pyulear(datafft,100,1000);

highf(im_num) = mean(log(p(400:length(p))));
medf(im_num) = mean(log(p(200:400)));
lowf(im_num) = mean(log(p(1:200)));

% End FFT

% Start Histogram stats
vari(im_num) = var(data);
skew(im_num) = skewness(data);
kurt(im_num) = kurtosis(data);
mead(im_num) = mad(data);
iqra(im_num) = iqr(data);

%disp(vari(im_num))
%disp(skew(im_num))
%disp(kurt(im_num))
%disp(mead(im_num))
%disp(iqra(im_num))

%sobels(im_num) = sum(sum(sobelim1));

figure(2)
SUBPLOT(2,2,1)
imshow(im1)
SUBPLOT(2,2,2)
imshow(im2)
SUBPLOT(2,2,3)
imhist(im1)
SUBPLOT(2,2,4)
imhist(im2)

toc
end
output = [vari.' mead.' highf.'];
csvwrite('JeetenAnalysis2.csv',output)
```